THE UNIVERSITY OF CHICAGO

THE STUDY, MANIPULATION, AND EVOLUTION OF MULTIPROTEIN SYSTEMS VIA T7 RNA POLYMERASE BIOSENSORS

A DISSERTATION SUBMITTED TO

THE FACULTY OF THE DIVISION OF THE PHYSICAL SCIENCES

IN CANDIDACY FOR THE DEGREE OF

DOCTOR OF PHILOSOPHY

DEPARTMENT OF CHEMISTRY

BY

JEFFREY ALEXANDER DEWEY

CHICAGO, ILLINOIS

AUGUST 2021

We stand not on the shoulders of giants, but on a mountain of dreams discarded by young scientists.

I dedicate this thesis to all forgotten scientists whose contributions are individually classified as minute, but together breathe life into each and every discovery.

TABLE OF CONTENTS

LIST OF FIGURES _____ v

ACKNOWLEDGMENTS _____ vi

ABSTRACT _____ vii

LIST OF PUBLICATIONS _____ viii

1. INTRODUCTION TO PROTEIN-PROTEIN INTERACTIONS _____ 1
   1.1 Forces and composition of PPIs _____ 1
   1.2 Targeting PPIs in disease _____ 5

2. RNA POLYMERASE TAGS TO MONITOR MULTIDIMENSIONAL PROTEIN-PROTEIN INTERACTIONS REVEAL PHARMACOLOGICAL ENGAGEMENT OF BCL-2 PROTEINS _____ 12
   2.1 Introduction _____ 12
   2.2 Results and discussion _____ 16
   2.3 Conclusion _____ 27
   2.4 Experimental details _____ 30

3. SPLIT T7 RNA POLYMERASE BIOSENSORS TO STUDY MULTIPROTEIN INTERACTION DYNAMICS: A PRACTICAL GUIDE _____ 34
   3.1 Introduction _____ 34
   3.2 Evolution of the split T7 RNA polymerase biosensor _____ 36
   3.3 RNAP analysis of Bcl-2 family PPIs _____ 43
   3.4 Summary _____ 57

4. A SYSTEM FOR THE EVOLUTION OF PROTEIN-PROTEIN INTERACTION INDUCERS _____ 58
   4.1 Introduction _____ 58
   4.2 Results _____ 62
   4.3 Discussion _____ 85
   4.4 Methods _____ 97

5. SUMMARY AND PERSPECTIVES _____ 104

REFERENCES _____ 108

LIST OF FIGURES

2.1 Split RNAP biosensors can detect Bcl-2 family PPIs in *E. coli* 14
2.2 Split RNAP biosensors can detect Bcl-2 family PPIs in mammalian cells 17
2.3 Split RNAP biosensors can monitor two Bcl-2 family PPIs simultaneously in mammalian cells 21
2.4 Spit RNAP biosensors can simultaneously monitor pharmacological engagement of two PPIs in live cells 21
2.5 Uncovering a series of orthogonal proximity-dependent C-terminal split RNAPs 23
2.6 Schematic of a system to detect 4 multidimensional PPIs simultaneously 26
2.7 Detection of 1x4 Bcl-2 family PPIs simultaneously in mammalian cells by RT-qPCR analysis of the unique RNA outputs 29

3.1 Schematic of several common methods for detecting PPIs 35
3.2 Example interactions detected via the evolved split RNAP biosensor 38
3.3 Plasmid designs for *e. coli* and mammalian assays and general workflow when using the split RNAP biosensor 42
3.4 Mcl1-tBID PPI detection in mammalian cells using a fluorescent RNA aptamer output 47
3.5 PPI competition and multidimensional analysis using the split T7 RNAP biosensor 50

4.1 Split RNAP biosensors detect molecular glue-induced PPIs 64
4.2 Rapid evolution of protein-protein interaction molecular glues (rePPI-G) to overcome the "hook" effect 68
4.3 rePPI-G improved molecular glue activity by altering binary interaction affinities 73
4.4 Expanding target scope of rePPI-G 77
4.5 Combination of continuous and noncontinuous phage assays escape local activity minima in rePPI-G 82
4.S1 Background RNAP assembly without molecular glue induction 88
4.S2 Molecular glue-dependent phage replication 89
4.S3 Negative selection PACE experiment 89
4.S4 Wildtype $RNAP_N$ can predict split RNAP compatibility 90
4.S5 Identifying new rePPI-G target proteins 90
4.S6 Background RNAP assembly without molecular glue induction 91
4.S7 Replicates of rePPI-G with ZB-Ulk1 molecular glue 92
4.S8 ZB-ULK1 rePPI-G variants and background activity 93
4.S9 Changes in eZB binding of ZA after rePPI-G 94
4.S10 Changes in eZB binding of off targets after rePPI-G 94
4.S11 Assessment of eZB(A1T, Q18R, W21R) as independent PPI inducer 95
4.S12 Co-immunoprecipitation of GABARAPL1-1/2 using either ULK1(wt) or ULK1(bp1081del) 96

ACKNOWLEDGEMENTS

I would like to acknowledge my advisor, Professor Bryan Dickinson, for his financial support and assistance in training me to be an independent, careful, and thoughtful scientist. I would also like to acknowledge my thesis committee members, Professors Joseph Piccirilli, Yamuna Krishnan, and Todd Emrick, for their time, insights, and support over the last 5 years, and 11 years in the case of Professor Emrick.

I would also like to acknowledge my friends and family. To avoid forgetting any friends I will say this, I am so grateful to every single graduate student and postdoc who helped bring joy to my life, or to those I care about. Even if this joy did not last for the entire Ph.D., it was important to my life nonetheless. My family has been incredibly supportive during my Ph.D. and kept me thinking about what is important in life.

ABSTRACT

Protein-protein interactions (PPIs) are critical to nearly all cellular functions. Despite more than 30 years of research detailing the impacts of specific PPIs in disease, there remain numerous undruggable interactions that lead to negative health outcomes. A major complication in the field of PPIs is understanding how multiprotein networks and complexes interact with one another over time. In particular, one challenge is a lack of methods to study the selective inhibition of one PPI vs. several others in a native cellular context. Another challenge is a lack of tools to selectively induce two proteins to interact with one another, enabling the control of cellular functions. In this thesis, I begin by discussing the character and importance of PPIs. I then detail a proof-of-concept method to study PPI networks and their selective inhibition in live mammalian cells, including a practical guide for using this method and expanding its use in the future. Finally, I describe a new directed evolution method for the rapid evolution of protein-protein interaction glues (rePPI-G) that is capable of evolving bivalent PPI inducers within a matter of days. Development of this new method also resulted in observations about optimal bivalent ligand design, presaging utility of the principles for optimizing small molecule bivalent glues. It is my hope that this work will catalyze new methodologies focused on modifying and studying multiprotein systems, which in turn fuels advancements in pharmacological tools to understand and treat human disease.

LIST OF PUBLICATIONS

1. **Dewey, J. A.**; Azizi, S. A.; Lu, V.; Dickinson, B. C. A System for the Evolution of Protein-Protein Interaction Inducers. *ACS Syn. Bio.*, Accepted (**2021**).

2. **Dewey, J. A.**; Dickinson, B. C. Split T7 RNA Polymerase Biosensors to Study Multiprotein Interaction Dynamics. *Methods Enzymol.* 641, 413-432 (**2020**)

3. Pu, J.*; **Dewey, J. A.***; Hadji, A.; LaBelle, J. L. & Dickinson, B. C. RNA Polymerase Tags To Monitor Multidimensional Protein–Protein Interactions Reveal Pharmacological Engagement of Bcl-2 Proteins. *JACS* 139, 11964-11972, doi:10.1021/jacs.7b06152 (**2017**). (* denotes equal contribution to this work)

CHAPTER 1

INTRODUCTION TO PROTEIN-PROTEIN INTERACTIONS

1.1 Forces and Composition of PPIs

All organisms rely on multipurpose biopolymers from DNA to branched carbohydrates. The biopolymers of particular interest in this thesis are proteins. Despite being composed of just five elements (H, C, N, O, S) and 20 repeating units, amino acids, proteins are capable of performing diverse functions. However, just as human civilization is defined by interpersonal coordination and cooperation rather than individuals, cells are defined by proteins interacting with a diverse suite of molecules including other proteins or even copies of themselves. Interactions between proteins, protein-protein interactions (PPIs), are abundant, necessary, and constantly shifting over time and space within every organism. Aberrations in PPIs are known to drive numerous diseases including autoimmunity and cancer.[1-3] Selective and effective modulation of PPIs, however, remains a challenge in disease contexts, despite the validation of PPIs as therapeutic targets more than 30 years ago. Before discussing the implications of PPIs in disease and cellular biology more broadly, I will first discuss the biophysical characteristics of PPIs. Understanding the forces that drive proteins to interact with one another, and indeed themselves, help the scientific community better understand and accurately predict PPI dynamics in diverse contexts.

Two specific phenomena dominate noncovalent protein interactions – electrostatic interactions and the hydrophobic effect. Electrostatic interactions take many forms. A common and intuitive interaction occurs between positively charged amino acids such

as lysine or arginine and negatively charged amino acids such as aspartate and glutamate. These fully charged interactions contribute 3-4 kcal/mol (3% of a C-H bond) to protein binding when poised < 3Å from one another.[4] Another important and common electrostatically driven interaction are hydrogen bonds. These atomic-scale interactions occur when an electronegative atom, such as oxygen or nitrogen, is covalently bonded to hydrogen atoms. The electronegative atom possesses a higher average electron density than their covalently bonded hydrogen atoms, creating electrostatic dipoles along the hydrogen bonds that can interact with one another or other electrostatic charges.[5] Hydrogen bonds between the amide backbone of proteins create repetitive nano-scale structures such as alpha helices and beta sheets. These structures organize amino acids and limit them to a particular suite of possible conformations, enabling proteins to display a selective and semi-stable interaction interface.

The hydrophobic effect is another dominant force shaping protein structures and interactions. The hydrophobic effect is an effect unique to hydrophobic molecules in environments surrounded by hydrogen bonds. For example, when a hydrophobic lipid enters water, the water molecules are forced in close proximity with the lipid to prevent formation of a special vacuum. The water molecules then orient themselves into discrete and semi-stable structures in order to form energetically favorable hydrogen bonds, but at a high entropic cost. Any change in the system to decrease the amount of exposed hydrophobic surface area will allow water molecules to move freely while retaining hydrogen bonds. Thus, decreasing hydrophobic surface area in a hydrogen

bond environment is energetically favorable, and referred to as the hydrophobic effect. Nearly half of the amino acids in biology have hydrophobic side chains. A protein chain typically folds in such a way to prevent exposing those hydrophobic regions to the surrounding water, but there are also hydrophobic patches that can interact tightly with patches on other proteins in order to prevent formation of those frozen waters.[6] Furthermore, there are narrow channels or pockets that are formed within proteins that selectively accept hydrophobic molecules with a specific structure and orientation.

Understanding the theoretical means by which proteins interact is important, but analyzing the motifs and components that repeat throughout the proteome can help us design proteins with new functions that also interface with the current endogenous protein interaction landscape. Categorizing and detailing different specific amino acid motifs has been carried out for over two decades.[7-11] Rather than detailing specific protein interaction domains, we will discuss the general principles that dictate all PPI interfaces. Analysis of crystal structures to determine which amino acids are overrepresented at PPI interfaces versus the protein's core or noninteracting outer shell revealed PPI interfaces are selectively enriched for particular amino acids.[12, 13] Three amino acids are overrepresented in PPI interfaces compared to the protein surface – tyrosine, tryptophan, and arginine. Tryptophan is a relatively rare amino acid, accounting for roughly 1% of protein surface area, but is amplified significantly (3-5%) at PPI interfaces. Arginine is only moderately amplified at PPI interfaces (~6-8% versus 9-10%), but this slight increase is a dramatic enrichment compared to other charged amino acids, which are all underrepresented at PPI interfaces.

The most consistently over enriched amino acid at PPI interfaces is Tyrosine. One study found that tyrosine comprises only 3% of the antibody surface area, but account for over 16% of protein interaction surface area.[12] Fellouse et al. performed phage-display based selections to determine if libraries of binding regions composed of only four unique amino acids could effectively discover protein binders.[14] They found that four amino acid combinations that contained tyrosine were most successful, with other combinations of amino acids failing to discover a single protein binder. Moreover, they crystallized their new binders and found that in some cases tyrosines made up 70% of the binding surface area. As a follow up study, the same group used binding regions consisting of only tyrosine and serine.[15] These minimal libraries discovered four antibody fragments with selective, low nanomolar affinity for diverse protein targets. Crystal structures revealed remarkable stacking interactions between tyrosine residues that reduced exposed hydrophobic phenyl rings, thus locking the tyrosine-containing region into a particular conformation that then makes selective contact with the protein target. Another crystal structure showed an alpha helix with serine amino acids performing a stabilizing backbone role and tyrosine amino acids branching in numerous directions from the helix core to form selective interactions. This study demonstrated the power of tyrosine in particular to not only interact with diverse targets, but also interact with other tyrosine molecules to generate structures capable of unique protein target recognition.

Considering electrostatic forces and the hydrophobic effect, along with the basic physical principles that no two atoms can occupy the same space and vacuums in space have an enormous energetic cost, allow us to predict how amino acid changes might result in increased or decreased PPI affinity. Later in this thesis we discover a mutation that switched an amino acid's charge resulting in a salt bridge that had a measurable contribution to interaction affinity. However, these changes are not always so clear from simple amino acid sequence. A simple binary code consisting of tyrosine and serine is capable of selectively recognizing unique protein targets. Moreover, crystal structures revealed the complex network of interactions formed by multiple tyrosine molecules that produced an orientation precisely fitting the protein target. Overall, understanding the fundamentals of PPIs is important when initially designing molecules or investigating the resulting impacts of mutations, but discovering and optimizing a PPI is still best left to nature's most powerful tool – evolution.

1.2 Targeting PPIs in Disease

The human genome contains ~20,000 proteins, but with an estimated 650,000 PPIs each protein interacts with dozens of others on average.[16] PPIs occur between intersecting networks of proteins, with a single protein playing multiple roles depending on the cellular environment. The cellular PPI network contains carefully balanced complexities and dynamics of to maintain cell homeostasis under equally complex and dynamic conditions. Thus, it follows that genetic mutations or environmental factors that modulate PPIs can disrupt cell homeostasis and in turn cause disease in humans. In this section I will discuss two cases where inhibiting select PPIs has a dramatic impact

on human disease. Analyzing these case studies will reveal the successes and current challenges in pharmacological PPI modulation and study. I will also discuss the status of PPI inducers in the treatment of disease. The research carried out in this thesis will hopefully reduce challenges faced in translational research, resulting in improved patient outcomes in the future.

The most common strategy in pharmacological modification of disease is inhibition of protein activity. Statistical analysis of commonly mutated genes in cancers identified numerous protein targets that drive disease, including extracellular signaling receptors such as GPCRs and intracellular kinases such as in the MAPK pathway, and triggered successful drug discovery campaigns for those protein targets.[17, 18] These genetic, and later biochemical, studies between 1980 and 2000 also identified several drivers of cancer that caused disease primarily via PPIs. Two genes or gene families we will discuss here are the B-cell lymphoma 2 (BCL2) family and the human epidermal growth factor receptor 2 (HER2).[19, 20]

The discovery and treatment of BCL2 family proteins revolves around PPI inhibition. The BCL2 gene was first identified as linked to cancer in 1985, and subsequent studies found that the Bcl-2 protein served as a guardian of apoptosis, or cell suicide.[21] Genetic alterations that amplify the amount of Bcl-2 protein in cells will prevent apoptosis, a necessary step in cancer progression given cancer cells must maximize growth and minimize death. Later biochemical characterization discovered Bcl-2 proteins bind and sequester a suite of proapoptotic peptides that are unstructured except for a Bcl-2

homology 3 (BH3) domain, earning them the name BH3-only peptides.[22] If left unbound within a cell, BH3-only peptide triggers apoptosis at the surface of mitochondria by binding the Bcl-2 associated X (BAX) protein.[23] Furthermore, researchers discovered there are multiple proteins that play homologous roles to Bcl-2, including myeloid leukemia cell differentiation protein 1 (Mcl1) and B-cell lymphoma-extra large (Bcl_{xL}). Given many cancers upregulate the expression of Bcl-2 protein, researchers hypothesized that if the PPI between Bcl-2 and BH3-only proteins is disrupted it would cause cancer cells to undergo apoptosis.

With this goal in mind, various companies began searching for inhibitors of the Bcl-2 protein's interactions with BH3-only peptides. In 1996 the crystal structure of Bcl_{xL} bound to a BH3-only peptide, enabling structure guided small molecule design.[24] In 2007 a small molecule that targeted Bcl-2 and its homologue Bcl_{xL}, navitoclax, entered phase I clinical trial.[25] Unfortunately, human thrombocytes rely on Bcl_{xL} expression to avoid apoptosis and so patients experienced severe thrombocytopenia that even resulted in death. Four years later, and 27 years after the initial correlation between Bcl-2 and cancer, a new small molecule that selectively targets the Bcl-2 protein, venetoclax, entered phase I clinical trials.[26] This drug was approved for the treatment of chronic lymphocytic leukemia with alterations in Bcl-2 protein expression in 2016. The story of Bcl-2 is one of perseverance and success in pharmacology. Sadly, venetoclax remains the only successful drug discovery campaign for an intracellular PPI inhibitor. Many other PPI inhibitors enter preclinical or clinical trials, but ultimately fail to treat

disease effectively or in a safe manner.[27] Thankfully for patients an alternative pipeline for PPI inhibitor discovery was optimized in the 1990's, but only for extracellular targets.

The inhibition of the HER2 PPI was not an outlier. In some ways research around HER2 sparked a 30+ year golden age in non-small molecule therapeutics. HER2 was first correlated with cancer in 1987 when it was observed to be hyper amplified in many breast cancer patients.[20] Mechanistic research identified HER2 as a membrane bound signaling receptor that activated cell growth upon extracellular binding of growth factors such as epidermal growth factor (EGF).[28] It was clear that cancerous cells overexpressed HER2 in order to more sensitively respond to these growth factors, thus maintaining an active growth state despite minimal growth signals. Moreover, HER2 activity is dependent on protein dimerization, which is also amplified when more HER2 proteins are expressed.[29] Inhibiting HER2's PPIs with itself and growth factors became a target in drug discovery campaigns.

In the 1990's a new class of protein modulator became viable as a pharmaceutical – antibodies. Advances in humanizing antibodies discovered in mice finally allowed safe and efficacious binding of extracellular proteins in humans.[30] Only five years after correlating HER2 to breast cancer, an antibody that binds to and inhibits HER2 PPIs enters phase I clinical trials.[31] Six years later this antibody therapeutic, Herceptin, is approved by the FDA for the treatment of HER2 positive breast cancer.[32] Unlike Bcl-2, the discovery of Herceptin was not a one-off. There are now over 80 FDA approved antibody therapeutics that operate via PPI modulation, including one that was approved

in after only one year for use treating SARS-COV-2 infection.[33, 34] The success of antibodies in part can be attributed to the power of the mammalian immune system, which discovers protein binders through a process of rapid continuous directed evolution. One might ask why an antibody therapy was not developed for inhibiting the Bcl-2 protein's interactions. Antibodies are limited to extracellular protein targets due to disulfide bonds and their large size, which complicates their intracellular delivery.[35] Moreover, antibody treatments are extremely expensive with one year costing over $90,000 on average.[36]

Another strategy for positively influencing human disease is inducing rather than inhibiting a particular protein's activity or interactions. A PPI inducer is a molecule that either binds to two proteins, bringing them in close proximity, or binds to one protein to change its conformation in such a way to bind another protein. The clinical success of the few known PPI inducers speaks for itself. Although less than 100 small molecule PPI inducers are known, seven are FDA approved.[37] These include not only natural products like Rapamycin, Taxol, Cyclosporin A, and FK506 that were evolved over the course of millennia to selectively induce a particular PPI, but also synthetic PPI inducers like, tafamidis, dexrozoxane, and thalidomide and its derivatives. Despite their success, campaigns to discover PPI inducers remain rare in both academia and industry. The biggest challenge facing the use of PPI inducers in the clinic is PPI validation. There is a limited set of endogenous PPIs, ~650,000 interactions, that already exist and so are targets for selective PPI inhibition. However, the number of PPIs that could be induced is upwards of 200,000,000 in theory given ~20,000 human genes.[16] Molecular biologists

need a method capable of rapidly generating high quality PPI inducers to begin validating or invalidating the most promising interactions. Antibody development allows these researchers to quickly begin screening extracellular targets, but as with PPI inhibitors, intracellular targets remain elusive with no versatile method exists to target these interactions.

Antibody therapies based on PPI induction are rare, there are only two FDA antibody therapies that induce PPIs, but as challenges in antibody engineering are overcome dozens more are in clinical trials for treating various cancers.[38, 39] Many of these therapies operate by performing a herculean feat – acting as a molecular bridge to induce the interaction between two cells. For example, blinatumomab is a bispecific antibody FDA approved in 2014 that kills B-cell lymphomas by bridging the interaction between two cell surface receptors, CD3 and CD19.[40] CD3 is overexpressed on T-cells while CD19 is a receptor commonly overexpressed on cancerous B-cells. When blinatumomab induces this new interaction it both stimulates the T-cell to destroy bound cells and brings the cancerous B-cell into the T-cell's killing range. Although still in their early stages, bispecific antibodies are a promising PPI inducer scaffold for extracellular targets. Again, mammalian immunity is a directed evolution system capable of producing excellent PPI modulators, but is limited to extracellular targets due to the antibody scaffold.

The examples of PPI modulators in disease described above make it clear that the scientific community needs a versatile directed evolution method similar to mammalian

immunity in order to discover PPI modulators with scaffolds amenable to intracellular delivery. Even when these modulators are initially discovered, it's also critically important that a suite of downstream mammalian cell assays are available to assess both how selective the modulator is for a given PPI and whether the modulator impacts PPI network dynamics in unexpected ways. The two methods described in this thesis represent the foundations for accomplishing both PPI modulator discovery and assessment.

CHAPTER 2

RNA POLYMERASE TAGS TO MONITOR MULTIDIMENSIONAL PROTEIN-PROTEIN INTERACTIONS REVEAL PHARMACOLOGICAL ENGAGEMENT OF BCL-2 PROTEINS

2.1 Introduction

As stated above, protein-protein interactions (PPIs) are fundamental to cellular organization, regulation, and cell signaling[41-43]. Although often considered "undruggable", the centrality of dysregulated PPIs in many complex disease states makes these biomolecular interactions enticing targets for therapeutic development[44-47]. A key challenge to understanding the physiological and pathological roles of target PPIs are a lack of tools for measuring competitive interactions within complex PPI networks in native biological contexts. An exemplar of both the challenges and opportunities in PPI-targeted therapeutics is the B cell lymphoma 2 (Bcl-2) family of apoptotic regulatory proteins, which function through highly interconnected and competitive interaction networks to control cell death[48].

A key hallmark of cancer is evasion of apoptosis, which is mediated by anti-apoptotic Bcl-2 family proteins such as Bcl-2, Bcl-X_L and myeloid cell leukemia 1 (Mcl-1). These proteins maintain cell survival by binding and sequestering their pro-apoptotic multidomain counterparts, such as Bcl-2-associate X protein (BAX) and Bcl-2 antagonist killer 1 (BAK), and Bcl-2 homology 3 (BH3)-only proteins such as Bcl-2 antagonist of cell death (BAD), truncated BH3-interacting domain death agonist (tBID), and Bcl-2-interacting mediator of cell death (BIM)[49, 50], through competitive PPIs. Venetoclax, a recently approved Bcl-2 inhibitor and first FDA approved intracellular PPI

inhibitor, is effective in patients with hematologic malignancies[51]. Mcl-1 dysregulation is a key mode of resistance to both Bcl-2 inhibitors such as Venetoclax[52], and chemotherapy more broadly, driving myriad cancers. Mcl-1 inhibitors, therefore, are a current focal point of cancer drug discovery efforts[53-56]. The complexity and interconnectivity of Bcl-2-family apoptotic regulation illustrates the need for tools to monitor the interactions in a native biological context, but is also representative of the broader challenges and opportunities in both understanding and exploiting disease-relevant PPIs.

A multitude of live cell-deployable technologies for measuring PPIs have been developed[57-66]. The yeast 2-hybrid system (Y2H) is being utilized to catalog the potential binary PPIs across the entire human proteome[67]. However, a key limitation of such yeast-based studies is that biological relevance is not guaranteed for each identified interaction, and the interactions may be differentially regulated in mammalian systems. Förster/bioluminescent resonance energy transfer (FRET/BRET)-based sensors permit detection of subtle changes in distance with high spatiotemporal resolution[68], and have even been adapted to rapidly and temporally measure changes in 40 cell signals under identical conditions[69]. Another widespread method for measuring PPIs in live mammalian cells is protein fragment complementation (PFC), which involves tagging two potential binding partners of interest with separate halves of a split protein reporter.

PFC systems have been developed for a variety of imaging modalities, such as green fluorescent protein (GFP)[61, 70-72], luciferase[73, 74], and horseradish peroxidase (HRP)[75], as well as other reporter systems such as tobacco etch virus (TEV) protease[76, 77], ubiquitin[78], and BS2 esterase.[79] The key advantage of most PFC technologies is that PPIs can be measured in real-time using simple imaging techniques. However, multiplexed and/or competitive detection of PPIs has only been reported in proof-of-concept demonstrations[80-83], and at most for a trimolecular PPI system. Although the need for multidimensional PPI analysis techniques is widely acknowledged[59], challenges with

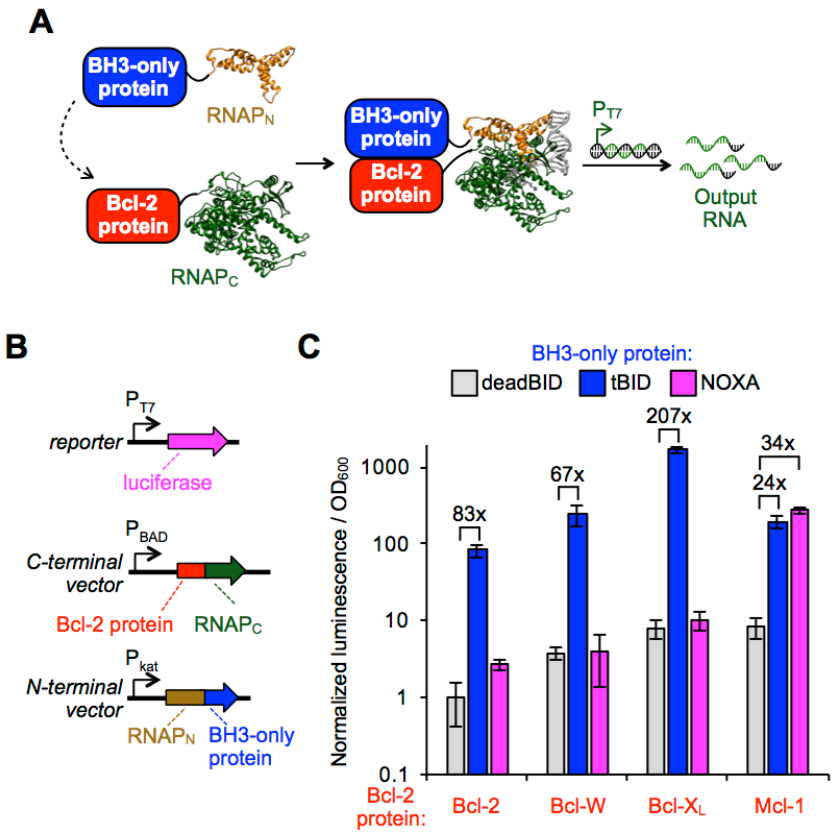

Figure 2.1. Split RNAP biosensors can detect Bcl-2 family PPIs in *E. coli*. (A) Schematic of split T7 RNAP tags to monitor Bcl-2-family PPIs. A target Bcl-2 protein is fused to a C-terminal T7 RNAP variant (RNAP$_C$) and a target BH3-only protein ligand is fused to an evolved proximity-dependent N-terminal T7 RNAP variant (RNAP$_N$). Interaction between the fusion proteins results in assembly of the RNAP and a transcriptional output signal. (B) Vector system to test Bcl-2 split RNAP detection system in *E. coli*. (C) Transcriptional output of split RNAPs with a series of Bcl-2 proteins interaction with a set of BH3-only peptides assayed in *E. coli* using the vectors shown in (B). Cells were induced for 3 h with arabinose and then analyzed for luminescence. Error bars are ± s.e.m., n = 4. "deadBID" is a modified tBID BH3-only peptide with the key binding portions removed as a negative control.

spectral overlap of reporters, incompatible PFC technologies, and differential sensitivities have largely precluded their development. Therefore, there is a need for generalizable PFC technologies to detect multidimensional PPIs in a competitive manner within mammalian systems.

Our group developed a proximity-dependent split RNA polymerase (RNAP) reporter system as a new method to measure target interactions in biological systems[84]. This involved evolving an N-terminal split RNAP tag, $RNAP_N$, to assemble with a C-terminal split RNAP tag, $RNAP_C$, in a PPI-dependent manner. The advantage of an RNAP-based reporter is that the RNA signal can be measured in a variety of sensitive ways, including fluorescence, sequencing, nanoparticle detection, etc.[85-89], and can be amplified by polymerase chain reaction (PCR)[90] or recombinase polymerase amplification (RPA)[91] for even more sensitive detection. Moreover, unlike optical reporters, RNAP-based reporters are not limited by spectral overlap considerations, as unique “barcode” sequences can, in principle, be encoded in orthogonal RNA outputs[86, 92]. Indeed, we recently demonstrated the possibility of performing multidimensional biochemical assays in mammalian cells using orthogonal protease-responsive RNAPs[93]. Finally, an RNA output offers control over genomic and transcriptomic processing through the production of mRNA, RNAi, or even gRNA, all of which have important applications in genetic screens and synthetic biology[94-98].

In principle, the evolved proximity-dependent split RNAP system lays the foundation for the generation of a new set of RNAP tags that encode multidimensional PPIs in RNA signals. The key to realizing such a technology is developing the approaches to deploy the tools in mammalian cells and the creation of a set of

orthogonal proximity-dependent split RNAPs that drive transcription from unique DNA promoters based on a target PPI, thereby producing a unique RNA output. In this report, we develop a series of orthogonal split RNAP tags for interrogating PPIs in mammalian systems and apply the new tools to probe Bcl-2-family interactions and their pharmacological engagement. Application of the tools in “one-by-four” interactome analyses of the Bcl-2 pathway reveals endogenous ligand competition and selectivity profiling of both clinical and preclinical drug candidates. Together, this work establishes split RNAPs as a versatile new addition to the PPI analysis toolbox, with particular advantages for multidimensional and competitive PPI interrogation, and future synthetic biology applications.

2.2 Results and Discussion

We first tested whether the proximity-dependent split RNAP tags can detect Bcl-2 family PPIs (Figure. 2.1A). To validate and optimize the protein sensors, we deployed an *E. coli*-based transcriptional reporter system[84, 99]. We cloned expression vectors that constitutively express the BH3 binding domains of tBID and NOXA each fused to the evolved $RNAP_N$ tag through a flexible linker. We also cloned a negative control, deadBID, that consists of tBID devoid of its necessary BH3 domain[23, 100]. In conjunction, we cloned a series of anti-apoptotic proteins including Bcl-2, Bcl-W, Bcl-X_L and Mcl-1, each fused to the T7 $RNAP_C$ tag, into an arabinose-inducible vector. To monitor *in vivo* transcriptional output of the assembled T7 RNAP, we used a reporter vector that produces luciferase in response to transcription from the T7 promoter. Reporter *E. coli* cells were then cotransformed with the three vectors, induced with arabinose, and

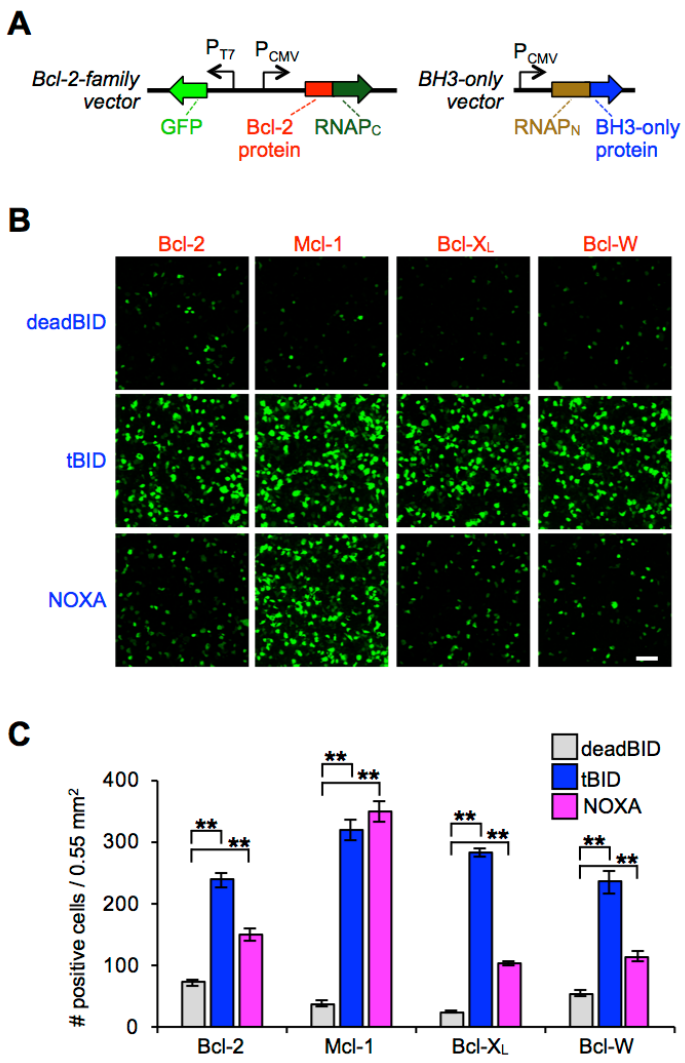

Figure 2.2. Split RNAP biosensors can detect Bcl-2 family PPIs in mammalian cells. (A) Vector system to test binary Bcl-2 split RNAP PPI detection system in mammalian cells using PPI driven GFP mRNA as the RNA output. (B) HEK293T cells cotransfected with the plasmids shown in (A). 30 h after transfection, the cells were analyzed for GFP expression by fluorescence microscopy. Interactions between tBID and Bcl-2, Mcl-1, Bcl-X_L, and Bcl-W, are readily detected compared to control, while NOXA is much more selective for interaction with Mcl-1. (C) Quantification of (B) (error bars are ± s.e.m, n = 5). Student's *t*-test; ** $P < 0.001$. 100 μm scale bar shown.

analyzed for luminescence output (Figure 2.1B). As expected, because all four Bcl-2-family proteins are known to interact with tBID[22], interactions of Bcl-2, Bcl-W, Bcl-X_L, and Mcl-1 with tBID each produced a robust enhancement of RNAP activity compared to the deadBID control, with between a 24-fold and 207-fold dynamic range (Figure 2.1C). More striking was that the NOXA-fused $RNAP_N$ only showed significant transcriptional output (34-fold) when combined with Mcl-1-fused $RNAP_C$, confirming NOXA selectively binds to Mcl-1 over the other anti-apoptotic proteins assayed[22, 101]. These experiments indicate that the split RNAP tags can reproduce known *in vitro* affinity measurements in live *E.*

coli with a robust RNA output signal.

Upon validating that the split RNAP tags can detect Bcl-2-family PPIs in *E. coli*, we sought to measure the performance of the system in a more physiologically relevant setting, mammalian HEK293T cells. We adapted the expression vectors for mammalian cell deployment by cloning a CMV-driven vector for each of the $RNAP_N$-tagged BH3-only protein fusions (Figure 2.2A). Next, we cloned a series of vectors that each featured a CMV-driven $RNAP_C$ tagged anti-apoptotic protein fusion, as well as a T7 promoter-driven GFP mRNA circuit[93, 102]. PPI-dependent RNAP assembly could therefore easily be measured by imaging GFP fluorescence, which is resultant from $RNAP_N$ and $RNAP_C$ reassembly, mRNA transcription, and GFP translation. Due to the signal amplification of this output, the data is qualitative, but the ease of analysis permits facile system optimization and validation. Cotransfection of any anti-apoptotic-$RNAP_C$ construct with the $RNAP_N$-deadBID vector resulted in cells with very low GFP fluorescence (Figure 2.2B, C). However, cotransfection of $RNAP_N$-tBID with each Bcl-2 family $RNAP_C$ fusion resulted in a dramatic enhancement of GFP fluorescence. Similar to the results in *E. coli*, and as expected based on *in vitro* measurements, $RNAP_N$-NOXA only induced robust GFP fluorescence when cotransfected with Mcl-1-$RNAP_C$ (Figure 2.2B, C). These imaging experiments indicate that the split RNAP tags are capable of measuring binary PPIs between Bcl-2-family proteins in mammalian cells.

Once we validated that split RNAP tags could measure single binary PPIs in mammalian cells, we sought to test whether we could detect two competing PPIs simultaneously. The goal would be to allow one BH3-only protein to interact with two different anti-apoptotic proteins in the same cell, such that each interacting pair drives a

different RNA output. Previously, we utilized an orthogonal $RNAP_C$[84], $RNAP_C$(CGG), that selectively transcribes from the "CGG" promoter upon assembly with the $RNAP_N$. In order to deploy this orthogonal system in conjunction with the T7-based system, we cloned a mammalian expression vector that produces Mcl-1-$RNAP_C$(CGG) and RFP expression via the CGG promoter. We first deployed this other reporter vector system with the Bcl-2-$RNAP_C$(T7) reporter and each of the $RNAP_N$-BH3-only proteins by cotransfecting cells with all three vectors and measuring GFP and RFP fluorescence (Figure 2.3A). This way, the interaction between the BH3-only protein and Bcl-2 would produce GFP fluorescence, while the interaction between the BH3-only protein and Mcl-1 would produce RFP fluorescence. Cells with $RNAP_N$-deadBID displayed low fluorescence in both channels, as expected (Figure 2.3B, C). However, $RNAP_N$-tBID produced robust fluorescent signal in both the RFP and GFP channels. Moreover, $RNAP_N$-NOXA produced more RFP than GFP fluorescence, recapitulating the *in vitro* and *E. coli* measurements in live mammalian cells. Intriguingly, in this competitive experiment tBID gave less signal than NOXA with Mcl-1, which is not what was observed in the individual PPI assays (Figure 2.2). This type of competitive binding effect can only be observed by monitoring multiple PPIs simultaneously. These results confirm that two PPIs can be monitored simultaneously in mammalian cells using this set of orthogonal split RNAP tags.

With the system to simultaneously measure two competitive PPIs in hand, we next sought to detect pharmacological engagement of PPI inhibitors in live cells. We tested the recently FDA approved Bcl-2 inhibitor ABT-199[26, 103] (Venetoclax) and the preclinical Mcl-1 inhibitor A-1210447[104] (A121). Treatment with ABT-199 blocked the

interaction between Bcl-2 and tBID (Figure 2.4A, B), while treatment with A-1210477 blocked the interaction between Mcl-1 and tBID. Coadministration of both inhibitors in a combination therapy experiment blocked both PPIs, though the level of Mcl-1 inhibition was less than in the single treatment conditions.

Intriguingly, the measured signal between Mcl-1 and tBID in the presence of competition with either Bcl-2 or Bcl-X_L was lower than when measured as a single binary interaction without competition (Figure 2.3 vs Figure 2.2). This is in-principle expected, because Mcl-1 is a roughly equal (Bcl-2) or lower (Bcl-X_L) affinity binder to tBID[22], and suggests that our dual-monitoring approach can recapitulate endogenous competitive interactions. Moreover, coadministration of both an Mcl-1 and Bcl-2 inhibitor in the competitive environment caused the Mcl-1 inhibitor to be less effective (Figure

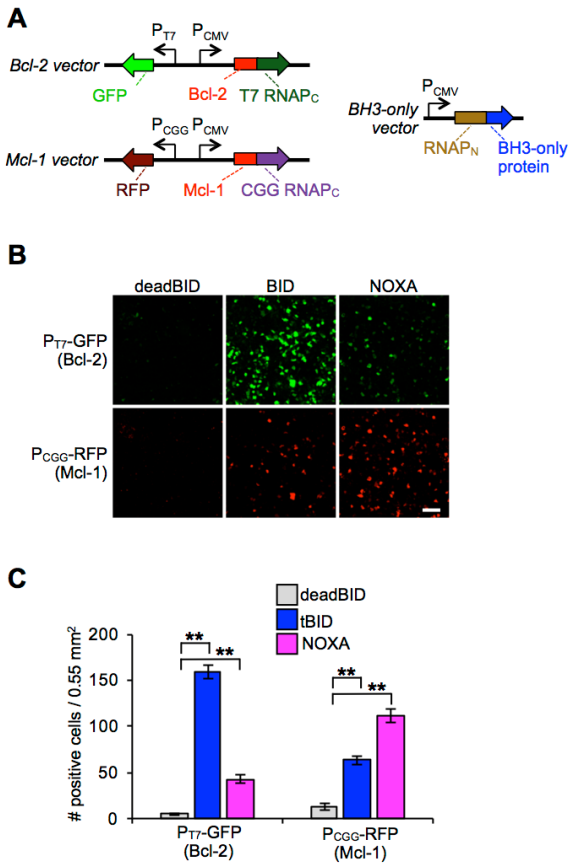

Figure 2.3. Split RNAP biosensors can monitor two Bcl-2 family PPIs simultaneously in mammalian cells. (A) Vector system to simultaneously monitor competitive interactions between Bcl-2 and Mcl-1 with BH3-only proteins in mammalian cells using mRNA for GFP and RFP as the two orthogonal RNA outputs from each PPI. (B) HEK293T cells cotransfected with the plasmids shown in (A). 30 h after transfection, the cells were analyzed for GFP and RFP expression by fluorescence microscopy. Bcl-2 and Mcl-1 were both found to interact with tBID, while NOXA was found to interact more with Mcl-1. (C) Quantification of (B) (error bars are ± s.e.m, n = 5). Student's *t*-test; $^{**}P < 0.001$. 100 μm scale bar shown.

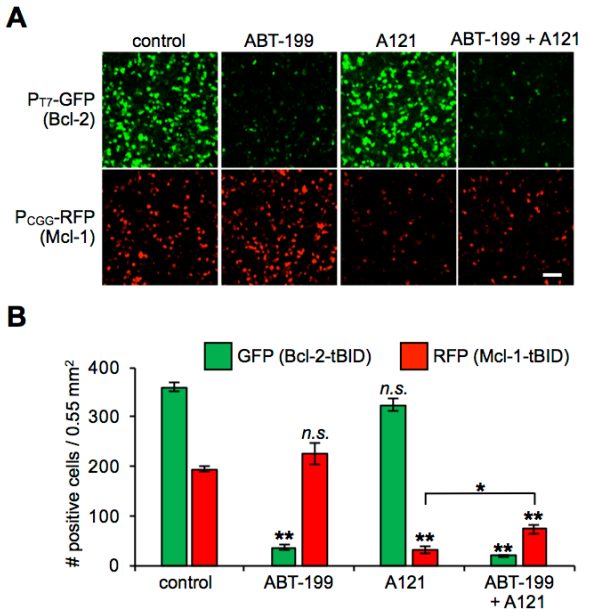

Figure 2.4. Spit RNAP biosensors can simultaneously monitor pharmacological engagement of two PPIs in live cells. (A) HEK293T cells cotransfected with the plasmids shown in Figure 2.3A. Upon transfection, DMSO carrier control, 0.5 μM ABT-199, 10 μM A1210477, or a combination of both 0.5 μM ABT-199 and 10 μM A1210447 were added to the cells. After 30 h, the cells were analyzed for GFP and RFP expression by fluorescence microscopy. (B) Quantification of (A) (error bars are ± s.e.m, n = 5). Student's *t*-test; $^{*}P < 0.01$, $^{**}P < 0.001$ (relative to control when not otherwise indicated). n.s. = not significant. 100 μm scale bar shown.

2.4B), presumably because more tBID was accessible in the system when not bound to Bcl-2 and may reflect differences in affinity between NOXA and tBID[105], or differences in pharmacological effectiveness.

Collectively, these data illustrate why multidimensional PPI analysis in live cells is critical

for understanding pharmacological engagement of competitively-interacting PPI networks.

Unlike fluorescent reporters, RNAP-based reporter systems are not limited by spectral overlap, and should therefore be capable of measuring higher-order PPI networks. In our spit RNAP system, orthogonality comes from the $RNAP_C$ tags that each drive transcription from unique DNA promoters upon RNAP assembly, thereby permitting the transcription of unique output RNA signals. Thus far, only T7 and CGG $RNAP_C$ tags have been developed as proximity-dependent split RNAP reporters. Therefore, we next sought to expand the approach by generating a panel of orthogonal tags for deployment in PPI network analysis experiments.

We mined the literature for mutations within our $RNAP_C$ tags that alter its DNA promoter specificity[106, 107], and cloned these variants into our *E. coli* luciferase reporter system to assay their ability to function as proximity-dependent split RNAP reporters. First, we tested orthogonality by measuring a series of eight putative $RNAP_C$ variants on a panel of five different DNA promoters, T7, CGG, K1F, CTGA, and T3. All of the variants displayed robust activity on their target promoter, but the variants differed in terms of overall activity and off-target activity on the other promoters (Figure 2.5A, B). Based on overall activity and selectivity, we selected T7, K1F-b, CTGA, and T3 $RNAP_C$ variants, along with their respective promoter sequences, as a series of four orthogonal $RNAP_C$ tags to pursue further. We omitted the CGG variant used in the one-by-two interaction analysis because it showed crosstalk with both the CTGA and T3 promoters. Critically, all of the variants, especially those selected for further study, maintained very good dynamic range for PPI detection when paired with the evolved $RNAP_N$ and split

isoleucine zipper peptides used previously[84, 108], displaying a 134-fold to 300-fold dynamic range (Figure 2.5C).

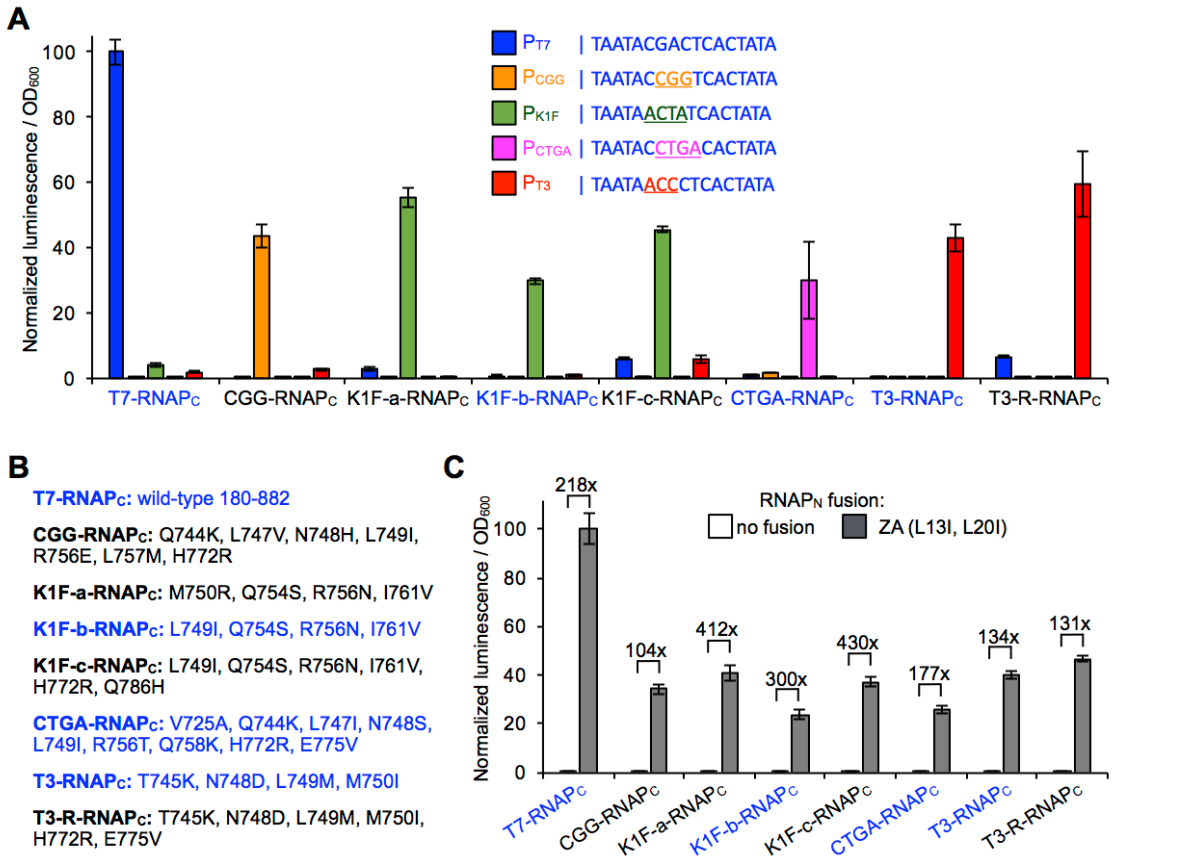

Figure 2.5. Uncovering a series of orthogonal proximity-dependent C-terminal split RNAPs. (A) *E. coli* transcriptional reporter assay for DNA promoter orthogonality of a series of split C-terminal T7 RNAP variants fused to ZB (ZB-RNAP$_C$) on putative DNA promoter sequences. Sequences for the five target DNA promoters are shown (T7-blue, CGG-orange, K1F-green, CTGA-magenta, T3-red). *E. coli* transformed with the vector system shown in Figure 2.1B: 1) an expression vector for an evolved N-terminal RNAP fused to ZA (RNAP$_N$-ZA), 2) an expression vector for a target RNAP$_C$ variant to be tested, and 3) a reporter vector that drives luciferase based on a target DNA promoter sequence. Cells were induced for 3 h with arabinose and then analyzed for luminescence. Error bars are ± s.e.m., n = 4. (B) Mutations shown for each RNAP$_C$ variant tested. (C) Proximity-dependent assembly of the series of ZB-RNAP$_C$ variants. *E. coli* transformed with the vector system shown in Figure 2.1B: 1) an expression vector for RNAP$_N$ fused to either nothing as a negative control or to ZA, 2) an expression vector for a target RNAP$_C$ variant to be tested, fused to ZB, and 3) a reporter vector that drives luciferase based on the target DNA promoter sequence of the variant being tested. Cells were induced for 3 h with arabinose and then analyzed for luminescence. Error bars are ± s.e.m., n = 4. The variants that were selected for further study are color-coded in blue.

With the four orthogonal $RNAP_C$ variants and four orthogonal promoters validated, we next sought to test whether we could monitor four Bcl-2 family PPIs simultaneously in mammalian cells. We envisioned a system in which one vector would express a target binding partner fused to $RNAP_N$, and a series of four other vectors would each express different protein targets fused to the four orthogonal $RNAP_C$ variants (T7, K1F-b, CTGA, and T3) (Figure 2.6A). The $RNAP_C$ expression vectors would also each contain gene circuits that drive transcription of unique RNA outputs from the four orthogonal promoters, thereby "encoding" each PPI in a separate RNA signal (Figure 2.6B).

To test the feasibility of a 1x4 interactome analysis with the split RNAP system, we cloned the orthogonal $RNAP_C$ variants into each of the Bcl-2 fusion vectors and swapped out the T7 promoter for the corresponding orthogonal promoter sequence matching each $RNAP_C$ variant. Rather than attempting to use four orthogonal fluorescent proteins, we aimed instead to measure each split RNAP assembly by direct quantitative RNA analysis. Aside from opening up future possibilities of doing even higher-order interaction analysis where spectral overlap of fluorescent proteins becomes prohibitive, we postulated that analyzing the RNA directly would also offer kinetic advantages and a more quantitative assay. Degradation of most fluorescent proteins is quite slow[100], meaning that even once we inhibit a PPI, the time it takes for that inhibition to change the intracellular fluorescent protein concentration is long. However, RNA turnover is much faster, meaning we should be able to detect inhibition of a target PPI in a more dynamic manner. To enable this approach, we then changed the RNA output on each orthogonal $RNAP_C$ fusion vector to a unique, arbitrary

sequence, and designed corresponding unique qPCR primers to analyze each output RNA. It should be noted that due to differences in primer efficiencies and promoter strengths, differences in outputs can only be measured in a relative manner between different conditions.

We transfected the set of 1x4 interactome vectors into HEK293T cells, allowed the cells to grow for 40 h, isolated total RNA from the cells, and then analyzed each unique PPI-dependent RNA output signal by quantitative reverse transcription PCR (RT-qPCR). First, we assayed whether we could recapitulate the deadBID, tBID, and NOXA binding interactions. As observed in the binary PPI analysis, we detected increased RNA production between all four Bcl-2 family proteins when the $RNAP_N$ was fused to tBID compared to dBID, but the NOXA fusion only showed enhanced RNA synthesis from the Mcl-1 fusion (Figure 2.7A). Furthermore, we again observed increased signal from the NOXA-Mcl-1 interactions compared to the tBID-Mcl-1 interactions in this competitive environment. Next, we assayed whether we could monitor competitive inhibition upon ABT-199 treatment in the context of tBID binding. We delivered the 1x4 interactome vectors using the $RNAP_N$-tBID binding partner and tested whether loading the cells with ABT-199 for 3 h, 24 h, or 40 h resulted in measurable PPI inhibition, and which PPIs were affected. We observed selective Bcl-2/tBID PPI inhibition at 3 h with enhanced inhibition at 24 h. At 3 h, we detected no other off-target inhibition. However, we observed Bcl-X_L/tBID PPI inhibition at the longer, 24 h, time point. This off-target activity has not previously been observed at the concentration used[26], but has been noted at higher concentrations. Because the kinetics of the inhibition differ between targets, this off-target effect could be due to pharmacological cross-talk, or biological

effects such as changes in endogenous Bcl-2-family binding partner levels. Collectively,

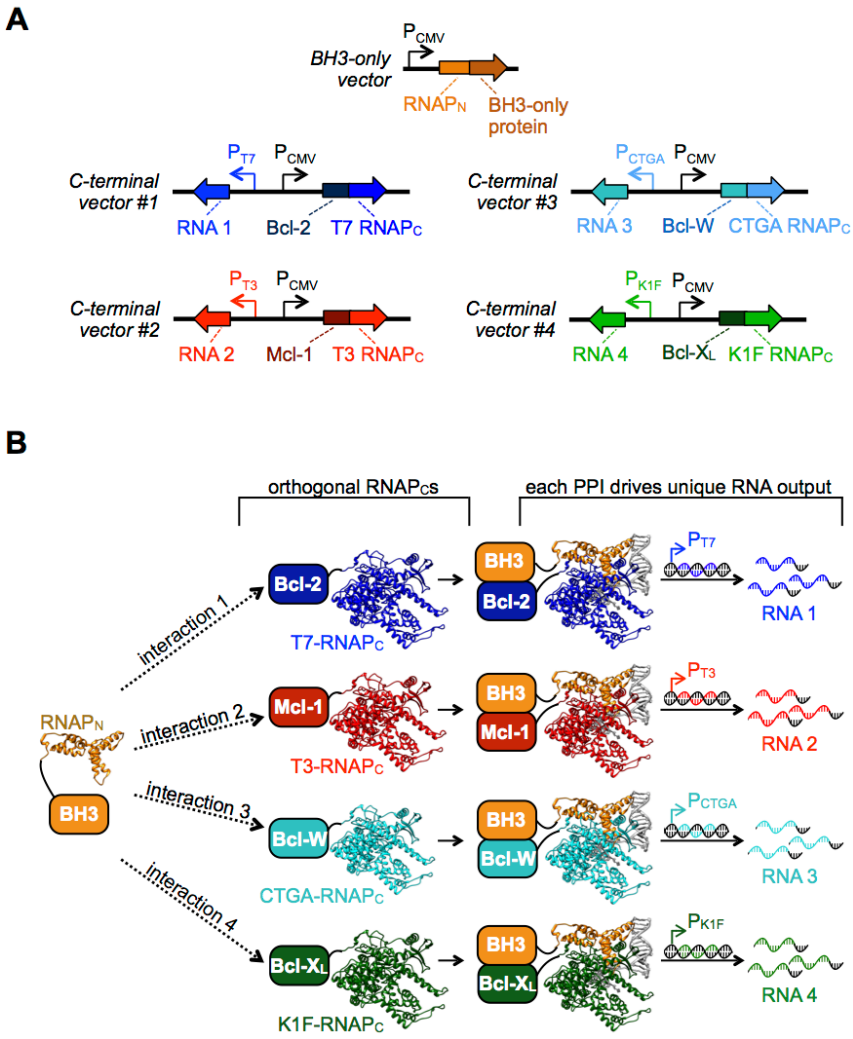

Figure 2.6. Schematic of a system to detect 4 multidimensional PPIs simultaneously. (A) Design of mammalian vector system to measure a one-by-four PPI network. Expression vectors for a series of anti-apoptotic-RNAP$_C$ using the orthogonal RNAP$_C$ variants developed in Figure 2.5 were engineered with a gene circuit that produces an orthogonal RNA output signal from transcription on the orthogonal DNA promoter. Four orthogonal vectors were created, which can then be deployed along with a BH3-only-RNAP$_N$ expression vector. (B) Schematic of one-by-four RNAP tagging system for multidimensional PPI analysis. The BH3-only peptide fusion on the RNAP$_N$ tag can competitively bind to a series of Bcl-2-family proteins, each themselves fused to orthogonal RNAP$_C$ tags. Interactions between each Bcl-2-family protein with the target results in the assembly of an orthogonal RNAP, which in turn transcribes an output RNA signal from an orthogonal DNA promoter. The relative amount of each PPI can be measured by RT-qPCR analysis of the output RNA signals.

these experiments indicate that the split RNAP PPI detection system can

simultaneously monitor four PPIs in mammalian cells and detect competitive PPI inhibition on relatively short time scales using RNA analysis techniques.

2.3 Conclusion

In conclusion, we developed and validated a series of split RNAP biosensors to monitor multidimensional PPI networks in live mammalian cells. Measuring endogenous biomolecular interactions in mammalian systems remains a substantial challenge, but an increasingly important problem as PPI modulators continue to gain momentum in the laboratory and clinic. The split RNAP biosensor approach described here can synergize with advances in nucleic acid sequencing technologies, by encoding new types of biological information in the high-throughput sequencing (HTS) data flow. Coupling the tools disclosed here with cell identifying bar-coding sequences in the RNA outputs or with direct *in situ* RNA sequencing technologies[86] would permit single-cell analysis of multidimensional PPI networks. By leveraging advances in nucleic acid computation[109, 110], the RNA outputs of the split RNAP sensors could be adapted for complex genetic screens, in which a series of interactions in a network are screened in parallel for specific effects. The RNA outputs could easily be engineered to mediate cell viability, leading to a very simple and inexpensive mammalian genetic screening platform. Moreover, proteins of interest could be genomically-tagged, improving physiological relevance and single-cell consistency. This would also allow even higher-order networks to be probed and screened for. Although we found that transient transfection worked well for the experiments presented here, removing the complications due to heterogeneity in transfection efficiency will likely decrease variability and sensitivity to

subtle effects. Finally, for synthetic biology applications, multiple split RNAP biosensors could analyze individual cells' interactomes to determine cell type or disease state and drive a therapeutic outcome, as has been done for microRNA detection systems[111].

We selected Bcl-2 family PPIs as a test bed to develop our split RNAP biosensor technology due to the availability of known small molecule inhibitors, which provided us with robust positive controls. Our observations of competitive effects of PPIs for the same target ligand upon pharmacological engagement of the Bcl-2 proteins is an excellent illustration as to why targeting PPIs therapeutically is so challenging. In future work, we will explore whether other therapeutically-relevant PPIs with known off-targets can also be assayed in our system. Integrating our rapid endogenous multidimensional PPI analysis approaches in the drug discovery process could substantially benefit the selection of pre-clinical molecules for both *in cellulo* efficacy and off-target interactions, thereby improving the drug discovery pipeline. Moreover, rather than measuring secondary treatment effects, direct PPI disruption measurements can be used to validate mechanisms of new therapeutic agents to gain enhanced understanding of targeted therapies prior to further preclinical development.

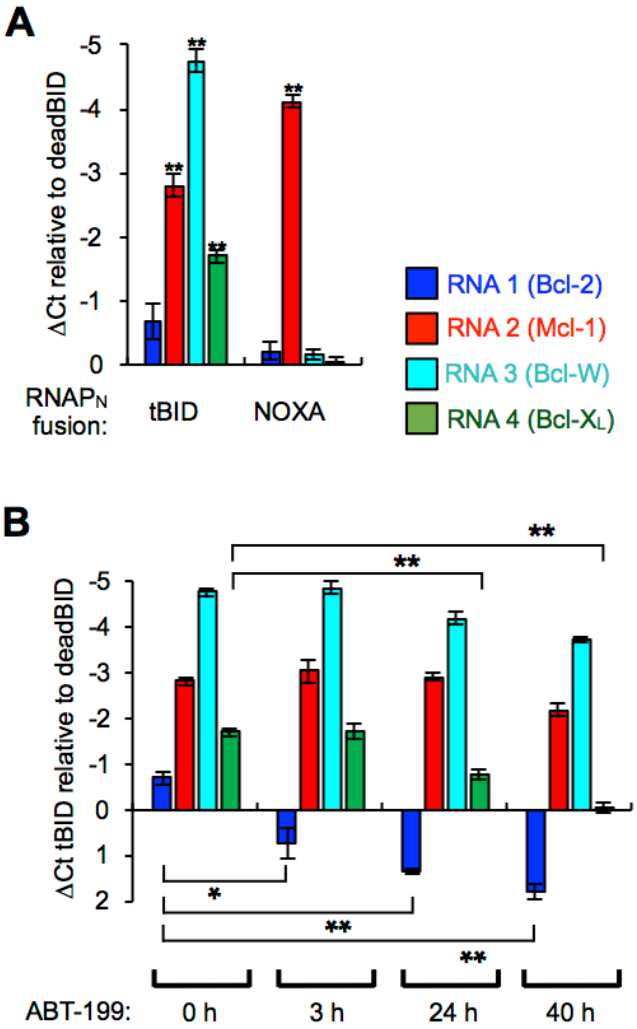

Figure 2.7. Detection of 1x4 Bcl-2 family PPIs simultaneously in mammalian cells by RT-qPCR analysis of the unique RNA outputs. (A) HEK293T cells were cotransfected with the plasmids shown in Figure 2.6A with the fusions indicated, grown for 40 h, lysed, and then total RNA was isolated and quantified by RT-qPCR. Separate PCR primers were used for each of the four unique RNA outputs to measure split RNAP assembly with each target. The data displayed is the delta-Ct value in comparison to cells transfected with the RNAP$_N$-deadBID "negative control". Therefore, a more negative value indicates more of a particular RNA is generated, and therefore more of a given interaction was present. (B) HEK293T cells were cotransfected with the plasmids shown in (Figure 2.6A) with the tBID-RNAP$_N$ fusion, grown for 40 h with 0.5 μM ABT-199 added at different time points, lysed, and then total RNA was isolated and quantified by RT-qPCR as described in (A). The data displayed is the delta-Ct value in comparison to cells transfected with the RNAP$_N$-deadBID "negative control". Error bars are ± s.e.m., n = 4. Student's *t*-test; **P* < 0.05, ***P* < 0.0005.

2.4 Experimental Details

Cloning. All plasmids were constructed by Gibson Assembly[112] from PCR products generated using Q5 DNA Polymerase (NEB) or Phusion Polymerase. All plasmids were sequenced at the University of Chicago Comprehensive Cancer Center DNA Sequencing and Genotyping Facility. Full vector sequences and annotated vector maps are available upon request.

Luciferase-based transcription assays of Bcl-2 proteins in *E. Coli*. Experiments were conducted as previously described[84]. Briefly, S1030 cells[113] were transformed by electroporation with three plasmids: (*i*) a T7 $RNAP_N$-linker-BH3 only expression plasmid, (*ii*) an Bcl-2 family protein-linker-T7 $RNAP_C$ expression plasmid, and (*iii*) a reporter plasmid that encodes luciferase under control of a T7 RNA polymerase promoter. Single colonies were then grown to saturation overnight at 37 °C, and then each well of a 96-well deep well plate containing 0.54 mL of LB with antibiotics and 10 mM arabinose was inoculated with 60 µL of the overnight culture. After growth with shaking at 37 °C for 3 h, 150 µL of each culture was transferred to a 96-well black wall, clear bottom plate (Nunc), and luminescence and OD_{600} was measured on a Synergy Neo2 Hybrid Multi-Mode Reader (BioTek). The data were analyzed by dividing the luminscence values by the background-corrected OD_{600} value, then subtracting out the background from the reporter vector alone. All values were then normalized to the transcription from Bcl-2/deadBID, which was assigned an arbitrary value of 1, allowing the values from each luminescence plot to be compared to one another.

Luciferase-based transcription assays of orthogonal C-terminal RNAP variants in *E. Coli*. Experiments were conducted as previously described[84] and similar to as noted

above. Briefly, S1030 cells[113] were transformed by electroporation with three plasmids: (*i*) a T7 $RNAP_N$-linker-ZA expression plasmid, (*ii*) a ZB-linker-$RNAP_C$ expression plasmid with the listed mutations, and (*iii*) a reporter plasmid that encodes luciferase under control of a given target promoter sequence. Single colonies were then analyzed as described above. The data were analyzed by dividing the luminescence values by the background-corrected OD_{600} value, then subtracting out the background from the reporter vector alone. The experiment was then repeated, but this time only assaying each variant on its target promoter and assessing proximity-dependence by comparing assembly with $RNAP_N$-linker-ZA with a plasmid that has no ZA fusion. For both experiments, values were then normalized to the transcription from the T7 $RNAP_C$ on the T7 promoter, which was assigned an arbitrary value of 100. Each variant was screened across all five promoters in this way.

Cell culture. HEK293T cells (ATCC) were maintained in DMEM (high glucose, L-glutamine, phenol red, sodium pyruvate; obtained from Gibco or Hyclone) supplemented with 10% fetal bovine serum (FBS, Gibco/Life Technologies, Qualified US origin) and 1% penecillin/streptomycin (P/S, Gibco/Life Technologies). Multiple biological replicates were performed with cells from different passages and freshly thawed aliquots.

Mammalian fluorescence imaging and inhibitor assay. HEK293T cells were cultured in DMEM (high glucose, glutamine, phenol red, pyruvate; Gibco/Life Technologies) supplemented with 10% fetal bovine serum (FBS, Gibco/Life Technologies, Qualified US origin). The cells were plated on an 8-well coverglass slide (Labtek) and transfected in the next day with 300 ng of Bcl2-family vector and 300 ng of

a BH3-only vector using 1.8 μL of Lipofectamine 3000 (ThermoFisher Scientific) following the standard protocol. For the inhibitor experiments, 500 nM ABT-199, 10 μM A-1210477, or DMSO control was added during cell culture and post transfection. The cells were imaged on an Olympus BX53 microscope using a GFP and RFP filter set and a 10x objective.

Image processing and quantification. For image analysis of fluorescent protein outputs, we counted the number of positive cells in each channel. Each image for a given condition was processed using identical conditions to adjust brightness and contrast to a level where background fluorescence was observed for control samples in ImageJ (Wayne Rasband, NIH). The fluorescent spots in each GFP image were counted as fluorescent cell number in ImageJ for quantification analysis. A macro batch script for each analysis was used to ensure the settings for each group were identical. The following script was used in the “Batch Process” of ImageJ: “setThreshold(239, 5000); setOption("BlackBackground", false); run("Convert to Mask"); run("Watershed"); run("Analyze Particles...", "size=100-Infinity pixel include summarize in_situ" “. The “Count” results were then used for quantification analysis. We found that counting the number of GFP-positive cells yielded the most reproducible results.

RT-qPCR analysis. HEK293T cells were transfected with split RNAP vectors. 400 ng for each of the five plasmids showed in Fig. 6A. 6 μL of Lipofectamine 3000 (ThermoFisher Scientific) was used for the transfection in 12-well plates (Corning) and biological replicates were performed in quadruplicate for each condition. The inhibitor ABT-199 was omitted, added during transfection, or added 16 h or 37 h after transfection, and the cells were harvested at 40h after transfection. RNA was purified

using an RNeasy Kit (Qiagen) and was reverse-transcribed using PrimeScript TM RT reagent Kit (TaKaRa). The transcribed cDNA was used as the qPCR template and the PCR reactions were performed on a LightCycler 96 Instrument (Roche) using FastStart Essential DNA Green Master (Roche).

CHAPTER 3

SPLIT T7 RNA POLYMERASE BIOSENSORS TO STUDY MULTIPROTEIN INTERACTION DYNAMICS: A PRACTICAL GUIDE

3.1 Introduction

Protein-protein interactions (PPIs) are involved in nearly all cellular processes, particularly in higher organisms. For example, although there are only approximately 21,000 protein coding genes in the human genome there are an estimated 650,000 unique PPIs, ranging from simple binary interactions to multiprotein complexes [16]. These interactions regulate information flow through the central dogma, cell signaling, metabolic processes, and more [114-116]. As the PPI estimation implies, individual proteins can take part in any number of distinct PPIs, with each one potentially involved in a different cellular process. Therefore, traditional methods for studying protein function, e.g., protein overexpression and knockdown, can impact several pathways simultaneously, convoluting experimental results. There are numerous instances where genetic aberrations cause human disease via PPI dysregulation or can be alleviated by manipulating selective PPIs [117, 118]. This central role of PPIs has led researchers to develop tools to study natural PPIs, and even to manipulate biology via synthetic PPI signaling [119].

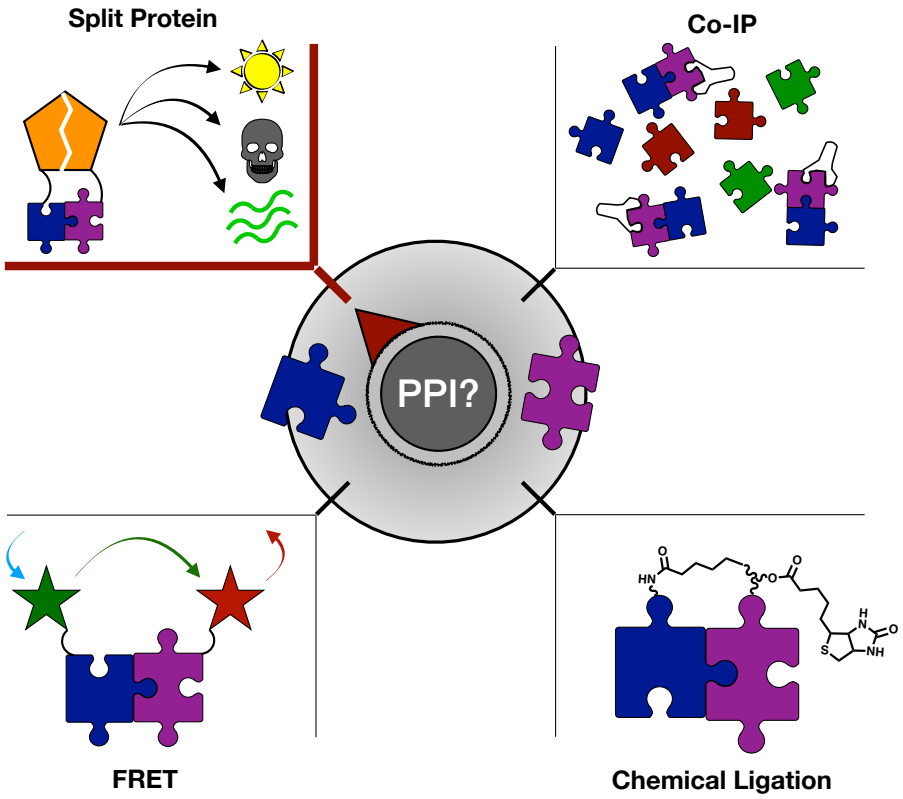

Figure 3.1. Schematic of several common methods for detecting PPIs. This chapter focuses on the split T7 RNAP, and so split proteins, which can produce diverse signals such as light, cytotoxic small molecules, or RNA, are highlighted.

A variety of methods have been developed to study PPIs, ranging from fixed-cell antibody-based endogenous coimmunohistology to live-cell FRET-based kinase sensors (Figure 3.1) [120, 121]. In this chapter, we will focus on measuring PPIs in live cells. In the context of live-cell PPI detection, protein fragment complementation (PFC) is one of the most widely-used and powerful approaches [122]. PFC assays work by splitting a reporter protein (GFP, luciferase, etc.) and genetically tagging each split protein fragment to different proteins of interest. Only when the tagged proteins come within close proximity to one another does the split reporter reassemble to produce an output signal. Indeed, this approach has been widely used with light-emitting reporters,

including GFP and luciferase, to study and discover chemical inhibitors of PPIs [80, 123-125]. More recently developed PFCs such as split horseradish peroxidase and split BS2 esterase convert PPIs into activation of chemical probes that release light, kill surrounding cells, or label surrounding proteins with chemical tags [75, 79]. While these aforementioned PFC tools are powerful for measuring a single PPI, they are often unable to measure or discern signals from multiple simultaneous interactions, largely due to a lack of orthogonal split components, or spectral overlap in output signals. Split RNAP-based biosensors, however, benefit from the vast information storage capacity of RNA to in principle encode an array of molecular interactions for subsequent multiplexed analysis. This chapter will therefore describe the evolved split T7 RNA polymerase (RNAP) as a novel PFC capable of converting multiple PPIs into unique RNA outputs simultaneously in live cells. This chapter represents an in-depth practical guide to deploying the split RNAP in various contexts, expanding on the research discussed in chapter 2.

3.2 Evolution of the split T7 RNA polymerase biosensor

3.2.1 Split T7 RNAP biosensor history and nomenclature

In 1985[126] it was discovered that the T7 RNAP, a single-domain, highly active, RNAP retained its transcriptional activity upon proteolysis into two fragments. Much later, Shis et al. confirmed the two fragments could reassemble when coexpressed [127]. In 2014 Segal-Shapiro et al. discovered that there are in fact multiple locations in T7 RNAP that are amenable to splitting and reassembly to produce a fully functional RNAP [107]. One split site at amino acid position 181 produced particularly robust signal when

the N-terminal half of the RNAP (aa's 1-180; wt$RNAP_N$) was co-expressed with the C-terminal half of the RNAP (aa's 181-883; $RNAP_C$), which contains the protein domain that recognizes the DNA promoter sequence. This group went on to introduce known amino acid mutations into this promoter recognition domain, generating a series of unique $RNAP_C$'s that recognize orthogonal DNA promoters. For example, the wild type $RNAP_C$ recognizes the T7 DNA promoter, and is termed the T7-$RNAP_C$, but an $RNAP_C$ mutant only recognizes the orthogonal CGG DNA promoter (CGG-$RNAP_C$).

The Voigt group also discovered that RNA output in *e. coli* increased 5-7 fold over that of background assembly when positive interacting proteins were fused to each half of the RNAP. This foundational work inspired our group to evolve the split $RNAP_N$ to reassemble with any $RNAP_C$ *only* when interacting proteins are fused to each half (Figure 3.2.a). In brief, we used a new modified Phage-Assisted Continuous Evolution (PACE) system to evolve proximity-dependency in the split RNAP system, thereby making it into a biosensor platform. See the following reference for an in depth look at the evolution in *e. coli* and initial characterization of the evolved $RNAP_N$ ($eRNAP_N$) in both mammalian and *e. coli* cells, as well as our recent review that compares the split T7 RNAP biosensor to other PFC technologies [84, 122].

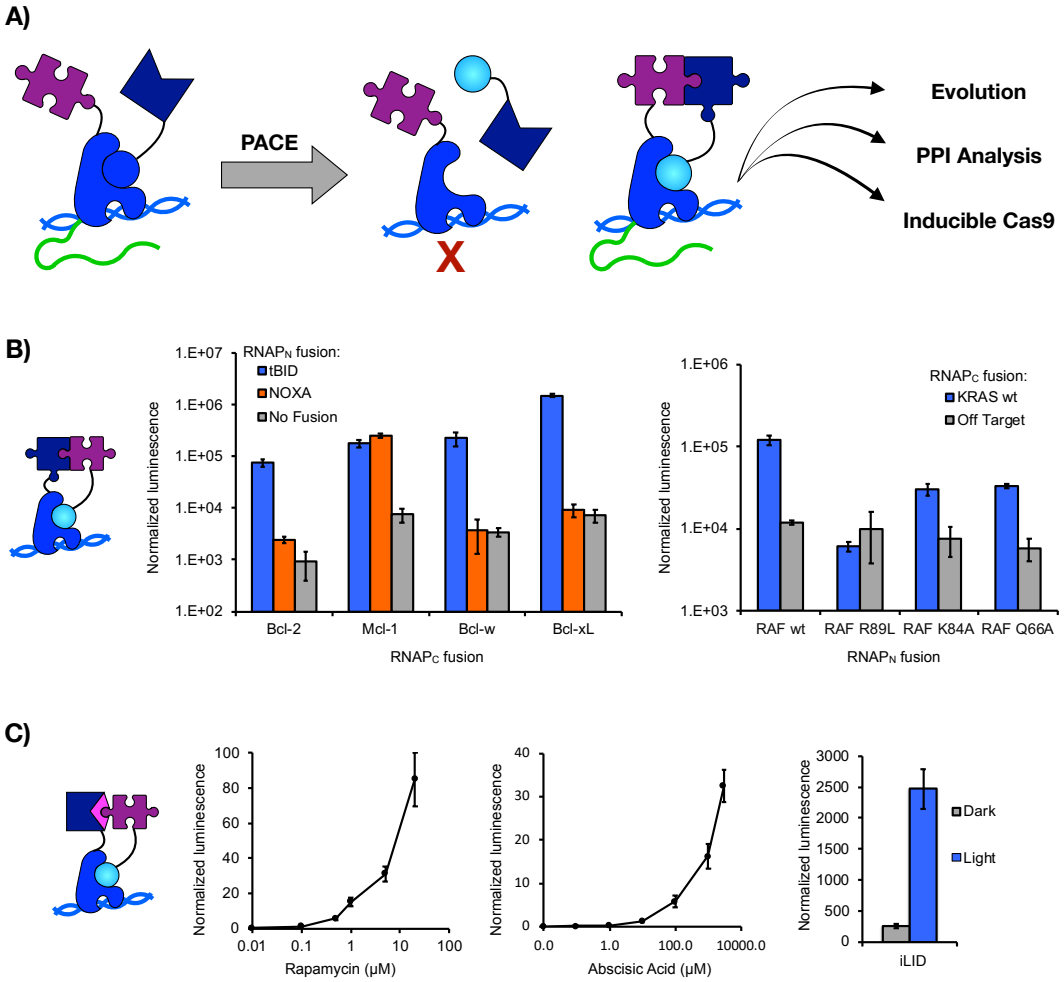

Figure 3.2. Example interactions detected via the evolved split RNAP biosensor. A) representation of the split T7 RNAP's PPI detection properties prior to and after evolution of the $RNAP_N$. The wild type $RNAP_N$ will assemble even without interacting fusion proteins (left), whereas the evolved $RNAP_N$ only assembles when interacting proteins are fused to each fragment (middle). B) *e. coli* luciferase assay results with Bcl-2 family (left) and KRas-Raf (right) interactions. C) *e. coli* luciferase assay results with the small molecule and light inducible PPIs FRB-FKBP (left), PYL-ABI (middle), and iLID (right).

3.2.2 eRNAP: applications and advances

Overall, evolution of the split RNAP increased the signal-to-noise ratio from 5-fold to 300-fold over background in *e. coli*. The evolved split RNAP not only provided robust signal-to-noise (Figure 3.2.b), but also tolerated fusion to interacting proteins with diverse structures and activities including short helix proteins, globular proteins, and

even activity-dependent PPIs that require small molecules or light to induce binding (Figure 3.2.c). We have recently used our evolved RNAP in two general ways: to study PPIs and for synthetic biology applications. For our usage in evolution and small molecule-induced Cas9 gene circuits, see the following references; [84, 128, 129]. Recently, our group employed the RNAP biosensor in two contexts. First, to rapidly screen thousands of amino acid mutations across a PPI interface and assess their effects on protein binding [130]. In this work, we used Darwinian evolutionary principles combined with high throughput sequencing to perform a deep mutational scan of the Ras/Raf binding interface. Second, we used the RNAP biosensor to perform numerous evolutions of modern and ancestral sequences of Bcl-2 family proteins, enabling the calculation of chance versus contingency in PPI evolution.[131]

In this chapter we will focus on our work using the RNAP biosensor in live mammalian cells to monitor up to four PPIs simultaneously, and to interrogate pharmacological inhibition of the competitive PPI network [132]. Along with these major advances, this technology is still undergoing development and characterization, and so nuances regarding its mechanism, advantages, and disadvantages remain open to exploration. Notably, however, our group's recent and ongoing work has identified several key factors to consider when designing an experiment utilizing the evolved split RNAP.

3.2.3 Considerations when using the split RNAP

One major consideration whenever deploying the split RNAP biosensor is its access to a DNA template. In eukaryotic cells, DNA is separated from most proteins by

lipid barriers that form the nucleus and other organelles. These physical barriers prevent the split RNAP from binding to its DNA promoter and subsequently transcribing an RNA signal. This is not usually a consideration when working with *e. coli* because they do not sequester DNA within compartments. Two notable exceptions are when investigating PPIs in the periplasm or extracellular space where DNA is inaccessible. Access to DNA is, however, a more pressing consideration when deploying this biosensor in mammalian cells, where many PPIs are localized within organelles that do not contain DNA, e.g., the Golgi or endoplasmic reticulum. Similarly, studying PPIs in the extracellular space and outer plasma membrane via the split RNAP is unlikely given that high concentrations of extracellular nucleotide triphosphates (NTPs), which are necessary to transcribe RNA, are toxic to cells[133]. The nucleus is therefore an optimal compartment for RNAP deployment because access to both DNA and NTPs is of minimal concern. Looking towards other compartments, manipulation of mitochondrial DNA to encode RNAP promoters, or DNA delivery techniques to endosomes/lysosomes in theory could enable PPI analysis via split RNAPs in these compartments[134].

A second major consideration when using the RNAP biosensor is the requirement for protein fusion. The RNAP tolerates different types of protein fusions, as our previous work has demonstrated. Yet, initially the $RNAP_C$ could not accept a C-terminal fusion because the wt $RNAP_C$ C-terminus is necessary for RNA transcription. In recent work, we overcame this disadvantage by evolving the $RNAP_C$ C-terminus to tolerate a protein fusion while retaining transcriptional capability[129]. With this advance, both RNAP halves can now tolerate fusions to either termini, as long as the fusion proteins themselves drive reassembly of the RNAP. It is important to investigate

whether a new PPI of interest, therefore, can properly orient the RNAP fragments. In our experience, there is a higher probability that protein fusions will be successful in the split T7 RNAP system if the proteins of interest have been previously used in other similar technologies, such as split GFP or split luciferase assays. If there is no precedent for protein fusion, then we find that crystal structure-based modeling or biochemical assays that reveal the roles of N- or C-termini in protein function, folding, and binding can greatly increase success when using the split T7 RNAP biosensor.

A third major consideration when deploying the split RNAP biosensor is the degradation, stability, folding, and overall activity of the fusion proteins. A relatively insoluble or unstable protein of interest fused to the RNAP fragments may result in differential expression of the resultant fusion protein, and in turn alter RNAP reassembly. As with all protein fusion approaches, the potential context-dependencies in protein stability or RNAP activity thus affect comparisons between PPIs. One PPI may produce a greater RNA signal simply due to improved RNAP folding/stability/activity rather than increased strength or frequency of the PPI in question. For this reason, it is crucial to run appropriate control experiments, particularly when comparing unique protein fusions to one another, or when assaying PPIs under different experimental conditions.

When designing experiments using the RNAP it is important to assess all of these factors and how they may change under each experiment's unique conditions. To ensure that results specifically reflect changes in PPIs of interest, and not changes in RNAP, the correct controls are critical. In the protocol below, we use our previous study of multiprotein interaction networks in live mammalian cells to describe the general

workflow for designing a PPI detection experiment using proximity-dependent split RNAPs. Within this protocol we include troubleshooting tips and additional protocols for control experiments that are particularly useful when testing new protein fusions.

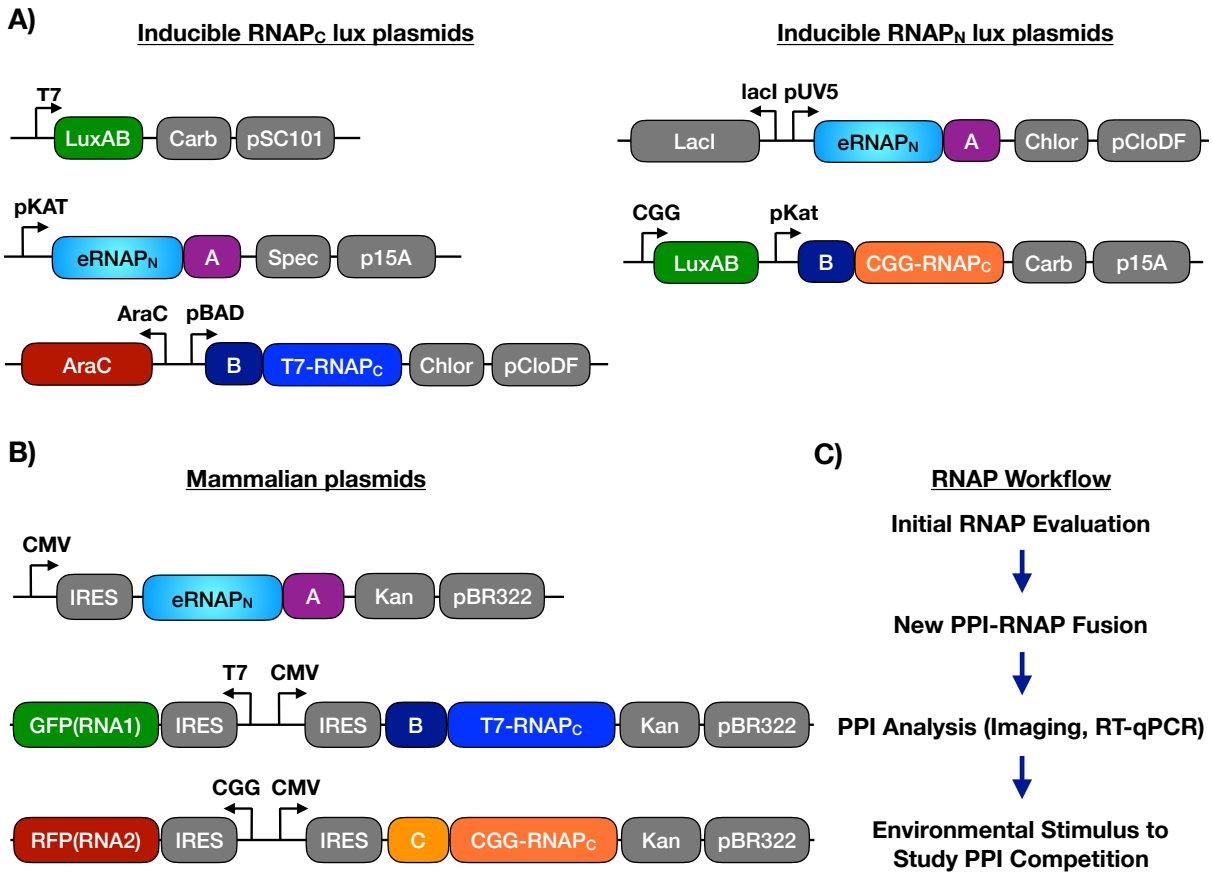

Figure 3.3. Plasmid designs for *e. coli* and mammalian assays and general workflow when using the split RNAP biosensor. Plasmid designs for measuring PPIs via bacterial luciferase in *e. coli* with arabinose induction of the RNAP$_C$ or IPTG induction of the RNAP$_N$. B) Mammalian expression plasmid designs for use in imaging and RT-qPCR analyses. C) General workflow when deploying RNAP biosensors to study proteins of interest. For more detailed assistance in designing experiments see “troubleshooting and advice” sections of each protocol.

3.3 RNAP analysis of Bcl-2 family PPIs

Many PPIs exist within networks that operate via selective interactions. Most methods only study these PPIs individually. However, crosstalk between PPIs is important to understand and quantify, particularly in the case of pharmacology. Bcl2 family proteins have been targeted by PPI inhibitors for cancer treatment, but resistance and off-target effects demand a holistic analysis of the Bcl-2 PPI-network. Three protocols below detail experiments to study: 1) individual PPIs in *e. coli* using bacterial luciferase, 2) two PPIs simultaneously with small molecule inhibition by fluorescence microscopy, and 3) four PPIs simultaneously with small molecule inhibition via RNA quantification. For protocols on basic techniques such as cloning, *e. coli* transformation, mammalian cell transfection, etc. see referenced materials in “precursor techniques” section below.

3.3.1 Materials, equipment and reagents

LightCycler 96 qPCR (Roche)

Synergy Neo2 Hybrid Multi-Mode Plate Reader (BioTek)

BX53 fluorescence microscope (Olympus)

Sterile Gard biosafety cabinet (Baker)

Cell culture incubator 5% CO_2 (Thermofisher Scientific)

NanoDrop 8000 (Thermofisher Scientific)

HEK293T mammalian cells (ATCC)

DMEM with high glucose, L-glutamine, phenol red, sodium pyruvate (Gibco or Hyclone)

Fetal Bovine Serum (Gibco)

Penecillin/streptomycin (Gibco/Life Technologies)

8-well cover glass slides (Labtek)

Lipofectamine 3000 (Thermofisher Scientific)

ImageJ image processing software (Wayne Rasband, NIH)

12-well plates (Corning)

RNeasy Kit (Qiagen)

PrimeScript TM RT reagent Kit (TaKaRa)

FastStart Essential DNA Green Master (Roche)

Opti-MEM I Reduced Serum Media (Thermofisher Scientific)

S1030 e. coli cells (Addgene)

96-well black wall clear bottom plate (Nunc)

Plasmids and sequence maps can be found on addgene

3.3.2 Protocols

3.3.2.1 Individual interactions in *E. Coli*

1. Transform 1030 *e. coli* cells [113] with 2-22 reporter plasmid, 8-1 $RNAP_N$-tBID expression plasmid, and 7-79 BclxL-T7-$RNAP_C$ expression plasmid OR 2-39 ZB-T7-$RNAP_C$ expression plasmid (links to electronic maps found in [132]). General plasmid design found in Figure 3.3.a. Grow cells on agar plates containing all four antibiotics (tet, carb, chlor, spec) and glucose (to repress $RNAP_C$ expression) for 14-18 hours at 37 degrees Celsius.
2. Grow four colonies of each plasmid combination in a 96 deep well plate until saturation (12-18 hours) in 1 mL of LB (miller) media containing all four antibiotics and glucose.

3. Transfer 60 µL of each saturated culture to 540 µL of LB (miller) media in a 96 deep well plate containing all four antibiotics and arabinose (to activate $RNAP_C$ expression).
4. After two hours (when cells are at ~0.2 optical density), and each hour thereafter, transfer 150 µL of culture to a clear bottom 96-well plate, and measure both absorbance at 600 nm to quantify *e. coli* optical density and luminescence output.
5. Analyze and normalize data using the following equation

$$\frac{lux_n - lux_0}{OD_n - OD_0}$$

Where lux_n is measured luminescence for a given sample, lux_0 is measured luminescence of LB media, OD_n is measured optical density for a given sample, and OD_0 is the optical density of LB media.

Troubleshooting and Advice –

Controls for split RNAP: *E. coli* lack many of the protein chaperones that mammalian cells rely on to properly fold newly-translated proteins. As a result, many mammalian proteins can be misfolded or aggregate in *e. coli*. If these misfolded proteins are fused to the RNAP they can interfere with, or completely eliminate, RNAP activity. Similarly, some proteins can cause the split RNAP to fold better, increasing its signal. The following control experiments are designed to test if a protein fusion changes RNAP activity.

Low Signal -

- Clone each protein of interest to the wild-type $RNAP_N$.
- Transform *e. coli* with the new $wtRNAP_N$ fusion protein or a no fusion $wtRNAP_N$ control, a T7-$RNAP_C$ control (no fusion or ZB fusion), and T7 promoted luciferase.
- Perform luciferase assay as described above.
- If no signal is observed compared to the control wild type split RNAP assembly then the $RNAP_N$ activity is disrupted by the protein fusion.
- If $wtRNAP_N$ signal is observed, clone the proteins of interest fused to T7-$RNAP_C$ and repeat experiment to assess if the protein of interest disrupts $RNAP_C$ activity.
- If signal is still observed with fusions to either RNAP half, but not when fused to test the proposed PPI itself, then the proteins do not interact with one another under these conditions.

High background -

- To test if a high signal is dependent on the PPI of interest and not enhanced RNAP folding or expression, perform the same troubleshooting as with “low signal” above, but fuse the proteins of interest to the $eRNAP_N$. Also, use the interaction between $eRNAP_N$ without a fusion protein and $RNAP_C$ as the background activity.

- If signal is observed above the no fusion eRNAP$_N$ control interaction then the protein of interest most likely alters RNAP$_N$ stability or expression. Simply normalize the PPI of interest's activity to this higher background for more accurate analysis.

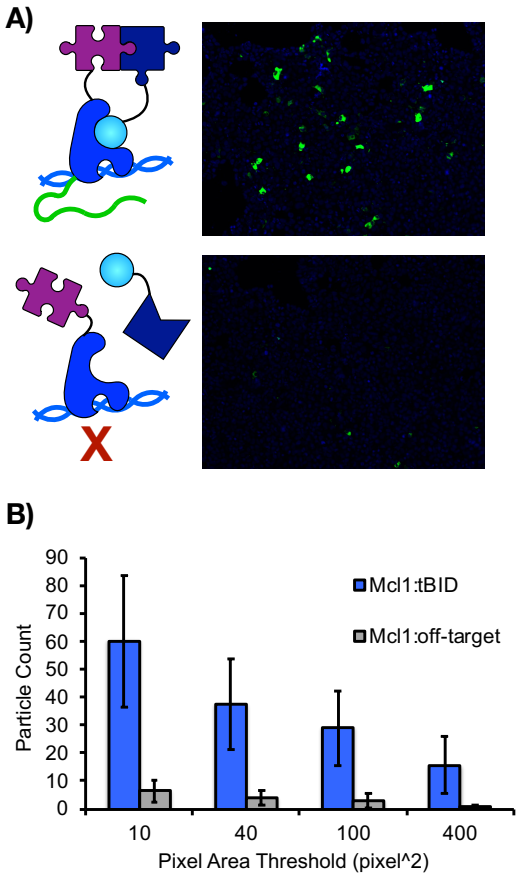

Figure 3.4. Mcl1-tBID PPI detection in mammalian cells using a fluorescent RNA aptamer output. A) Cells transfected with the RNAP$_N$ fused to either tBID (top image) or a truncated form of BID (bottom image), T7-RNAP$_C$ fused to Mcl1, and a T7 transcribed fluorescent RNA aptamer. An increased number of fluorescent cells was observed when positive interacting proteins were fused than non-interacting proteins. B) Graph demonstrating how analysis can vary if different pixel threshold values are used.

3.3.2.2 Imaging Multiple Interactions in Mammalian Cells

1. Culture HEK293T cells in triplicate for each PPI combination to 70-90% confluence in a 8-well cover glass slide dish with 250 µL antibiotic free DMEM

media, supplemented with 10% fetal bovine serum and either 500 nM ABT-199 or appropriate DMSO control.

2. Transfect each well with 300 ng of 9-49 $RNAP_N$-tBID OR 9-52 $RNAP_N$-DeadBID mammalian expression plasmid, 300 ng of 9-54 T7 promoted GFP and BclxL-T7-$RNAP_C$ expression plasmid, 9-53 CGG promoted RFP and Mcl1-CGG-$RNAP_C$ expression plasmid, and 2.4 microliters of lipofectamine 3000, while closely following the transfection protocol referenced in precursor techniques. See Figure 3.3.b for general mammalian plasmid designs.
3. After 24-36 hours wash cells with 250 µL PBS incubate each well with 1 µM DAPI in PBS for at least 30 minutes to stain cell nuclei.
4. Within two hours, using a fluorescence microscope with a 10x objective, take white light, DAPI filtered (461 nm emission), GFP filtered (509 nm emission), and RFP filtered (583 nm emission) images of three random locations for each well.
5. Analyze GFP and RFP images using the following FIJI (Fiji is just image J) macro. For basic instructions on using ImageJ and designing ImageJ macros see precursor techniques below. “setThreshold”(X,4095); setOption(“BlackBackground”, false); run(“Convert to Mask”); run(“Watershed”); run(“Analyze Particles…)”, “size = Y-Infinty pixel include summarize in_situ”. Where “X” is the threshold value at which 1% of total fluorescence remains for the average positive control sample, and where “Y” is the pixel size required to count a cell as “positive”, which can affect results (Figure 3.4.b).
6. This script will provide the number of counted particles in a given image.

Troubleshooting and Advice –

DNA delivery:

Most cells of interest will not contain the T7 DNA promoter with a downstream reporter such as GFP or luciferase, so these sequences of DNA will need to be delivered by some method. Most of our work relies on transient transfection, which is outlined in the precursor techniques section below. However, some cells are resistant to transient transfection. To determine if DNA can be delivered to your cells of interest, the transfection protocol above can be used with a DNA plasmid that constitutively expresses a reporter protein such as GFP.

Maximum split RNAP activity

After successful DNA delivery, the RNAP activity itself should be assayed. Clone or purchase a plasmid(s) with the following DNA elements: A T7 promoter-driven reporter protein (GFP, luciferase, etc.), constitutively expressed T7-RNAP$_C$, and constitutively expressed wtRNAP$_N$. Deliver the plasmid(s) and measure the signal via RT-qPCR, microscopy, or plate reader assay under your particular experimental conditions. To estimate a signal-to-noise ratio, conduct an experiment comparing reporter expression in the presence of wtRNAP$_N$, versus the eRNAP$_N$.

PPI fusion protein controls

Perform the same control experiments as described above for the *e. coli* luciferase assay, instead using the appropriate plasmids for mammalian expression. First use fusions to the wtRNAP$_N$ to assess if protein fusion diminishes split RNAP activity. Next, use fusions to the eRNAP$_N$ to measure if protein fusion increases evolved split RNAP activity.

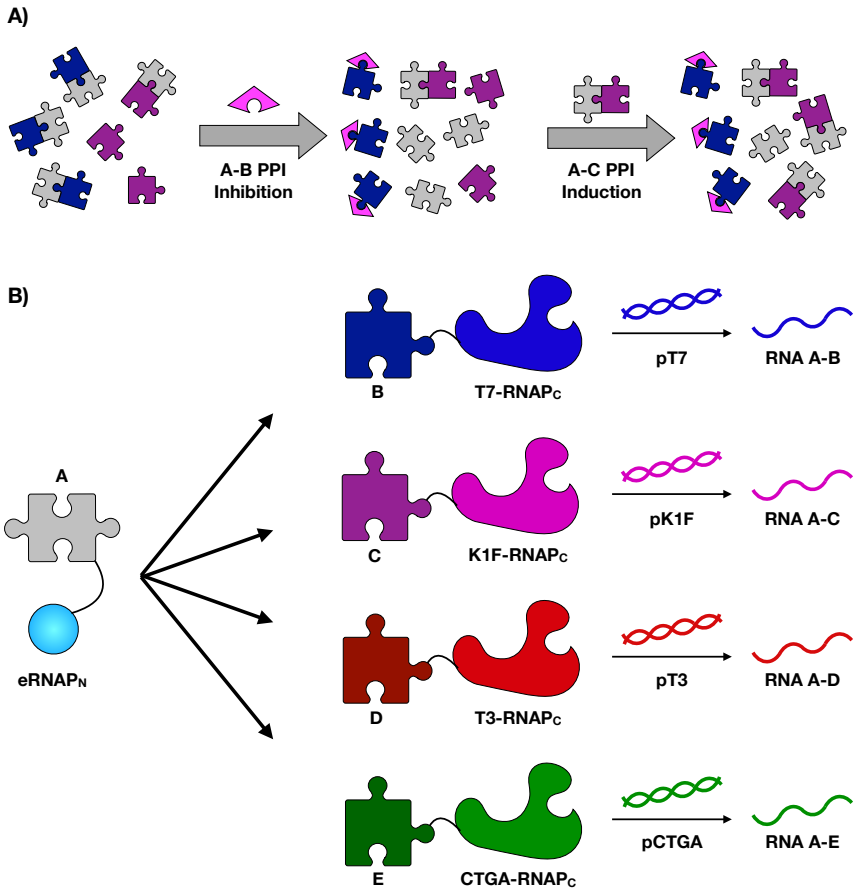

Figure 3.5. PPI competition and multidimensional analysis using the split T7 RNAP biosensor. A) cartoon representing the importance of measuring multiple PPIs simultaneously in a given sample. Specifically, when a single PPI is inhibited (pink), it increases the unbound concentration of one binding partner (gray). The increased unbound protein concentration can increase its interactions with other proteins (purple), which may have different downstream impacts. B) cartoon portraying how the split RNAP biosensor can distinguish between at least four PPI simultaneously. In brief, the RNAP$_N$ can assemble with any of the mutant RNAP$_C$, but each RNAP$_C$ is orthogonal to one another. A protein fused to RNAP$_N$ will produce a different RNA signal depending on which RNAP$_C$ its protein partner is fused to. In this way, each PPI produces a unique RNA signal.

Multiple simultaneous PPI effects

It is important to remember that the $RNAP_C$ contains the DNA promoter recognition domain and that mutations in this domain do not affect $RNAP_C$ assembly with $RNAP_N$. Therefore, all PPI experiments effectively involve one "hub" protein fused to the $RNAP_N$ and several potential binding partners fused to each orthogonal $RNAP_C$. For example, if, two $RNAP_N$ protein fusions, $RNAP_N$-A and $RNAP_N$-B, were introduced with a T7-$RNAP_C$ protein fusion into the same cells, it would be impossible to distinguish whether RNA signal was produced from $RNAP_N$-A, $RNAP_N$-B, or a combination of the two. Simply performing multiple experiments with different $RNAP_N$ protein fusions, and then normalizing the results to a control $RNAP_N$ or fusion protein can overcome this limitation.

One advantage of the split RNAP is its ability to measure competition between PPIs. For example, protein A might interact with both proteins B and C when tested individually, but when all three are expressed simultaneously or selectively inhibited, the A-B PPI may outcompete the A-C PPI (Figure 3.5.a). The split RNAP can take advantage of orthogonal $RNAP_C$ to encode a unique RNA signal for each PPI (Figure 3.5.b). However, any analysis of multiple simultaneous PPIs cannot assume the only difference between signals is due to PPI frequency. Along with considerations mentioned above in section 2.3, each orthogonal $RNAP_C$ and DNA promoter pair has a different activity and orthogonality profile. See figure 5.a in the following reference for a large panel of $RNAP_C$ and DNA promoter pairs screened in *e. coli*. For example, The

T7-RNAP$_C$ is able to recognize the K1F promoter to a significant degree. This means that decreasing T7-RNAP$_C$ PPIs will also decrease K1F RNA signal, which could be mistaken for decreased K1F-RNAP$_C$ PPIs. There was no combination of RNAP$_C$ mutants and promoter pairs that would not have some mixed signal for a 1:4 (hub:potential partner) PPI based experiment. However, for a 1:3 PPI experiment, we would predict that using CTGA, K1F, and T3 promoters would have the fewest off target effects, while for a 1:2 PPI experiment, using the T7 and CGG promoters would have the fewest off target effects (especially notable, since the original RNAP$_N$ evolution used these promoters).

Combining purified reagents and split RNAP tags

Combining split RNAP tags to study the perturbation or manipulation of PPIs by external triggers (like inhibitors) or endogenous signaling events presents an additional challenge: how to monitor PPIs over relatively short time periods. Split RNAP tags are empowered by the versatility of RNA. The signal can manifest in unique RNA sequences, RNA aptamers (e.g., spinach or broccoli) [85], or mRNA for reporter proteins such as GFP and luciferase. However, certain RNA signal outputs are more desirable in different situations. GFP and luciferase are commonly used due to reliability and cost effectiveness, but when monitoring signal changes within short time periods these slow folding and/or degradation of these proteins limit their use. When deploying split RNAP tags to monitor changes in PPIs on short time scales, which is common when using exogenous reagents, it's more effective to directly measure unique RNA sequences via either RT-qPCR or fluorescent RNA aptamers.

3.3.2.3 Monitoring a 4-by-1 PPI network during inhibitor treatment

1. Culture HEK293T cells in triplicate for each PPI combination to 70-90% confluence in 12-well culture plates with 250 µL antibiotic free DMEM media supplemented with 10% fetal bovine serum.
2. Transfect each well with 400 ng of 9-49 $RNAP_N$-tBID OR 9-52 $RNAP_N$-DeadBID mammalian expression plasmid, 400 ng of 9-54 T7 promoted GFP(RNA1) and Bcl2-T7-$RNAP_C$ expression plasmid, 10-52 T3 promoted RNA2 and Mcl1-T3-$RNAP_C$ expression plasmid, 11-63 CTGA promoted RNA3 and Bclw-CTGA-$RNAP_C$ expression plasmid, 12-75 K1F promoted RNA4 and BclxL-K1F-$RNAP_C$ expression plasmid and 6 microliters of lipofectamine 3000, while closely following the transfection protocol referenced in precursor techniques.
3. Add 500 nM ABT-199 or DMSO control during transfection, 24 hours after transfection, 36 hours after transfection, and 45 hours after transfection.
4. 48 hours after transfection extract total RNA from cells using the RNAeasy kit from Qiagen. Note- when handling RNA be sure to use RNAse free reagents wipe down workbench with RNAse inhibitor.
5. Measure RNA concentration.
6. Perform reverse transcription. We recommend using PrimeScript TM RT kit. We didn't encounter issues when following the PrimeScript TM RT protocol.
7. Design qPCR primers for your RNA of interest and a housekeeping gene like GAPDH, or use those we used in the following reference [132].

8. Measure DNA concentration via qPCR. cDNA from reverse transcription was diluted 1:20, or even 1:100 before adding to qPCR mixture. We found this necessary because the T7 RNAP biosensor produces enough RNA in cells to saturate the machine. Save remaining DNA and rerun qPCR if CT values are less than 15 (implying too much cDNA) or above 32 (implying too little cDNA).
9. Subtract all Ct values by each sample's GAPDH Ct value to normalize RNA signal. This will ensure that samples with greater or fewer numbers of cells can still be compared to one another. Also, measuring the level of T7 RNA polymerase can help normalize for changes due to transfection.
10. Next, subtract from this GAPDH normalized value the average Ct value of an off-target control. For example, in this experiment we use a truncated form of tBID that no longer interacts with its binding partners. This provides a "ΔΔCt value" where the first Δ represents GAPDH normalization, and the second Δ represents off target normalization.
11. To calculate RNA fold changes from Ct values simply use 2^{Ct}, so a ΔΔCt value of 4 would represent a 2^4 or 16 fold change in RNA between the sample and an off target control.

3.3.3 Precursor techniques

3.3.3.1 Cloning

Our group prefers cloning with the following techniques – electronic plasmid design, polymerase chain reaction (PCR), spin column DNA clean up, Gibson Assembly, and

chemically competent *e. coli* transformation. Listed below are references for each technique.

Plasmid design – There are many electronic tools to aid in plasmid design. Our group uses the online services found on www.benchling.com. Benchling helps with many aspects of plasmid design including primer design, sequencing alignment, plasmid export, and guide RNA design.

PCR – Our group amplifies sequences for later assembly using PCR. We purchase reagents from New England Biolabs (NEB), and follow their protocols. See the following website for a protocol using the high-fidelity Phusion DNA polymerase. https://www.neb.com/protocols/0001/01/01/pcr-protocol-m0530

DNA clean up – Although there are several ways to purify DNA, we purchase DNA spin/vacuum manifold columns from econospin, but use buffers and protocols found on Qiagen's website. Also, we use DpnI treatment and/or gel purification to eliminate plasmid templates or alternative products from PCR reactions. https://www.qiagen.com/us/resources/resourcedetail?id=e0fab087-ea52-4c16-b79f-c224bf760c39&lang=en

Gibson Assembly – There are also many ways to assemble DNA into a plasmid. Our group uses a technique called Gibson Assembly. The following reference details this method[112].

e. coli transformation – Our group uses protocols found in the following reference [135].

3.3.3.2 Mammalian cell work:

Transient transfection – See the following reference on mammalian cell transfection as a first look into this technique[136]. We use lipofectamine 3000 or 2000, but PEI can also be used. See the following references for Lipofectamine and PEI https://www.thermofisher.com/content/dam/LifeTech/global/life-sciences/CellCultureandTransfection/pdfs/Lipofectamine_3000_Protocol_6Dec2013.pdf [137].

ImageJ – For help setting up a batch process see the following link.

https://imagej.net/Batch_Processing

3.4 Summary

The split RNAP biosensor is a powerful tool to study multiple PPIs simultaneously in live cells. In particular, split RNAP tags are capable of studying changes in several PPIs

over time depending on cellular environment and PPI competition. The most important consideration when deploying the split RNAP that isn't common to other protein fragment complementation assays is its requirement for a DNA template. Considering its limitations, we believe the split RNAP biosensor can spearhead a thorough PPI network analysis within cell nuclei, specifically when investigating PPI inhibition and competition. More critically, due to its versatility and robust RNA output, the proximity-dependent split RNAP technology can be used for applications beyond just detection of PPIs, including synthetic biology applications engineering gene circuits for cell control, selectin, and evolution.

CHAPTER 4

A SYSTEM FOR THE EVOLUTION OF PROTEIN-PROTEIN INTERACTION INDUCERS

4.1 Introduction

Protein-protein interactions (PPIs) regulate nearly all cellular processes, functioning as signaling hubs, structural components, modifiers of biocatalytic complexes, and recognition motifs for intercellular communication[9, 115, 138-141]. Dysregulated PPIs have been attributed to diverse pathologies, including cancer, neurodegeneration, and autoimmunity[142-150] and are therefore important therapeutic targets. PPIs are also increasingly recognized as engineerable nodes for the control of cellular information flow. Indeed, synthetic biologists have harnessed PPIs to engineer increasingly complex artificial biological systems, sensors, and materials[151-157]. Therefore, technologies for the generation of molecules that create or alter PPI networks have value both as therapeutic strategies and for synthetic biology applications.

While PPI inhibitors have been the focus of extensive research[27, 158-161], culminating after 30 years in the first and only FDA-approved intracellular PPI inhibitor[118], molecules that instead induce interactions between proteins, i.e., “molecular glues”, are garnering increased attention[37, 162-164]. Approximately one hundred confirmed small molecule PPI inducers or glues, largely discovered by serendipity, currently exist, seven of which are FDA-approved for clinical use, including important medicines like rapamycin, taxol, tafamidis, and lenalidomide. However, as there are in principle at least 200,000,000 possible PPIs among members of the human proteome, these molecules barely scratch the surface of what is possible. This potential is further illustrated by the advent of proteolysis targeting chimeras (PROTACs), bifunctional molecules that degrade

proteins of interest (POIs) by inducing an interaction between the POI and an E3 ubiquitin ligase[165-171]. While over a dozen PROTACs are entering phase I and II clinical trials, they are limited to the current pool of potent E3 ligase- and POI-binding small molecules[172]. Moreover, PROTACs and all bifunctional molecular glues are susceptible to the “hook effect”: decreased effectiveness of the molecule at higher concentrations due to target protein saturation[173]. The “hook effect” is also dependent on protein target concentration, requiring screening of each new target with a panel of target- and E3 ligase-binding ligands at a wide range of concentrations.

Besides rationally designing bivalent molecules such as PROTACs, there are two other distinct molecular glue discovery methods: random screens and evolutions. Random screens, whether carried out *in silico* and/or *in vitro*, have been somewhat successful in identifying PPI inducers, particularly for the 14-3-3 protein family[174-184]. However, evolution has been by far the most successful method for discovering PPI inducers. There are already six evolutionarily derived FDA-approved drugs (four small molecule natural products and two bispecific antibodies) and dozens more bispecific antibodies in clinical trials[38, 185-187]. However, while powerful therapeutic approaches, antibody therapies are limited to extracellular POIs, and the success of bispecific antibodies in particular can be attributed to the immune system, which itself essentially functions as a robust, modular, and rapid directed evolution method for creating POI binders.

Directed evolution – the cyclic process of diversifying, selecting, and amplifying molecules based on activity – has generated molecules with a wide range of new

activities, including metabolically altered organisms, stably expressed proteins, and selective small molecule processing enzymes[188-195]. In the realm of PPIs, pioneering and robust directed evolution methods such as phage, mRNA, and ribosomal display technologies have generated PPIs with sub-nanomolar binding affinities[196-198]. A range of powerful continuous evolution technologies that reduce the need for human intervention, accelerate evolution, and evolve molecules in unique biological contexts have emerged, including Phage-Assisted Continuous Evolution (PACE), Orthorep, mammalian phage assisted continuous evolution (mPACE), and viral evolution of genetically actuating sequences (VEGAS)[199-204]. While powerful, all of these directed evolution approaches are limited by the selection systems that can be deployed, and a robust method to evolve molecules to drive a desired intracellular PPI is lacking.

Here, we present rapid evolution of Protein-Protein Interaction Molecular Glues (rePPI-G), a new selection and continuous evolution platform for creating PPI inducers based on PACE. A powerful continuous evolution system, PACE requires linking a desired function of interest to the expression of gIII, a required phage gene. We reasoned that a PACE system for evolving PPI inducers would require a biosensor system that can convert induced protein interactions into a robust and quantifiable gene expression output. To this end, we leveraged our proximity dependent split T7 RNA polymerase (RNAP) technology – which uses RNA transcription to trigger either reporter or gIII gene expression – as a versatile detector of PPI inducer-based interactions in live cells[84, 107, 129]. The coupling of these two technologies forms rePPI-G. We validated rePPI-G using a panel of engineered bifunctional molecular glues that drive interactions between

otherwise non-interacting POIs. To optimize the engineered molecular glues, we developed workflows that combined PACE-based continuous evolution with phage-based selection systems. These evolutionary approaches yielded bifunctional molecular glues with decreased “hook effect” properties, which we attribute in part to tuned interaction affinities between each half of the bifunctional molecule. Overall, this work validates rePPI-G in key proof-of-concept experiments and lays the foundation for approaches to rapidly generate molecular PPI inducers through the process of evolution.

4.2 Results

Split RNAPs can detect PPI inducers

In previous work, we developed proximity dependent split T7 RNA polymerase (RNAP) variants that assemble into functional RNA polymerases and drive programmed gene expression outputs only when a PPI brings the two RNAP fragments together[84]. We demonstrated the split T7 RNAP can detect selective PPIs, light-induced dimerization events, and the presence of small molecules. Critically, we demonstrated that the split T7 RNAP system can detect validated molecular glues, including both the rapamycin-induced pairing of FRB/FKBP[84, 205] and the abscisic acid-induced interaction of PYL/ABI[128, 206]. Moreover, we recently developed "Phage-Assisted Continuous Selection – Deep Mutational Scanning" (PACS-DMS), a method that links PPIs between a target protein and a library of binding variants to phage fitness, thereby allowing the interrogation of mutations that impact PPI formation[207]. Therefore, we hypothesized that the proximity dependent split RNAP system could be used to convert induced PPIs into gIII production, thus developing a new PACE system for evolving PPI inducers.

We first tested whether we could drive the assembly of two non-interacting proteins using a rationally designed bifunctional inducer molecule composed of binding partners for each target protein (Figure 4.1A). As a model, we selected KRas and NOXA, which have no known interaction with one another[208, 209]. We tagged KRas with the C-terminal portion of the proximity-dependent spit RNAP system ($RNAP_C$) and NOXA with the N-terminal portion of the split RNAP system ($RNAP_N$) and tested the background assembly of the split protein using a previously established *E. coli* luciferase gene

expression assay[113]. As expected, we observed luminescence signal comparable to the background levels of the split RNAP system itself, confirming that KRas and NOXA do not interact (Figure 4.S1). Next, we tested whether we could promote an interaction between KRas and NOXA with a bivalent PPI inducer expressed from an IPTG-inducible vector. We generated a rationally designed PPI inducer of KRas and NOXA by fusing Raf, a KRas binder, to Mcl1, a NOXA binder[209]. In the absence of IPTG, we observed only background levels of luminescence. However, addition of IPTG resulted in a dose-dependent enhancement of luminescence signal, with a maximum 58-fold increase in gene expression based on the engineered inducer (Figure 4.1B). As a control, we substituted Bcl_{XL}, a protein related to Mcl1 that does not bind NOXA[209], for Mcl1 in our bivalent inducer. As expected, this control molecule did not trigger enhanced gene expression (Figure 4.1B). Taken together, these data confirm that the split RNAP system can detect functional bivalent PPI inducers and trigger a robust increase in gene expression.

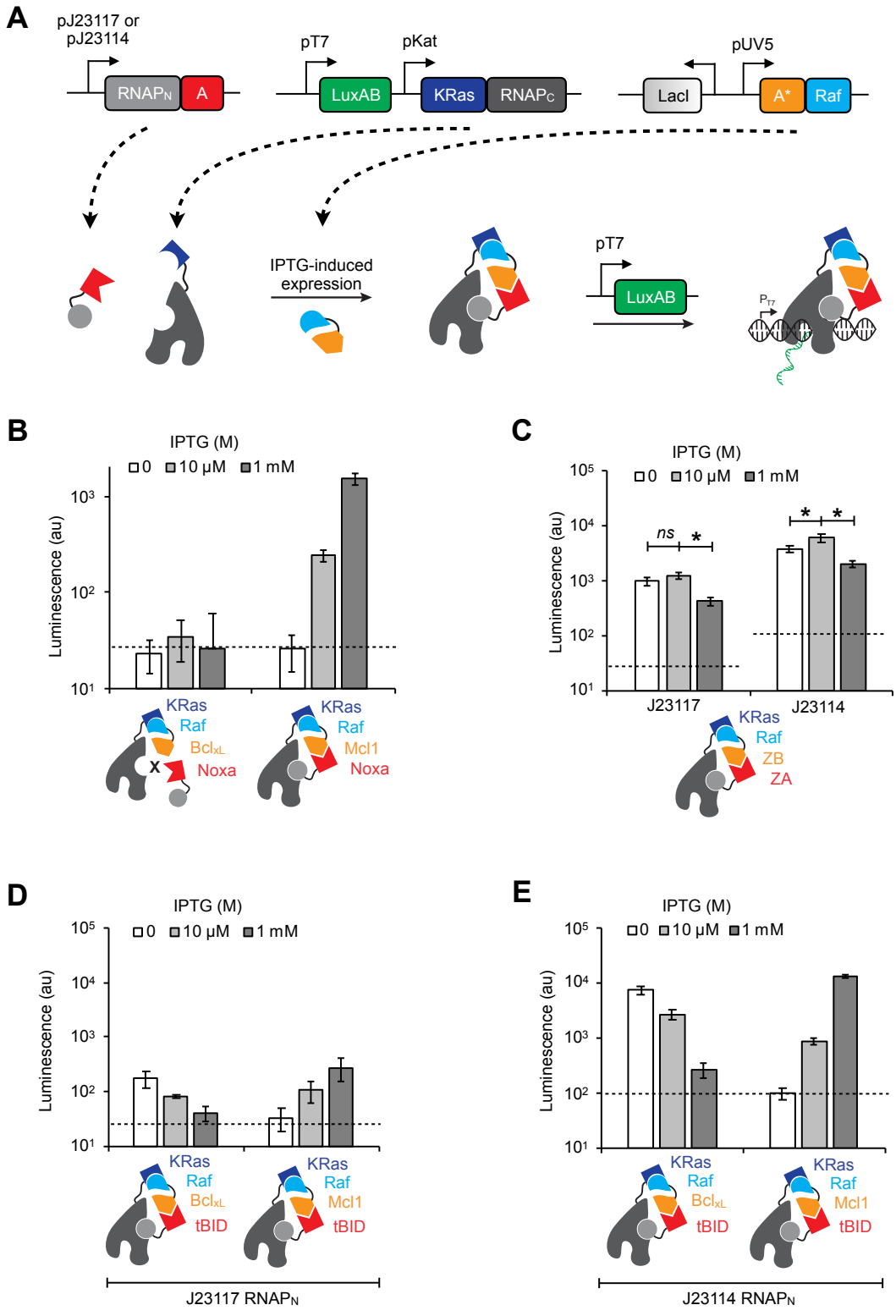

Figure 4.1. Split RNAP biosensors detect molecular glue-induced PPIs. (A) Schematic of plasmid maps used in the inducer detection assay and cartoon representation of inducer detection assay mechanism. (B) Luminescence data from molecular glues with

Figure 4.1. Split RNAP biosensors detect molecular glue-induced PPIs continued. a mismatched PPI (Bcl_{xL} and Noxa) and an interacting PPI (Mcl1 and Noxa) at various molecular glue expression levels as controlled by IPTG concentration. (C) Luminescence data obtained with the ZB-Raf molecular glue with low (J23117 promoter) or high (J23114 promoter) $RNAP_N$ expression. (D) Luminescence data from Bcl_{xL}-Raf and Mcl1-Raf molecular glues with low $RNAP_N$ expression. (E) Luminescence data from Bcl_{xL}-Raf and Mcl1-Raf molecular glues with high $RNAP_N$ expression. Dashed lines indicate baseline luminescence signal from PPI-independent RNAP reassembly as reported in Figure 4.S1. * = $p < 0.05$, *ns* = $p > 0.05$.

We next sought to test the generality of the system and the ability to detect PPI inducers of varied affinities. We substituted ZA – a leucine zipper peptide which also has no known interaction with KRas – for NOXA in our PPI detection system. We then designed a bivalent inducer by fusing Raf to ZB, a peptide that forms a tight PPI with ZA^{210}. As expected, this second inducer system also triggered a robust increase in gene expression (Figure 4.1C). In this case, we observed gene expression activation even without IPTG induction, as well the "hook effect," with the highest concentrations of IPTG inducer causing a significant decrease in gene expression. To investigate this, we increased the expression of the $RNAP_N$-tagged ZA by swapping the promoter from J23117 to the stronger J23114. With the stronger promoter, we observed higher levels of inducible gene expression, albeit with a more pronounced hook effect (Figure 4.1C). Such an effect is expected as the bivalent inducer eventually decreases ternary complex formation due to separate bivalent molecules independently binding each of the protein partners rather than bridging a ternary complex[173].

Finally, we tested a third inducible system, this time exchanging ZA for tBID, a protein that does not bind KRas, but does interact with both Mcl1 and Bcl_{XL}. As expected, both the Raf-Bcl_{XL} and Raf-Mcl1 resulted in enhanced luciferase reporter gene expression

(Figure 4.1D). We again observed a hook effect dependent on the expression of the bivalent inducer. With low expression of $RNAP_N$-tagged tBID (via the J231117 promoter), we observed a decrease in signal with increasing Raf-Bcl_{XL} inducer expression, although there was a significant signal over background even without IPTG induction. With the same low expression of the $RNAP_N$-tagged tBID, we observed an expected IPTG-dependent increase in RNAP activity with increasing Raf-Mcl1 inducer expression. With high $RNAP_N$-tagged tBID expression (driven by the J231114 promoter), we observed the same trends, though greatly magnified (Figure 4.1E). Previous work in our group and reported in the literature found that the binary PPI between Mcl1 and tBID is weaker than the PPI between Bcl_{xL} and tBID[132, 209, 211], which could explain these differences in signal response and varied hook effect magnitude.

Overall, these data indicated that the split RNAP system is capable of robustly detecting bivalent molecule-induced interactions between non-interacting protein pairs. Tuning bivalent inducers to properly drive a set of non-interacting partners without succumbing to the hook effect or losing potency is a major challenge in the rational design of inducible systems. Therefore, we next sought to develop a PACE system for optimizing PPI inducers, with the proof-of-concept goal being to overcome the hook effect.

Design and validation of rePPI-G

To convert our PPI inducer detection assay into a PACE system, we made two key changes. First, we cloned the ZB-Raf inducer from the IPTG inducible plasmid to the M13 bacteriophage's gIII region under a high expression ProB promoter[212] (Figure

4.2A). The high expression promoter should produce enough ZB-Raf inducer to decrease its overall activity via the “hook” effect. Second, we changed the downstream RNAP output protein from bacterial luciferase (LuxAB) to gIII, the protein necessary for bacteriophage replication. We next assessed whether ZB-Raf phage can replicate in a manner dependent on the selectively induced interaction between ZA and KRas.

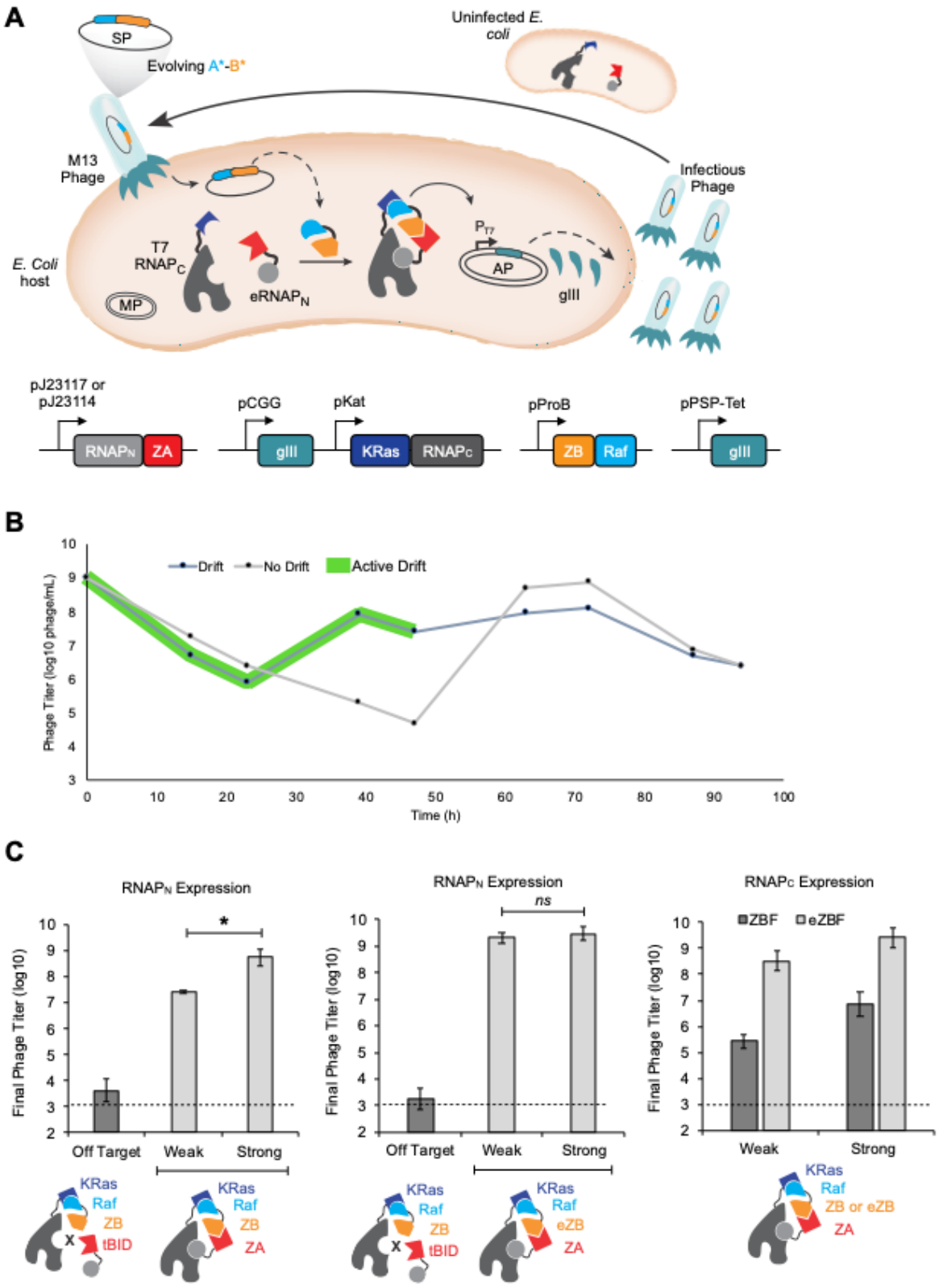

Figure 4.2. Rapid evolution of protein-protein interaction molecular glues (rePPI-G) to overcome the "hook" effect. (A) Schematic of plasmid maps used in the molecular glue

Figure 4.2. Rapid evolution of protein-protein interaction molecular glues (rePPI-G) to overcome the "hook" effect continued.
PACE and cartoon representation of molecular glue PACE components and mechanism. (B) ZB-Raf molecular glue phage titers over time during PACE experiment. Green background indicates active genetic "drift" cells. (C) Quantification of phage replication in overnight growth assays. Wildtype ZB-Raf molecular glue phage activity with a mismatched target (tBID and ZB) and a weak (J23117 promoter) or strong (J23114 promoter) $RNAP_N$-tagged ZA (left panel) compared to the PACE-evolved ZB-Raf molecular glue phage with the same targets (center panel). Wildtype (dark) compared to evolved (light) ZB-Raf molecular glues with weak (sd6 RBS) or strong (SD8 RBS) $RNAP_C$-tagged KRas expression. * = $p < 0.05$, *ns* = $p > 0.05$.

To measure phage replication, we used overnight growth assays. In this assay, a small number of phage (10^3/mL) are used to infect engineered *E. Coli* host cells for 24 hours, at which point the final phage titer is quantified using plaque assays[213]. We found that ZB-Raf phage that infected cells expressing $RNAP_N$-tagged tBID and $RNAP_C$-tagged KRas did not replicate at all (Figure 4.S2). However, when these phage infected cells expressing $RNAP_N$-tagged ZA and $RNAP_C$-tagged KRas, they replicated >30,000-fold to a population of ~10^7/mL (Figure 4.S2). These results confirm that the materials for the rePPI-G system can drive the replication of engineered phage based on their production of a PPI inducer. Next, we sought to transition from these overnight phage growth assays to a more stringent, continuously evolving PACE format.

We initially performed the PACE of ZB-Raf phage with two different host cells, each featuring a different selection system design. One set was transformed with the combination of a $RNAP_N$-tagged ZA plasmid and a $RNAP_C$-tagged KRas plasmid, along with a mutagenesis plasmid to increase genetic variation (Figure 4.2A). The second set of cells were designed to provide phage with their missing gIII protein regardless of inducer activity. To accomplish this, we first cloned a tetracycline-repressed phage

shock promoter upstream of gIII so that both tetracycline addition and phage infection are required for gIII expression[113]. This selection pressure-free genetic "drift" plasmid was transformed into the second set of host cells, along with a mutagenesis plasmid and a plasmid encoding the third antibiotic resistance gene. We began the PACE experiment with an equal mixture of these two cell populations in two lagoons, with tetracycline added to one lagoon to activate the "drift" expression cassette. After 39h, the tetracycline-treated lagoon (i.e., active "drift") had 400-fold higher phage titers than the lagoon without tetracycline, confirming "drift" cell efficacy (Figure 4.2B). After 47h we removed the "drift" cell population, thus increasing the overall evolutionary selection pressure and allowing noninfectious phage variants to wash out of the "drift" lagoon. Between the 47h and 63h timepoints, the phage titer in the lagoon without active "drift" cells increased by 10,000x, while the active "drift" lagoon retained its high titers, indicating the presence of active phage in both lagoons. Next, another PACE experiment was conducted with ZB-Raf-expressing phage without "drift" cells and with the addition of a negative selection plasmid (Figure 4.S3). This new plasmid expresses gIIIneg, a dominant negative mutant of gIII, under the control of an orthogonal RNAP promoter controlled by an orthogonal $RNAP_C$ mutant fused to ZBneg, a protein that does not interact with any other protein in the PACE system. The phage again evolved within 48-72 hours, but produced a somewhat diminished final phage titer due low expression of gIIIneg from small off-target interactions. We then subjected the ZB-Raf phage from the 63h timepoint of the original PACE to another round of PACE and observed a similar timing for phage titer increase, but significantly higher final phage

titers (Figure 4.S3). Based on phage titers, these experiments indicated multiple successful PACE runs.

We next used overnight growth assays to assess whether the phage from these PACE experiments possessed different replication properties when compared to wild type phage. We first compared wildtype vs. evolved phage replication with different $RNAP_N$-tagged ZA expression levels. We found that the original ZB-Raf inducer phage replicated 21-fold less when a lower level (J23117 promoter) of $RNAP_N$-tagged ZA is expressed (Figure 4.2C). By contrast, the evolved phage replicated with identical efficiency regardless of the $RNAP_N$-tagged ZA expression level. In addition, these evolved phage remained incapable of replicating with cells expressing $RNAP_N$-tagged tBID and $RNAP_C$-tagged KRas, confirming that these phage are dependent on inducing a specific PPI. Modulation of the $RNAP_C$-tagged KRas expression led to increased replication with increasing $RNAP_C$ expression for both the wildtype and evolved phage (Figure 4.2C). Notably, however, the evolved phage replicated over 300-fold more overall than wildtype phage at both $RNAP_C$ expression levels. Taken together, these data confirm the PACE experiments generated evolved phage that replicate more effectively than wildtype phage while remaining dependent on selective PPI induction.

The observed PACE-evolved phage could have mutated in at least three ways to increase RNAP assembly at high ZB-Raf expression levels and thus mitigate the “hook” effect: 1) the inducer promoter strength could have been weakened to reduce ZB-Raf concentration; 2) the ZB affinity for ZA could have weakened to match the KRas-Raf

interaction; or 3) the affinity of Raf for KRas could have increased to match the ZB-ZA interaction. To assess these possibilities, we Sanger-sequenced individual phage variants from each lagoon to determine which components evolved most frequently in the PACE experiments. We found that all variants had single or double mutations in the ZB region (Figure 4.3A) and only observed one mutation in the Raf protein (N71K) that was rare after the first PACE, but common after the second negative selection PACE. No mutations were observed in the ProB promoter region. We cloned the most common variant, termed ZBF(3-2), into an IPTG-inducible expression vector and tested to what degree ZBF(3-2) induced the interaction of $RNAP_N$-tagged ZA and $RNAP_C$-tagged KRas, as compared to ZB-Raf. ZBF(3-2) produced up to a 6-fold increase in RNAP activity compared to ZB-Raf at all inducer expression levels and did not decrease in activity with moderate inducer expression (10 μM IPTG), demonstrating increased resistance to the “hook” effect (Figure 4.3B). We next cloned each ZB or Raf variant as a fusion to the $RNAP_C$ or $RNAP_N$, respectively, to perform a binary PPI luciferase assay that measures variant binding to ZA or KRas respectively. $RNAP_C$-tagged ZB variants produced a 3- to 17-fold reduction RNAP activity when co-expressed with $RNAP_N$-tagged ZA, indicating that the evolution selected solely for mutations that negatively impact ZB-ZA assembly and avoid the “hook” effect (Figure 4.3C). The Raf(N71K) mutation increased KRas-Raf assembly by ~3-fold, again supporting the hypothesis that the ZB-Raf inducer evolved to balance each PPI’s relative affinity (Figure 4.3D). After this successful proof-of-concept evolution, we sought to expand our scope to a new PPI and evolve an inducer composed of short peptides.

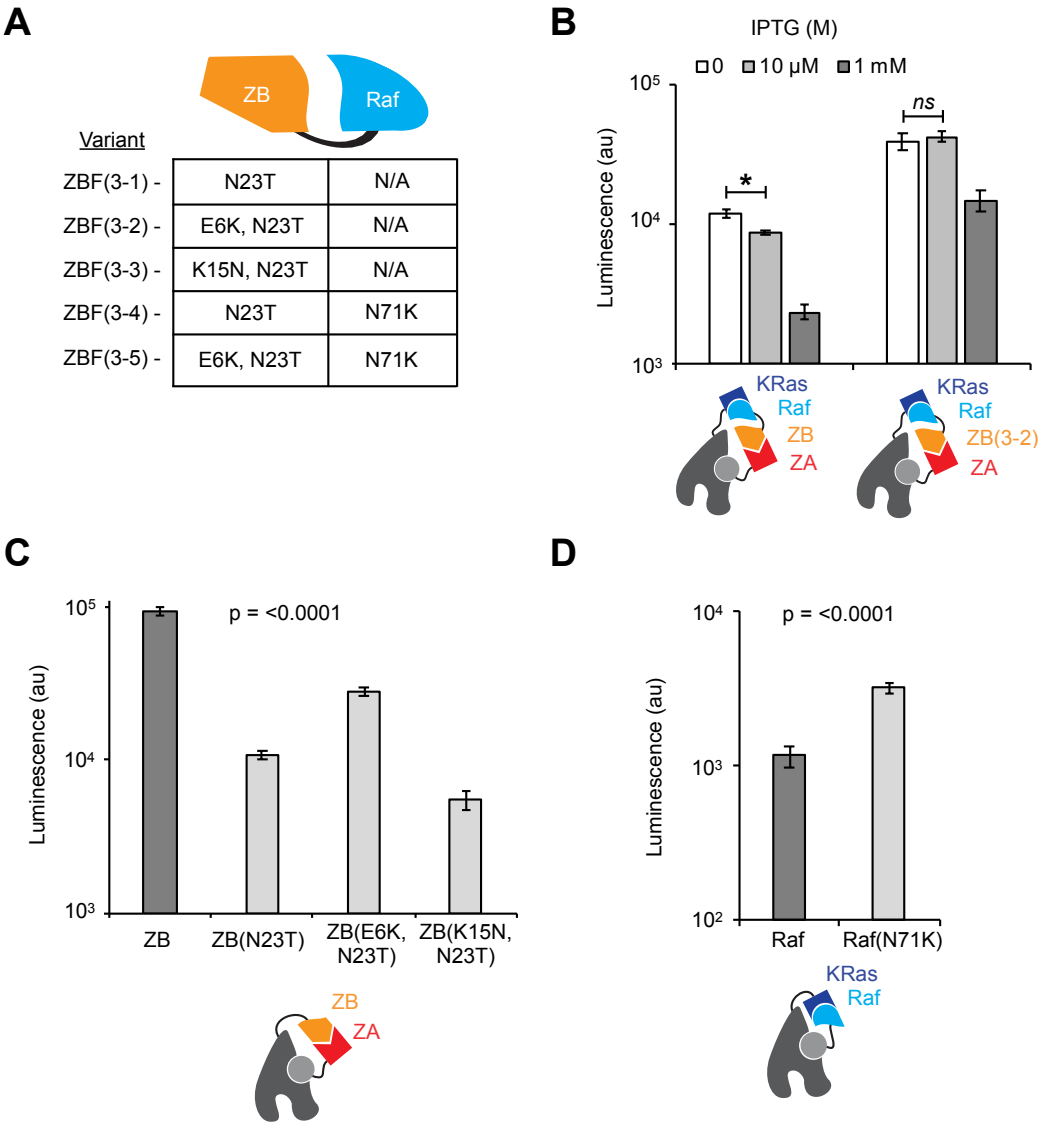

Figure 4.3. rePPI-G improved molecular glue activity by altering binary interaction affinities. (A) Common mutations discovered in the PACE experiment. (B) Luminescence data of ZB-Raf or ZBF(3-2) molecular glues inducing an interaction between ZA and KRas at different concentrations. (C) Luminescence data of individual binary interactions between $RNAP_C$-tagged ZB or ZB variants with $RNAP_N$-tagged ZA. All mutants had p = <0.0001 compared to ZB(wt) activity. (D) Luminescence results of binary interactions between $RNAP_C$-tagged KRas with $RNAP_N$-tagged Raf or Raf(N71K). p = <0.0001. * = $p < 0.05$, *ns* = $p > 0.05$.

Expanding target scope of rePPI-G

One challenge when identifying new protein targets for split reporter-based systems is avoiding false negatives stemming from either inherent instability in the new protein fusion or interference with split reporter assembly or activity. To avoid this pitfall, we first developed an assay to determine whether a new protein of interest (POI) can be fused to split RNAP reporters while retaining high signal-to-noise. We replaced the evolved $RNAP_N$ with the wildtype $RNAP_N$, which is capable of reassembling with the $RNAP_C$ with or without a PPI (Figure 4.S4)[84, 214]. We fused several POIs to either the $RNAP_N$ or $RNAP_C$ and co-expressed these fusions with a cognate $RNAP_C$ or $RNAP_N$ fusion protein capable of folding and reassembling to form an active RNAP. Using this assay, we rapidly identified GABARAP and LC3B as protein targets with high RNAP activity, albeit with >5-fold less activity than previously validated targets, KRas and tBID (Figure 4.S5). Neither GABARAP nor LC3B greatly increased RNAP folding or expression, as evinced by their low background activity when fused to the evolved $RNAP_N$ (Figure 4.S5 and 4.S6).

We next searched the literature for peptides that bind GABARAP and/or LC3B. A recent publication screened and identified peptides from human proteins that selectively bind various autophagic adaptor proteins, including GABARAP and LC3B[215]. Two short peptides from the ULK1 and Fyco1 proteins possessed particularly high affinities for GABARAP and LC3B, respectively. We cloned PPI inducers composed of ZB or ZB(E6K, N23T), now termed eZB, fused to either ULK1 or Fyco1 and measured their ability to activate the split RNAP with GABARAP or LC3B fused to the $RNAP_C$. Both

eZB-ULK1 and ZB-ULK1 induced RNAP activity when ZA and GABARAP were fused to the $RNAP_N$ and $RNAP_C$, respectively (Figure 4.4A). ZB-Fyco1 induced a strong interaction between ZA-LC3B, and a weaker, yet significant, interaction between ZA-GABARAP (Figure 4.4B). Notably, increasing concentrations of the ZB-ULK1 and eZB-ULK1 inducers resulted in enhanced RNAP activity. Furthermore, the eZB-ULK1 inducer produced higher overall signal compared to ZB-ULK1, suggesting that the weaker eZB-ZA interaction is closer in affinity to the ULK1-GABARAP interaction than ZB-ZA. These data led to the hypothesis that the ULK1-GABARAP interaction is low affinity and thus a prime candidate for optimization via rePPI-G.

To test this possibility, we cloned the ZB-ULK1 and eZB-ULK1 inducers into the bacteriophage genome and altered the RNAP output gene to gIII. Host *E. Coli* cells were transformed with plasmids expressing $RNAP_N$-tagged ZA and $RNAP_C$-tagged GABARAP, along with a mutagenesis plasmid, and we performed a PACE experiment using these host cells and two lagoons, one containing ZB-ULK1 inducer phage and one containing eZB-ULK1 inducer phage. After 48h, eZB-ULK1 phage titers increased ~50-fold while ZB-ULK1 titers remained the same (Figure 4.4C). However, after 84h, both PPI inducer phage populations remained below 10^7 phage/mL, indicating a stagnation in the evolution. Both repeating the evolution under the same conditions and increasing the evolutionary selection pressure by decreasing the expression of $RNAP_N$-tagged ZA resulted in similarly low phage titers (Figure 4.S7). We speculate that these evolutions were repeatedly stuck in activity minima that may require numerous mutations to overcome. While very rare phage with mutational combinations might

escape the relative activity minima, it could take days or even weeks for these to overtake the population, especially given the rigorous selection pressure that continuous flow represents. Fine-tuning the PACE experiment components has proven successful in similar situations but can require weeks or months of optimization and evolution[84]. To sidestep this challenge, we developed an alternative evolution strategy.

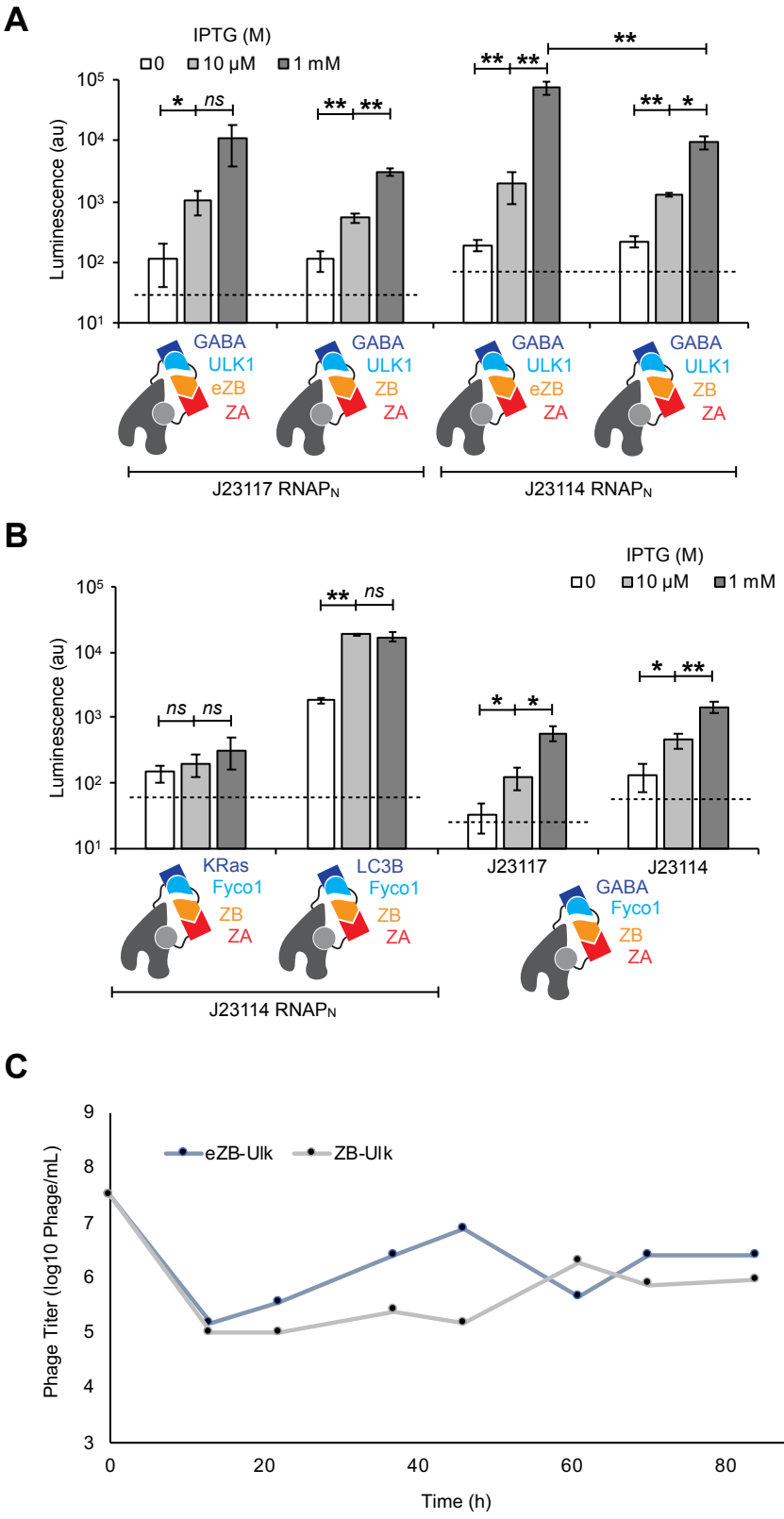

Figure 4.4. Expanding target scope of rePPI-G. (A) Luminescence data from ZB-ULK1 and eZB-ULK1 molecular glues inducing the interaction between GABARAP and ZA at

Figure 4.4. Expanding target scope of rePPI-G continued.
low (J23117 promoter) and high (J23114 promoter) $RNAP_N$ expression levels. (B) Luminescence data obtained with the ZB-Fyco1 molecular glue with an off-target PPI (KRas and ZA) and two on-target PPIs (LC3B or GABARAP and ZA). (C) PACE of eZB-ULK1 (blue) and ZB-ULK1 (gray). Dashed lines represent background RNAP assembly as reported in Figure 4.S6. * = $p < 0.05$, ** = $p < 0.005$, *ns* = $p > 0.0$

Rapidly overcoming local activity minima in rePPI-G

Similar to an activity minimum, immeasurable starting activity is a common roadblock when carrying out PACE experiments. This challenge has typically been overcome by performing numerous rounds of phage assisted noncontinuous evolution/selection (PANCE/S) or traditional antibiotic selection screening[216-218]. Although these methods can take months to develop and achieve suitable activity to begin a PACE experiment, they are excellent at amplifying rare variants from a large pool. We hypothesized that a short round of "Phage-Assisted Non-Continuous Selection" (PANCS), a combination of PANCE[216] and PACS[207], could quickly amplify rare PACE variants capable of escaping the PPI inducer activity minima.

Before performing the PANCS experiment, we first amplified the final phage titers from previous PACE experiments in a selection-free manner using 1059 cells, which supply gIII in an activity-independent manner[199]. Next, we diluted these phage 10,000-fold into host *E. Coli* cells identical to those used in the PACE experiment, which express $RNAP_N$-tagged ZA, $RNAP_C$-tagged GABARAP, and gIII when the RNAP is assembled. Importantly, we decided not to include a mutagenesis plasmid, thereby both decreasing the chance of genetic recombination and testing our hypothesis that highly mutated variants existed in the PACE. After the first round of PANCS the phage populations increased 630- and 158-fold (Figure 4.5A). We then performed another round of PANCS by diluting each sample to a concentration of ~10^5 phage/mL and incubating them overnight with host cells. Both phage populations increased 10,000-fold after the

second round of PANCS, indicating the phage population had developed increased PPI induction efficacy. We then combined the PANCS amplified phage populations and subjected them to a final PACE experiment. After three days of PACE, phage achieved 20,000-fold greater titers than eZB-ULK1 inducer phage under continuous flow (Figure 4.5A). Moreover, the final phage population was more readily detectable using one of the most stringent assessments of phage activity, the activity dependent plaque assay. This experiment is similar to an overnight growth assay, except the phage and host cell mixture are incubated together in an agar gel matrix[213]. Only phage that acquire enough gIII to replicate robustly can inhibit host cell growth to a degree that is detectable by eye. After the first PACE experiment plaques were noticeable, but not robust. After the PANCS and second PACE experiment plaques were very clearly visible (Figure 4.5A).

Characterization of evolved eZB-ULK1 variants

Having successfully evolved the phage to replicate significantly more than wildtype, we Sanger sequenced the phage from each PACE experiment to assess the mutations in each binding partner. The first three PACE experiments resulted in three unique dominant phage. The mutant from the first PACE, ZU(1), had a deletion at base pair 1081 that changed the ending ULK1 coding sequence from -PAQFPGDLVA* to the remarkably similar, yet more positively charged -PRNFRGT* (Figure 4.5B). The mutant from the second PACE experiment, which included an increase in selection pressure after 48h, produced a phage, ZU(1*) with a deletion at base pair 1084 that resulted in the identical amino acid sequence. The replicate of the original PACE experiment did not produce any deletion mutants, instead resulting in a double mutant in the ULK1

sequence, ZU(2). Phage resulting from the PANCS and final PACE experiment, ZU(3), contained the ULK1 base pair 1081 deletion along with a threonine-to-alanine mutation within the amino acid sequence after the base pair deletion (T*21A). Furthermore, this variant had three mutations in the eZB domain (A1T, Q18R, W21R). These evolved inducers were cloned into the IPTG-inducible plasmids used previously and assessed for improved induction of the ZA and GABARAP PPI. Both ZU(1) and ZU(2) had 6- to 10-fold increases in RNAP activity at all concentrations of inducer, as compared with wildtype phage (Figure 4.5C). Strikingly, these mutants also had nearly identical activity profiles at all IPTG concentrations. These mutants also exhibited no increase in RNAP activity between moderate and high inducer expression at lower $RNAP_N$-tagged ZA expression levels (Figure 4.S8), indicating a measurable “hook” effect. On the other hand, ZU(3) possessed 40- to 95-fold increased activity compared to the wildtype PPI inducer, a >2000-fold overall signal to noise ratio at maximum expression, and no “hook” effect, even with low $RNAP_N$-tagged ZA expression (Figures. 4.5C and 4.S8). Importantly, none of the variants dramatically increased off-target ZA-LC3B PPI induction, meaning the mutations did not impact overall split RNAP assembly and activity. After confirming the evolution was successful, we sought to characterize how these mutations impact the individual PPIs in our engineered and evolved bifunctional molecular glues.

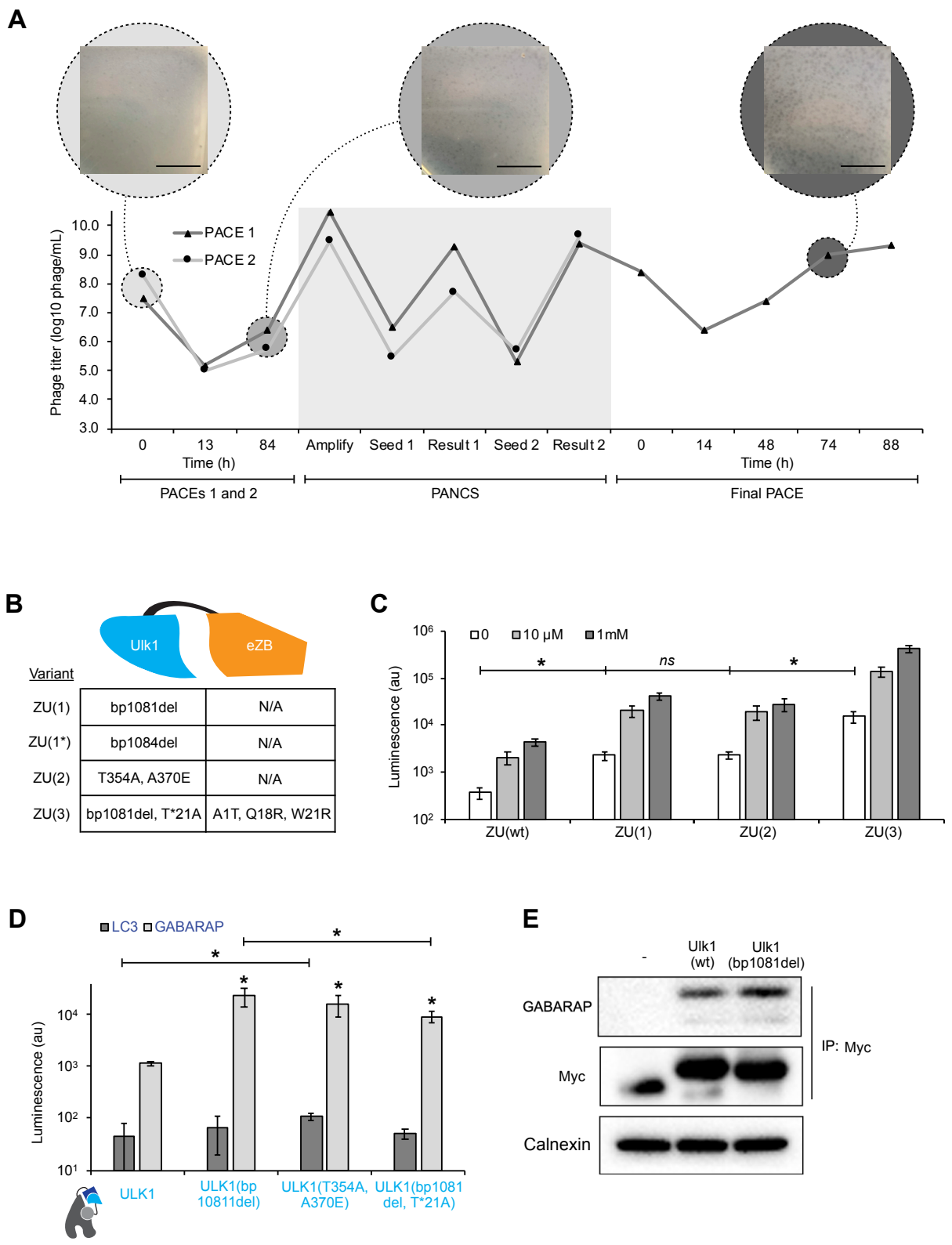

Figure 4.5. Combination of continuous and noncontinuous phage assays escape local activity minima in rePPI-G. (A) Phage titers across full eZB-ULK1 molecular glue

Figure 4.5. Combination of continuous and noncontinuous phage assays escape local activity minima in rePPI-G continued.
evolution including original PACE, PACE replicate, PANCS (light background), and final PACE along with pictures of activity dependent plaque assay results at different time points (scale bar = 1cm). (B) Common mutations discovered from rePPI-G eZB-ULK1 evolutions. (C) Luminescence data measuring each IPTG inducible eZB-ULK1 variant's ability to induce the interaction between $RNAP_N$-tagged ZA and $RNAP_C$-tagged GABARAP. (D) Luminescence results from $RNAP_N$-tagged ULK1 rePPI-G variants paired with either $RNAP_C$-tagged LC3B (dark) or GABARAP (light). (E) Co-immunoprecipitation of Myc-tagged ULK1 or ULK1(bp1081del) to measure GABARAP pulldown efficiency with calnexin loading control and Myc output control.

We cloned each unique ULK1 variant to the $RNAP_N$ to assess changes in the ULK1/GABARAP interaction. Both the ULK1(bp1081del) and ULK1(T354A, A370E) mutants had a 20-fold increase in RNAP activity compared to ULK1(wt) when paired with GABARAP (Figure 4.5D). Interestingly, the ULK1(T354A, A370E) mutant also had a small, yet significant, 2-fold increase in LC3B binding. Somewhat surprisingly, the ZU(3) ULK1 mutant had a ~2-fold decrease in GABARAP binding compared to the ZU(1) and ZU(2) ULK1 variants. To determine how the ZU(3) inducer evolved to radically improve overall inducer activity, we cloned its eZB mutant as a fusion to the $RNAP_C$. We observed no difference in RNAP activity between eZB(A1T, Q18R, W21R) and eZB when interacting with ZA, but we did observe a small, significant increase in RNAP activity when ZB(A1T, Q18R, W21R) interacted with the off-target tBID (Figure 4.S9). Binary binding assays with ULK1 variants and LC3B confirmed that these mutations also conferred a small increase in binding affinity to these off-target proteins (Figure 4.S10). We next cloned eZB and eZB(A1T, Q18R, W21R) into IPTG inducible plasmids to assess whether this new promiscuous peptide was capable of inducing a PPI between either ZA and LC3B or ZA and GABARAP. We observed a small, yet significant, increase in RNAP signal when the eZB(A1T, Q18R, W21R) peptide was

expressed at its highest concentration and inducing the interaction between ZA and LC3B (Figure 4.S11). It is possible that these nearly undetectable interactions reflect the molecular glue's ability to bring multiple proteins within close proximity to one another.

Finally, we validated that changes in PPI affinities observed and optimized in *E. Coli* translate to mammalian cell experiments. To measure induced PPIs in mammalian cells, we inserted the highest affinity ULK1 mutant – ULK1(bp1081del) – within a Myc-tagged protein, and then performed a co-immunoprecipitation to probe for its interaction partners, GABARAPL1-1/2. Expression of the ULK1(bp1081del) mutant construct pulled down significantly more endogenous GABARAP protein compared to the ULK1(wt) sequence (Figure 4.5E). Expression of the Myc-tagged protein alone resulted in no GABARAP signal, confirming this interaction is dependent on the ULK1 peptide. Experiment replication and image quantification confirmed this observation is consistent and significant (Figure 4.S12).

4.3 Discussion

During our validation of rePPI-G, we discovered affinity-altering mutations that parallel those found in previous studies. For example, our group used PACS to perform deep mutational scanning on the KRas/Raf1 interaction interface[207]. While most mutations in Raf1 resulted in either no change or a decrease in enrichment, N71K resulted in the most positive enrichment score, indicating this mutation increases the interaction affinity. Not only did we also observe the N71K mutation in this work when evolving the ZB-Raf1 inducer, but we also confirmed it increases the interaction affinity between KRas and Raf1 ~3-fold (Figure 4.3). Crystal structures of the PPI complex reveal that the Raf1 N71 residue is ~2.5 Å away from the negatively charged D33 residue on KRas, an optimal distance for a potential salt bridge interaction[208]. The mutations discovered in our eZB-ULK1 evolution also matched those found in previous studies by other groups. In-depth point mutation screens of the ULK1 LC3 interaction region (LIR), the same peptide used in our evolution, revealed T47 as a key residue for LC3B binding[215]. This observation mirrored the T47A, A63E double mutant discovered in our evolution that demonstrated a small yet significant increase in LC3B binding when compared to the wildtype ULK1 peptide (Figure 4.5D). These data, along with the mammalian cell co-immunoprecipitation experiment and previous work[84, 131, 207], support the theory that observed changes in activity translate beyond the split RNAP system to biologically relevant interactions.

While designing and validating rePPI-G we also learned several key lessons in bivalent inducer engineering. The “hook” effect makes fine-tuning any PPI inducer a challenge,

particularly in a therapeutic context, where target protein concentrations are dynamic and uncontrollable. We consistently found that alterations in protein binder affinity were sufficient to overcome the “hook” effect. When inducing a tBID/KRas interaction, for instance, the higher affinity Bcl_{xL}/tBID interaction results in a dramatic “hook” effect relative to the Mcl1/tBID interaction (Figure 4.1D). In the case of the ZB-Raf inducer evolution, all ZB mutations resulted in weaker ZA binding. This not only diminished the “hook” effect, but also produced more ZA/KRas interaction at all expression levels, implying changes that reduce the “hook” effect may actually produce an overall more efficient PPI inducer (Figure 4.3B and 4.4C). Finally, in the case of the eZB-ULK1 inducer, we found that increasing the potency of one ligand (ULK1) provided increased potency until a “hook” effect developed, at which point the paired protein binder (eZB) became the limiting factor in increasing inducer potency (Figure 4.5). These results make it clear that increased interaction affinity of one protein binder does not always result in overall increased molecular glue potency. Together, these findings suggest a new strategy for discovering bivalent PPI inducers, including PROTACs, wherein binders with different affinities for protein “A” and protein “B” are screened as a matrix of unique bivalent molecules to discover the optimal molecular glue for each target interaction.

In this proof-of-concept work, engineered bifunctional molecular glues – which already have affinity for both targets – were our starting point, but rePPI-G could in principle use naïve libraries to evolve molecules *de novo*. While theoretically feasible, implementing phage libraries in PACE often presents technical challenges, including gIII

recombination or limited library size, that preclude identification of functional starting points. Nonetheless, based on our results here and in previous PACE-based evolutionary campaigns[216-218], a combination of PANCE/PACS with PACE may be the solution to implementing libraries with rePPI-G. An advantage of the rePPI-G pipeline is that the same split RNAP-based biosensors used for the evolution can also be used to measure target activity in live mammalian cells[132, 211]. Most recently, we showcased a PPI evolution system for PACE that features both positive and negative selection, which permitted the rapid reprogramming of PPI specificity via PACE[131], further demonstrating the potential of PACE-based evolutions and suggesting the rePPI-G platform can be expanded to evolutions of selective molecular glues.

This work showcases evolution as a strategy to find unique and even unimaginable solutions to biological challenges. In the case of eZB-ULK1, rePPI-G discovered single base pair deletions that dramatically increased individual PPI affinity and a triad of mutations that conferred a subtle promiscuity resulting in optimized molecular glue activity. More broadly, now that we have validated the proximity dependent split RNAP as a system to select for and evolve molecular glues, this opens up the possibility of implementing this selection scheme with other evolution technologies. For example, implementing the molecular glue selection with the yeast-based Orthorep, mammalian-based mPACE, or VEGAS systems would allow for evolution of molecules that drive the interactions between proteins that cannot be expressed in *E. coli*, a key limitation of PACE-based methods[201-204]. As the repertoire of rapid evolutionary technologies

expands, so too will our ability to harness evolution to solve problems in synthetic biology and therapeutic design.

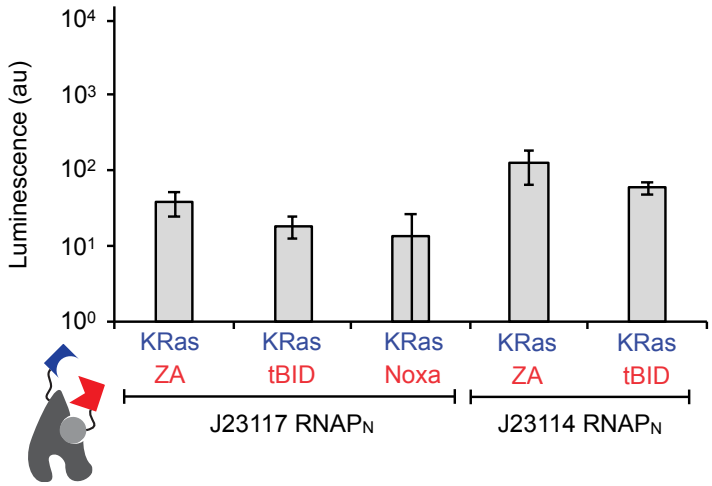

Figure 4.S1. Background RNAP assembly without molecular glue induction. Background luminescence signals from different combinations of RNAP$_N$-tagged protein fusions (red) and RNAP$_C$-tagged protein fusions (blue) at low (J23117) and high (J23114) RNAP$_N$ expression levels.

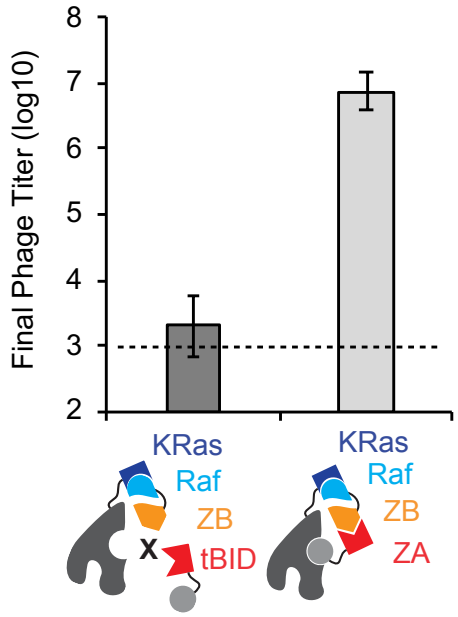

Figure 4.S2. Molecular glue-dependent phage replication. Overnight growth assays quantifying molecular glue expressing phage replication without an interaction (dark) compared to with an interaction (light)

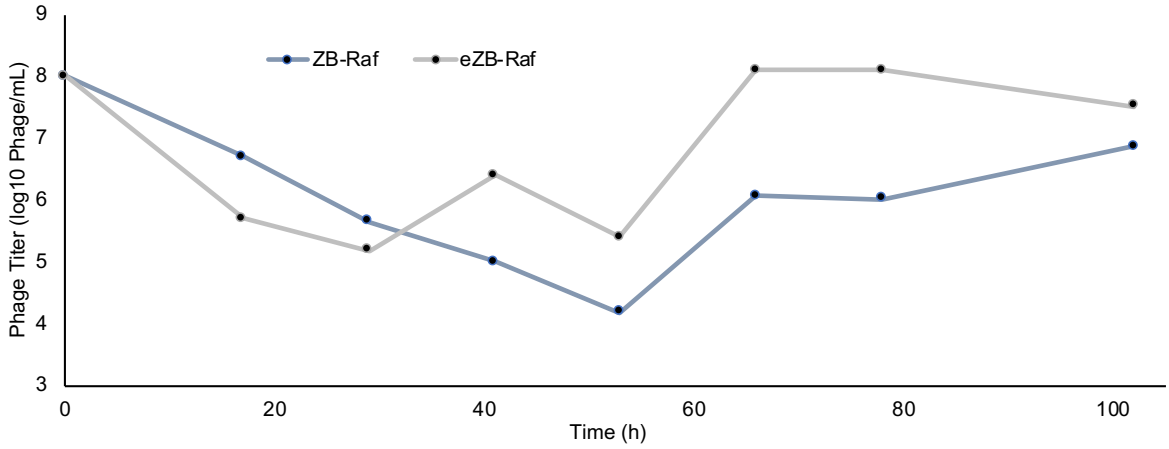

Figure 4.S3. Negative selection PACE experiment. PACE that includes a negative selection plasmid to prevent mutations that induce general binding to off-targets. This experiment was conducted starting with either ZB-Raf (blue) or the previously PACE-evolved ZB-Raf (gray) molecular glue phage.

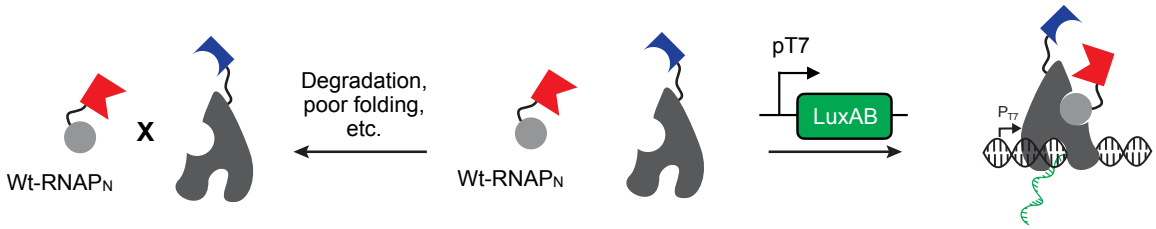

Figure 4.S4. Wildtype RNAP$_N$ can predict split RNAP compatibility. Schematic demonstrating how the wildtype RNAP$_N$ can be used to detect protein folding, degradation, and impact on RNAP assembly.

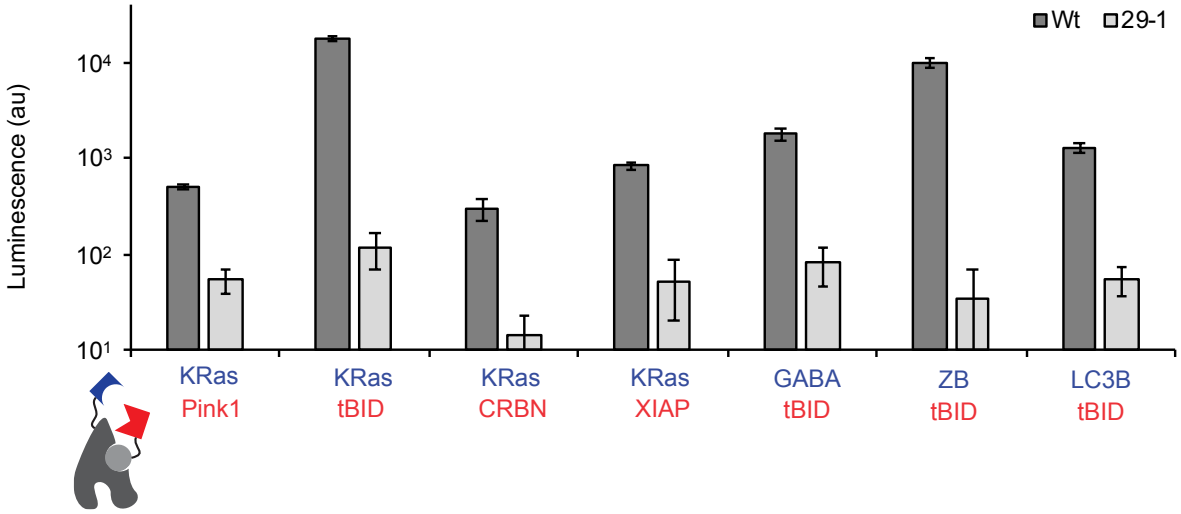

Figure 4.S5. Identifying new rePPI-G target proteins. Luminescence signals from different combinations of either wildtype (dark) or mutant (light) RNAP$_N$-tagged protein fusions (red) and RNAP$_C$-tagged protein fusions (blue).

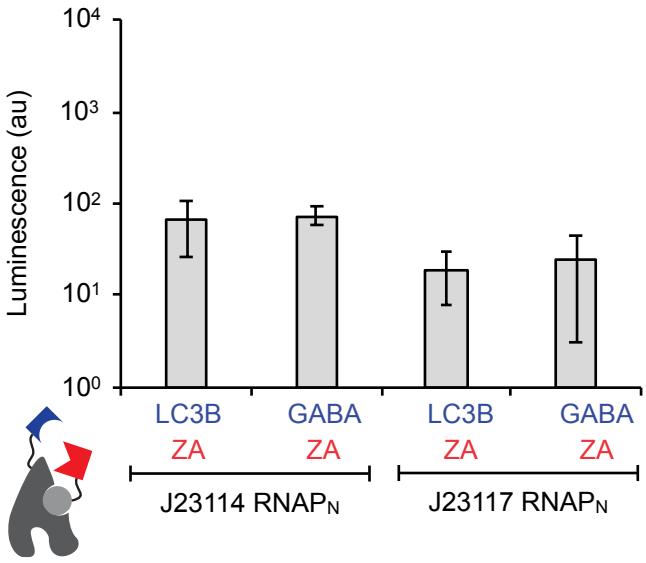

Figure 4.S6. Background RNAP assembly without molecular glue induction. Background luminescence signals from different combinations of $RNAP_N$-tagged protein fusions (red) and $RNAP_C$-tagged protein fusions (blue) at low (J23117) and high (J23114) $RNAP_N$ expression levels.

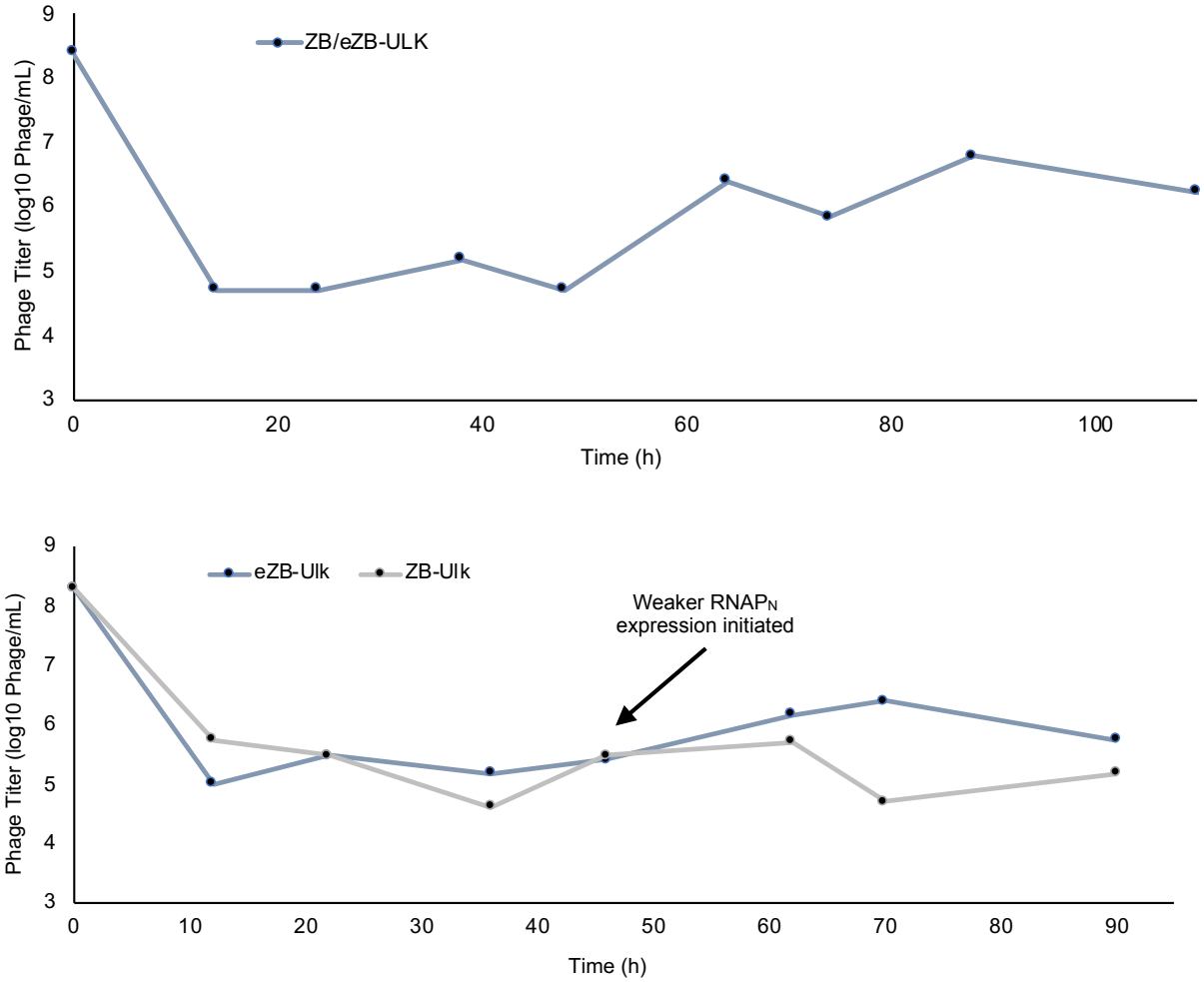

Figure 4.S7. Replicates of rePPI-G with ZB-Ulk1 molecular glue. A replicate of the original ZB- and eZB-Ulk1 evolution using a mixture of the two phage as the starting point (top). Replicate of the original ZB- and eZB-Ulk1 evolution until 48h when cells expressing lower levels (J23117) of RNAP$_N$-tagged ZA replaced the original evolution cells (bottom).

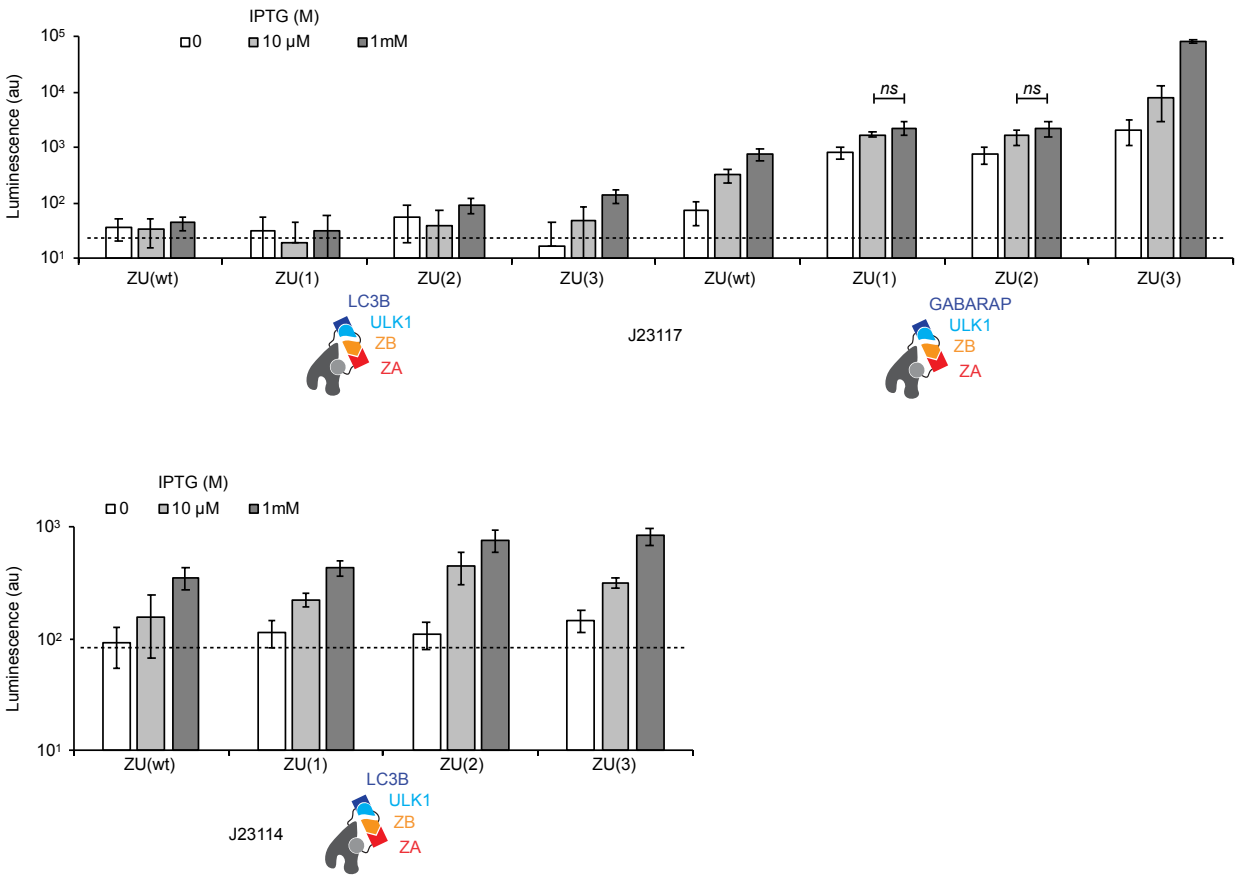

Figure 4.S8. ZB-ULK1 rePPI-G variants and background activity. Luminescence data of ZB-ULK1 rePPI-G variants inducing the interaction between GABARAP or LC3B and ZA at low (top) and high (bottom) $RNAP_N$-tagged ZA concentrations. Dashed lines indicate background RNAP assembly based on data from Figure 4.S6. *ns* = p > 0.05

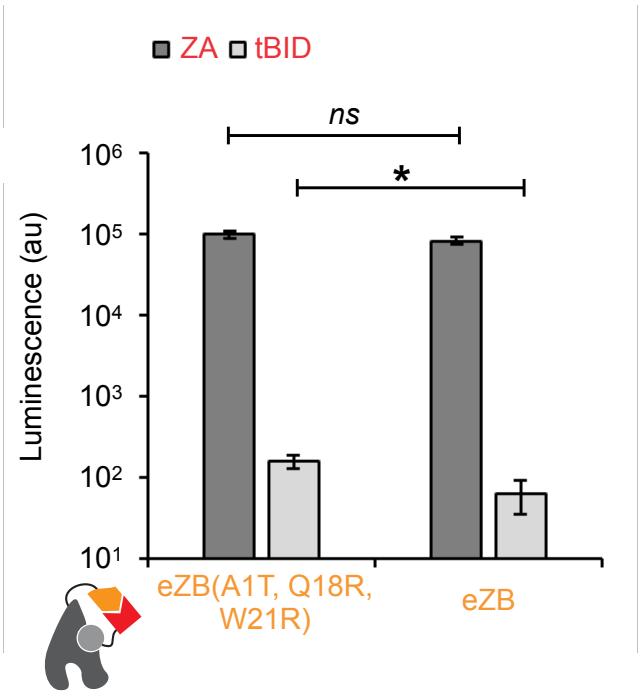

Figure 4.S9. Changes in eZB binding of ZA after rePPI-G. Luminescence data comparing the binary interaction between ZA (dark) or tBID (light) and eZB or eZB(A1T, Q18R, W21R). * = $p < 0.05$, *ns* = $p > 0.05$

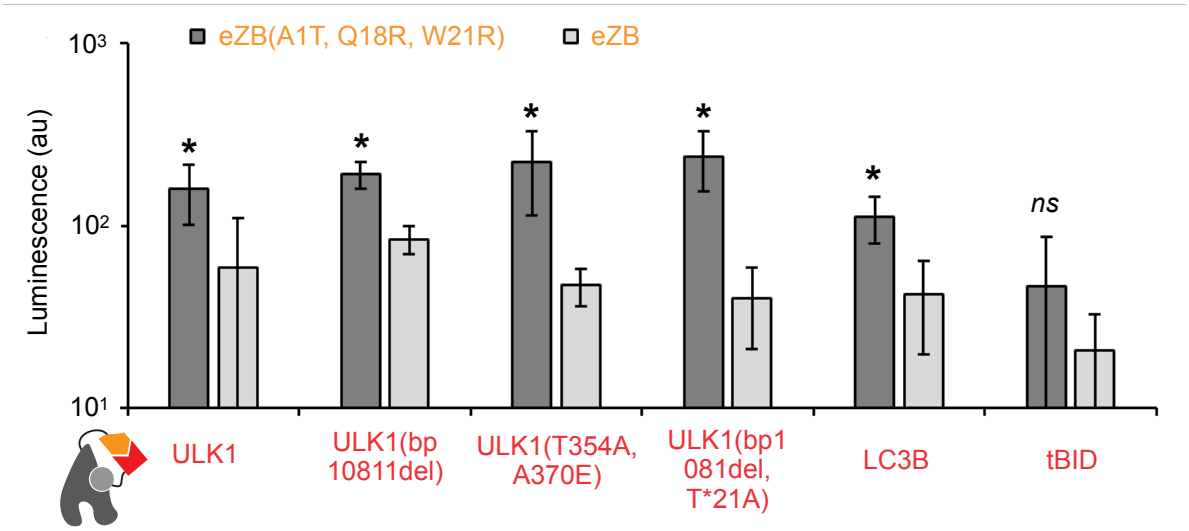

Figure 4.S10. Changes in eZB binding of off targets after rePPI-G. Luminescence data comparing the binary interaction between eZB(A1T, Q18R, W21R) (dark) or eZB (light) to ULK1 variants, LC3B, or tBID expressed using the stronger J23114 promoter. Statistical comparisons were made between eZB and eZB(A1T, Q18R, W21R). * = $p < 0.05$; *ns* = $p > 0.05$.

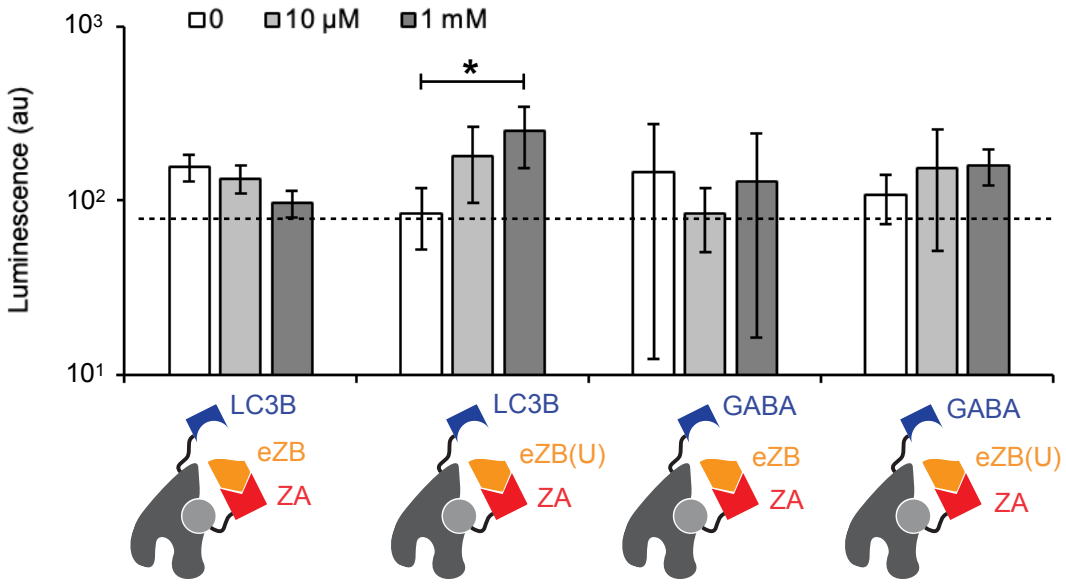

Figure 4.S11. Assessment of eZB(A1T, Q18R, W21R) as independent PPI inducer. Luminescence data from induced binary interactions between LC3B (left) or GABARAP (right) via expression of either eZB or eZB(A1T, Q18R, W21R), termed eZB(U) here. ZA expressed using the stronger J23114 promoter. * = $p < 0.05$

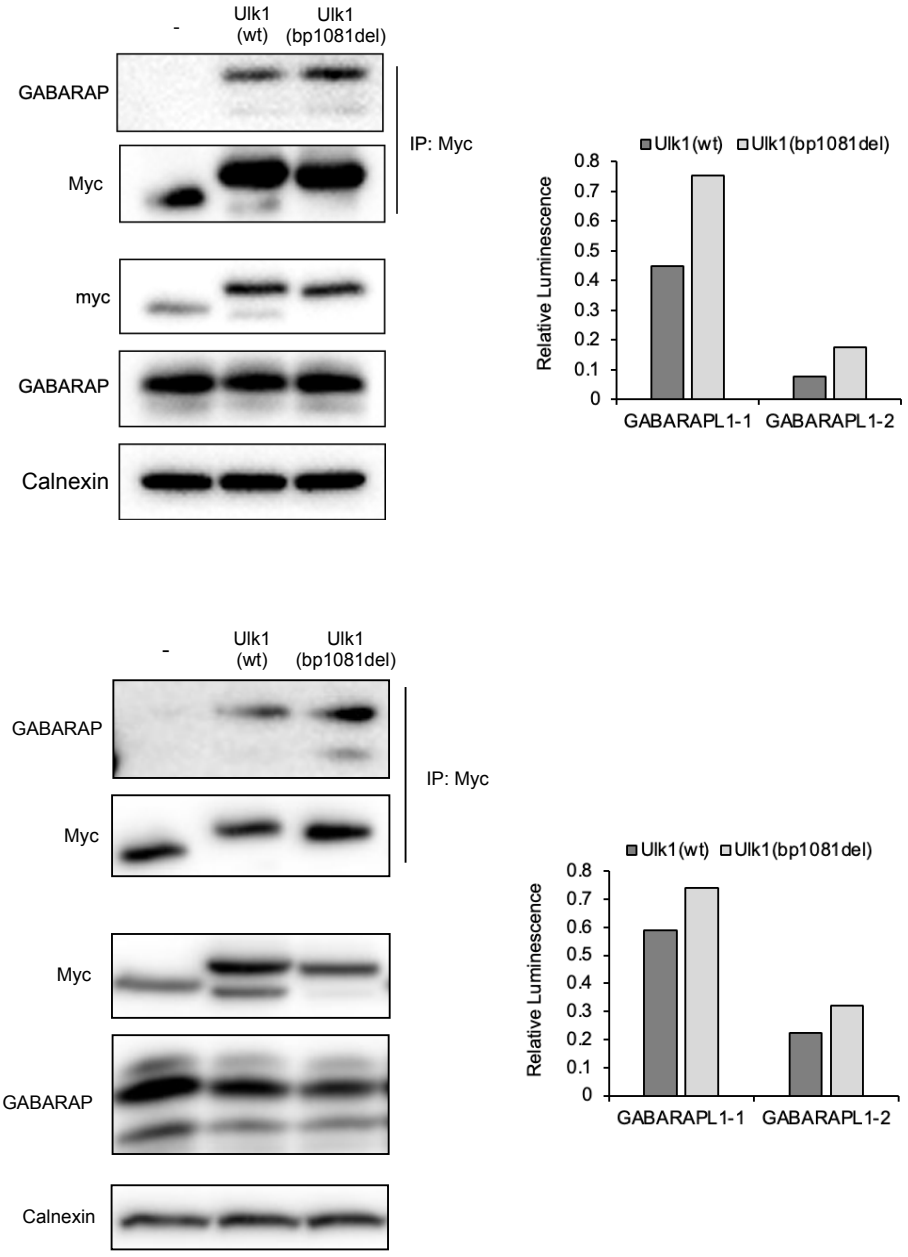

Figure 4.S12. Co-immunoprecipitation of GABARAPL1-1/2 using either ULK1(wt) or ULK1(bp1081del). Hek293T cells transfected with Myc-tagged proteins with an internal Ulk1(wt) sequence, Ulk1(bp1081del) sequence, or no Ulk1 sequence (dash) were immunoprecipitated to assess GABARAPL1-1/2 interaction affinity. Calnexin was used as a loading control, and images were quantified using the ratio between output GABARAPL1-1 or GABARAPL1-2 and output Myc-tagged protein construct.

4.4 Methods

DNA Plasmid Cloning

All plasmids were cloned using Phusion or Q5 DNA polymerases (NEB) for PCR amplification of specific DNA fragments, Gibson Assembly to generate new plasmids from PCR fragments, DH10β *E. Coli* cells for transformation, and Sanger Sequencing via the University of Chicago Comprehensive Cancer Center DNA Sequencing and Genotyping Facility to verify plasmid sequence fidelity and integrity[112]. DNA primers were ordered from Integrated DNA Technologies (IDT) or Sigma-Aldrich. All plasmid maps, descriptions, annotations, and gene DNA/amino acid sequences are available in supplementary materials online along with links to full DNA sequences for each plasmid used in this study. Additionally, key vectors will be deposited to Addgene for distribution and all vectors are available upon request.

Split RNAP luciferase assay in *E. Coli*

Chemically competent S1030 or S2060 *E. Coli* cells (available from Addgene) were transformed with $RNAP_N$ and $RNAP_C$ fusion protein plasmids that also contain T7 driven LuxAB. If a third plasmid is needed, as is the case when testing a PPI inducer, chemically competent cells of the doubly transformed *E. Coli* were prepared and transformed with the third plasmid. *E. Coli* colonies were then picked in quadruplicate into 500 µL of LB (miller) broth (US Biological Life Sciences) with antibiotics (GoldBio) in a 96-well deep well plate and incubated in a shaker at 220 RPM for 12-16h overnight. 10 µL of each overnight growth was then transferred to 500 µL of LB media containing antibiotics and any inducing small molecule such as IPTG (GoldBio). After 4-5h when

the cells are between 0.3 and 0.5 OD_{600}, 150 µL of cells were transferred to a 96-well imaging plate (costar) and assayed for luminescence and OD_{600} on a Synergy Neo2 hybrid multimode plate reader (BioTek Instruments, Inc.).

Quantifying Phage Titer with Plaque Assays

Chemically competent S1030 or S2060 *E. Coli* cells (available from Addgene) were transformed with plasmid 6-64 that contains phage shock promoter driven gIII. These cells are also termed 1059 cells here and in the literature. A colony of 6-64 containing cells was picked into antibiotics media and grown to 0.5-0.9 OD_{600}, or grown overnight and diluted to 0.5-0.9 OD_{600}. 50 µL of diluted 6-64 cells were then aliquoted into 4 1.5 µL Eppendorf tubes for each phage sample to be measured. 1 µL of phage sample was pipetted to the first tube, mixed vigorously by flicking, and then 1 µL of that solution was transferred to the next tube using a new tip to prevent inflated titers. This serial dilution was repeated for the remaining tubes so that the final tube represents a 125,000,000x dilution from the original phage sample. 750 µL of 50 °C top agar (7 g/L agar, 25 g/L LB broth) was added to each tube and then quickly transferred in order of increasing phage concentration to a 10 cm quad plate coated in bottom agar (15 g/L agar, 25 g/L LB broth). Plaques should be visible after 12-24h and can be counted to quantify phage titer. Note: place warm top agar in a tight-fitting Styrofoam container whenever pipetting at room temperature to delay agar solidification.

Quantifying Phage Activity with Overnight Growth Assays

To quantitatively compare phage activity between samples, we first measured each sample's phage titers as described above. Next we diluted each phage sample in LB broth containing appropriate antibiotics to the same titer (final concentration between 1000 and 10,000 phage/mL for best signal to noise). 500 µL of the diluted phage were added to a 96 deep well plate in triplicate. A colony of S1030 or S2060 *E. Coli* cells containing the desired activity selection plasmids (for example tagged split RNAP biosensors) was picked into each well and the plate was incubated for 24h. The contents were spun down and immediately used in a plaque assay to quantify final phage titers as described above.

Phage Assisted Continuous Evolutions

For the most in depth and up to date protocol for performing a phage assisted continuous evolution (PACE) see the following reference[200]. One significant difference in all of our PACE protocols is that we use a more affordable Forma 3960 environmental chamber (ThermoFisher Scientific) rather than a warm room to house and conduct PACE experiments[84]. To perform rePPI-G specifically, we first transformed S1030 *E. Coli* cells with an MP4 mutagenesis plasmid (available from Addgene), an $RNAP_N$-tagged protein expression vector, and an $RNAP_C$-tagged protein expression vector that also contains CGG driven gIII expression. These cells were plated on LB agar containing appropriate antibiotics along with 20 mM glucose to suppress the MP4 mutagenesis plasmid activity. The next day, a single colony was picked for each chemostat into two 15 mL culture tubes with 6 mL of LB media, and one tube containing

20 mM glucose and the other containing 20 mM arabinose. Davis Rich Media (also called Harvard Custom Media C, US Biological Life Sciences) was prepared or purchased and autoclaved in 7.5L batches. Davis Rich Media supplement (also called Harvard Custom Media A, US Biological Life Sciences) was prepared or purchased and sterile filtered as previously described in the references above. The media base was added to the environmental chamber to equilibrate to 37 degrees Celsius overnight. The next day the sterile filtered supplement was added to the media base by a flame to prevent contamination. After 14-16h of growth, the arabinose induced cells were checked for greatly diminished growth compared to the glucose repressed cells, which suggests an active MP4 plasmid. The glucose-containing tube was added to a 500 mL chemostat and 100-200 mL of Davis Rich Media at 37 degrees Celsius was pumped into the chemostat over the course of two hours. Once cells reached approximately 0.4-0.8 OD the lagoon pump was activated to allow chemostat cells to fill the 50 mL lagoons to a volume of 20 mL at a flow rate of 1 v/h. Syringes containing 20% w/v arabinose and 18 mM $MgSO_4$, which we find improves phage titers by ~5 fold, in water began pumping into each lagoon at a rate of 0.5 mL/h. To activate “drift” cells, 2 µg/mL of tetracycline (GoldBio) was added to the syringe solution along with the previously mentioned arabinose and $MgSO_4$. The PACE system was allowed to equilibrate concentration for 1-2h before adding 1 mL of the desired phage at a concentration of of $>10^9$ phage/mL to each lagoon, at which point the lagoon and syringe pumps were paused for 30-60 minutes to provide phage ample time for initial host cell infection. After 30-60 minutes, the syringe and lagoon pumps were reactivated. Samples were extracted from lagoons in the morning and evening, and plaque assays performed each day to monitor phage

titer. 1 μL of phage sample was then directly added to a PCR to amplify phage variants for Sanger sequencing. New chemostats were added after 48h to ensure cells remained at maximal infectivity. Also, all chemostats and lagoons were kept below 50% maximum volume and constantly stirred via magnetic stir bars to ensure cells were properly aerated.

Phage Assisted Noncontinuous Selection

For the most detailed and up to date protocol on PANCE experiments see the following reference[200]. PANCS experiments were carried out as follows. 50 μL of phage samples from PACE experiments were added to 5 mL of LB broth along with a colony of 1059 cells. After 24h of growth the sample was spun down, and the supernatant was passed through a 0.2 μM filter to remove all *E. Coli* cells while collecting phage. Phage titer was measured as described above. Phage samples were diluted 10,000x into 500 μL LB broth along with 1% by volume of overnight selection cell culture. Samples were grown at 37 degrees Celsius for 20-24h, spun down, and then phage titer was quantified. The resulting phage were passed through a 0.2 μm filter to remove all *E. Coli* cells and then diluted to a final phage titer of 10^5 phage/mL in 500 μL LB broth along with 1% by volume of overnight selection cell culture. As with PACE samples, 1 μL of phage sample was then directly added to a PCR to amplify phage variant DNA for Sanger sequencing. This cycle can be repeated with variable phage dilution or selection cells to alter selection pressure until desired activity emerges indicating a successful selection or phage titer drops below 10^3 phage/mL indicating no active phage were present in the original sample.

Mammalian Cell Culture

HEK293T cells (ATCC) were maintained in DMEM (high glucose, L-glutamine, phenol red, sodium pyruvate; obtained from Gibco or Hyclone) supplemented with 10% fetal bovine serum (FBS, Gibco/Life Technologies, Qualified US origin) and 1% penicillin/streptomycin (P/S, Gibco/Life Technologies). Multiple biological replicates were performed with cells from different passages below 20 and freshly thawed aliquots. Transfections were carried out using Lipofectamine 3000 (Thermo Fisher).

Co-Immunoprecipitation of Myc-tagged Proteins

For co-immunoprecipitation, cells were lysed in SDS-free RIPA (0 mM Tris, 150 mM NaCl, 0.5% deoxycholate, 0.1% SDS, 1.0% Triton X-100, pH 7.4) supplemented with PMSF and a protease inhibitor cocktail on ice for 10 minutes, followed by centrifugation at 13,000xg for 20 min. Protein (20 µg, “input”) was removed and lysate was added to Protein G Dynabeads (Invitrogen: 10003D) pre-incubated with c-Myc antibody (Santa Cruz sc-40). After 12 hours of enrichment, beads were washed (3x, SDS-free RIPA) and total protein eluted with 50 mM glycine, “output.” Both input and output protein were subjected to separation by SDS-PAGE. After SDS–PAGE, proteins were transferred onto methanol-preactivated Immobilon-P PVDF membranes (pore size 0.45 µm; Millipore) using a semi-dry transfer cell. After transfer, membranes were treated in accordance with standard Western blotting procedures, using a solution of 3% BSA (ThermoFisher) in either TBST (20 mM Tris, pH 7.5, 150 mM NaCl, 0.1% Tween-20). Membranes were probed with GABARAP (Abcam), c-Myc (Santa Cruz), and calnexin

(Abcam) antibodies overnight. Following secondary antibody incubation, membranes were visualized using SuperSignal West Pico PLUS chemiluminescent substrate (ThermoFisher) and recorded on a chemiluminescent Western blot imaging system (Azure Biosystems C300).

Chapter 5

SUMMARY AND PERSPECTIVES

The criticality of PPIs cannot be overstated. Many methods exist to measure individual PPIs, but few exist that can measure multidimensional and completive PPI dynamics. Even if a select PPI is identified to have a role in disease, disrupting that PPI selectively is a nearly impossible task for small molecule inhibitors, in part due to a poor understanding of PPI compensatory mechanisms in cells. Besides understanding how inhibitors alter multiprotein systems, inducing a new multiprotein system with a PPI inducer is a little pursued goal. Unlike with PPI inhibitors, this is not due to a lack of success in clinical trials. Instead, it is difficult to know which induced PPIs would alleviate disease because there is no versatile toolkit to systematically screen induced PPIs in cellular contexts. In this thesis I detailed research in developing two key methods - the only method to simultaneously monitor four PPIs in live mammalian cells and the only directed evolution method to optimize PPI inducers. Both methods are dependent on the split T7 RNA polymerase biosensor that our group evolved and showcased in 2017.[84] Although in their proof-of-concept stage, I hope these methods generate new tools to study and modulate multiprotein systems. In this last section I will expound upon future experiments these new methods may enable.

In this thesis I described using multiple orthogonal split RNAP tags to monitor four PPIs and their selective inhibition simultaneously. However, these split RNAP tags could be used to study other interesting biological phenomena. The split RNAP tags are only effective when a DNA template is present. Specifically, PPI events in the cell nucleus

and selective induction of PPIs. The most viable area to deploy split RNAP tags in cells is the nucleus because the RNAP is only effective when a DNA template is present. Thus, using split RNAP tags to investigate PPI dynamics specifically in the nucleus is a promising next endeavor. For example, transcription factors and RNA splicing machinery are regulated by a dynamic network of nuclear PPIs.[219-221] Understanding how these networks change with various stimuli could lead to a better understanding of how pharmacological inhibitors might alter these dynamics positively or negatively.

There are two simple changes that are necessary in order to deploy split RNAPs in the nucleus. The first is a nuclear localization signal added to the RNAP tag.[222] This signal will trigger both components of the RNAP to primarily remain within the nucleus where both the protein target naturally and RNAP DNA template reside. The second change is cloning multiple different expression plasmids for each RNAP half to tune protein concentrations in a way that maximally reduces background assembly. Protein concentrations in the nucleus will initially be roughly ten times higher given the nucleus is roughly one tenth the volume of the cell. Our group and others have already tested mammalian expression plasmids with variable expression based on altered variants of the CMV promoter.[223] However, we have yet to assess these in the context of split RNAPs in the nucleus.

Another exciting use of split RNAP tags is a subcategory of nuclear PPI measurement – screening of small molecule proteolysis targeting chimeras (PROTACs). PROTACs are molecules composed of an E3 ligase binding small molecule, a linker, and a target

binding small molecule.[171] PROTACs bridge the interaction between E3 ligases and target proteins, ubiquitinylating the target, which signals its degradation. Recently PROTACs have been developed for BRD4, a nuclear transcription factor upregulated in various cancers, and several other nuclear target proteins.[224] One challenge when developing PROTACs is ensuring they are capable of both penetrating the cell membrane and nuclear pores while retaining potent binding to the target of interest.[225] As was discussed in chapter 4, PROTACs are also subject to the hook effect, and so changes in protein or small molecule concentration, which would occur in the cell nucleus versus in vitro, can alter PROTAC efficacy. One half of the split RNAP could be tagged to a catalytically inactive nuclear E3 ligase, such as VHL, while the other is tagged to a on target and off target proteins, such as BRD1-4. The selective interaction between different PROTACs could thus be measured using split RNAP tags.

The other method developed in this thesis work is the rapid evolution of protein-protein interaction glues (rePPI-G) discussed in chapter 4. I successfully optimized multiple PPI inducers in a matter of days, analyzed how the molecular changes from each evolution, and laid out a protocol that spans from target screening to overcoming local binding minima in evolutions. One next step is to screen random phage-encoded libraries in rePPI-G to discover *de novo* PPI inducers. This would eliminate the requirement for known protein binding partners, enabling PPI inducers to be generated for any protein pair that express in *E. Coli*. This is a common challenge facing PACE-based methods. Indeed, no PACE has evolved activity from fully randomized amino acid sequences. My recent experience overcoming local activity minima using a combination of PACE and

PANCS to led me to hypothesize that discovering *de novo* PPI inducers from phage libraries would require a similar process. My initial experiment consisted of subjecting a phage encoded library of randomized linear peptides to two rounds of PANCS (data not shown). I observed no increase in phage titer, but decided to use these phage in a PACE experiment. When I began the PACE with the library itself the phage quickly decreased in titer until none were detectable. When on the other hand I began a PACE with the PANCS-ed library phage titers always increased to very high levels (~10^9 phage/mL). Unfortunately, these phage were able to replicate in a PPI inducer independent manner, meaning a copy of gIII had recombined into their genome, eliminating the need for a PPI inducer to activate the split RNAP. From my experience, PANCS does not result in phage recombination, perhaps due to low overall phage and *E. Coli* titers. Library preparation on the other hand requires very high concentrations of phage and *E. Coli* (~$10^{10\text{-}12}$), which increase the chance of gIII protein recombination. Thus, altering phage library preparation protocols to decrease phage and *E. Coli* concentrations may enable *de novo* PPI inducer discovery.

The methods described in this thesis work, multidimensional split RNAP tags and rePPI-G, will hopefully contribute to exciting developments in studying multiprotein biology and PPI modulator development. Moreover, the limitations and strengths of each technology were analyzed to understand where they can be immediately applied to yield scientific discoveries. I hope this thesis work lays a solid foundation on which future scientists can build their research.

REFERENCES

1. Sanchez-Vega, F.; Mina, M.; Armenia, J.; Chatila, W. K.; Luna, A.; La, K. C.; Dimitriadoy, S.; Liu, D. L.; Kantheti, H. S.; Saghafinia, S.; Chakravarty, D.; Daian, F.; Gao, Q.; Bailey, M. H.; Liang, W. W.; Foltz, S. M.; Shmulevich, I.; Ding, L.; Heins, Z.; Ochoa, A.; Gross, B.; Gao, J.; Zhang, H.; Kundra, R.; Kandoth, C.; Bahceci, I.; Dervishi, L.; Dogrusoz, U.; Zhou, W.; Shen, H.; Laird, P. W.; Way, G. P.; Greene, C. S.; Liang, H.; Xiao, Y.; Wang, C.; Iavarone, A.; Berger, A. H.; Bivona, T. G.; Lazar, A. J.; Hammer, G. D.; Giordano, T.; Kwong, L. N.; McArthur, G.; Huang, C.; Tward, A. D.; Frederick, M. J.; McCormick, F.; Meyerson, M.; Cancer Genome Atlas Research, N.; Van Allen, E. M.; Cherniack, A. D.; Ciriello, G.; Sander, C.; Schultz, N., Oncogenic Signaling Pathways in The Cancer Genome Atlas. *Cell* **2018,** *173* (2), 321-337 e10.

2. Tuller, T.; Atar, S.; Ruppin, E.; Gurevich, M.; Achiron, A., Common and specific signatures of gene expression and protein-protein interactions in autoimmune diseases. *Genes Immun* **2013,** *14* (2), 67-82.

3. Sahni, N.; Yi, S.; Taipale, M.; Fuxman Bass, J. I.; Coulombe-Huntington, J.; Yang, F.; Peng, J.; Weile, J.; Karras, G. I.; Wang, Y.; Kovács, I. A.; Kamburov, A.; Krykbaeva, I.; Lam, M. H.; Tucker, G.; Khurana, V.; Sharma, A.; Liu, Y. Y.; Yachie, N.; Zhong, Q.; Shen, Y.; Palagi, A.; San-Miguel, A.; Fan, C.; Balcha, D.; Dricot, A.; Jordan, D. M.; Walsh, J. M.; Shah, A. A.; Yang, X.; Stoyanova, A. K.; Leighton, A.; Calderwood, M. A.; Jacob, Y.; Cusick, M. E.; Salehi-Ashtiani, K.; Whitesell, L. J.; Sunyaev, S.; Berger, B.; Barabási, A. L.; Charloteaux, B.; Hill, D. E.; Hao, T.; Roth, F. P.; Xia, Y.; Walhout, A. J. M.; Lindquist, S.; Vidal, M., Widespread macromolecular interaction perturbations in human genetic disorders. *Cell* **2015,** *161* (3), 647-660.

4. Debiec, K. T.; Gronenborn, A. M.; Chong, L. T., Evaluating the strength of salt bridges: a comparison of current biomolecular force fields. *J Phys Chem B* **2014,** *118* (24), 6561-9.

5. Espinosa, E.; Souhassou, M.; Lachekar, H.; Lecomte, C., Topological analysis of the electron density in hydrogen bonds. *Acta Crystallogr B* **1999,** *55* (Pt 4), 563-572.

6. Eriksson, A. E.; Baase, W. A.; Zhang, X. J.; Heinz, D. W.; Blaber, M.; Baldwin, E. P.; Matthews, B. W., Response of a protein structure to cavity-creating mutations and its relation to the hydrophobic effect. *Science* **1992,** *255* (5041), 178-83.

7. Van Roey, K.; Uyar, B.; Weatheritt, R. J.; Dinkel, H.; Seiler, M.; Budd, A.; Gibson, T. J.; Davey, N. E., Short linear motifs: ubiquitous and functionally diverse protein interaction modules directing cell regulation. *Chem Rev* **2014,** *114* (13), 6733-78.

8. Pawson, T.; Gish, G. D.; Nash, P., SH2 domains, interaction modules and cellular wiring. *Trends Cell Biol* **2001,** *11* (12), 504-11.

9. Perkins, J. R.; Diboun, I.; Dessailly, B. H.; Lees, J. G.; Orengo, C., Transient protein-protein interactions: structural, functional, and network properties. *Structure* **2010,** *18* (10), 1233-43.

10. Pawson, T.; Nash, P., Assembly of cell regulatory systems through protein interaction domains. *Science* **2003,** *300* (5618), 445-52.

11. Mosavi, L. K.; Cammett, T. J.; Desrosiers, D. C.; Peng, Z. Y., The ankyrin repeat as molecular architecture for protein recognition. *Protein Sci* **2004,** *13* (6), 1435-48.

12. Lo Conte, L.; Chothia, C.; Janin, J., The atomic structure of protein-protein recognition sites. *J Mol Biol* **1999,** *285* (5), 2177-98.

13. Bogan, A. A.; Thorn, K. S., Anatomy of hot spots in protein interfaces. *J Mol Biol* **1998,** *280* (1), 1-9.

14. Fellouse, F. A.; Wiesmann, C.; Sidhu, S. S., Synthetic antibodies from a four-amino-acid code: a dominant role for tyrosine in antigen recognition. *Proc Natl Acad Sci U S A* **2004,** *101* (34), 12467-72.

15. Fellouse, F. A.; Li, B.; Compaan, D. M.; Peden, A. A.; Hymowitz, S. G.; Sidhu, S. S., Molecular recognition by a binary code. *J Mol Biol* **2005,** *348* (5), 1153-62.

16. Stumpf, M. P.; Thorne, T.; de Silva, E.; Stewart, R.; An, H. J.; Lappe, M.; Wiuf, C., Estimating the size of the human interactome. *Proc Natl Acad Sci U S A* **2008,** *105* (19), 6959-64.

17. Ferguson, F. M.; Gray, N. S., Kinase inhibitors: the road ahead. *Nat Rev Drug Discov* **2018,** *17* (5), 353-377.

18. Usman, S.; Khawer, M.; Rafique, S.; Naz, Z.; Saleem, K., The current status of anti-GPCR drugs against different cancers. *J Pharm Anal* **2020,** *10* (6), 517-521.

19. Tsujimoto, Y.; Cossman, J.; Jaffe, E.; Croce, C. M., INVOLVEMENT OF THE BCL-2 GENE IN HUMAN FOLLICULAR LYMPHOMA. *Science* **1985,** *228* (4706), 1440-1443.

20. Slamon, D. J.; Clark, G. M.; Wong, S. G.; Levin, W. J.; Ullrich, A.; McGuire, W. L., Human breast cancer: correlation of relapse and survival with amplification of the HER-2/neu oncogene. *Science* **1987,** *235* (4785), 177-82.

21. Tsujimoto, Y.; Cossman, J.; Jaffe, E.; Croce, C. M., Involvement of the bcl-2 gene in human follicular lymphoma. *Science* **1985,** *228* (4706), 1440-3.

22. Chen, L.; Willis, S. N.; Wei, A.; Smith, B. J.; Fletcher, J. I.; Hinds, M. G.; Colman, P. M.; Day, C. L.; Adams, J. M.; Huang, D. C. S., Differential targeting of

prosurvival Bcl-2 proteins by their BH3-only ligands allows complementary apoptotic function. *Molecular Cell* **2005,** *17* (3), 393-403.

23. Zha, H. B.; AimeSempe, C.; Sato, T.; Reed, J. C., Proapoptotic protein Bax heterodimerizes with Bcl-2 and homodimerizes with Bax via a novel domain (BN3) distinct from BH1 and BH2. *Journal of Biological Chemistry* **1996,** *271* (13), 7440-7444.

24. Muchmore, S. W.; Sattler, M.; Liang, H.; Meadows, R. P.; Harlan, J. E.; Yoon, H. S.; Nettesheim, D.; Chang, B. S.; Thompson, C. B.; Wong, S. L.; Ng, S. L.; Fesik, S. W., X-ray and NMR structure of human Bcl-xL, an inhibitor of programmed cell death. *Nature* **1996,** *381* (6580), 335-41.

25. Chauhan, D.; Velankar, M.; Brahmandam, M.; Hideshima, T.; Podar, K.; Richardson, P.; Schlossman, R.; Ghobrial, I.; Raje, N.; Munshi, N.; Anderson, K. C., A novel Bcl-2/Bcl-X(L)/Bcl-w inhibitor ABT-737 as therapy in multiple myeloma. *Oncogene* **2007,** *26* (16), 2374-80.

26. Souers, A. J.; Leverson, J. D.; Boghaert, E. R.; Ackler, S. L.; Catron, N. D.; Chen, J.; Dayton, B. D.; Ding, H.; Enschede, S. H.; Fairbrother, W. J.; Huang, D. C. S.; Hymowitz, S. G.; Jin, S.; Khaw, S. L.; Kovar, P. J.; Lam, L. T.; Lee, J.; Maecker, H. L.; Marsh, K. C.; Mason, K. D.; Mitten, M. J.; Nimmer, P. M.; Oleksijew, A.; Park, C. H.; Park, C. M.; Phillips, D. C.; Roberts, A. W.; Sampath, D.; Seymour, J. F.; Smith, M. L.; Sullivan, G. M.; Tahir, S. K.; Tse, C.; Wendt, M. D.; Xiao, Y.; Xue, J. C.; Zhang, H. C.; Humerickhouse, R. A.; Rosenberg, S. H.; Elmore, S. W., ABT-199, a potent and selective BCL-2 inhibitor, achieves antitumor activity while sparing platelets. *Nature Medicine* **2013,** *19* (2), 202-208.

27. Mabonga, L.; Kappo, A. P., Protein-protein interaction modulators: advances, successes and remaining challenges. *Biophys Rev* **2019,** *11* (4), 559-581.

28. Margolis, B. L.; Lax, I.; Kris, R.; Dombalagian, M.; Honegger, A. M.; Howk, R.; Givol, D.; Ullrich, A.; Schlessinger, J., All autophosphorylation sites of epidermal growth factor (EGF) receptor and HER2/neu are located in their carboxyl-terminal tails. Identification of a novel site in EGF receptor. *J Biol Chem* **1989,** *264* (18), 10667-71.

29. Rubin, I.; Yarden, Y., The basic biology of HER2. *Ann Oncol* **2001,** *12 Suppl 1*, S3-8.

30. Glennie, M. J.; Johnson, P. W., Clinical trials of antibody therapy. *Immunol Today* **2000,** *21* (8), 403-10.

31. Baselga, J., Phase I and II clinical trials of trastuzumab. *Ann Oncol* **2001,** *12 Suppl 1*, S49-55.

32. Baselga, J.; Norton, L.; Albanell, J.; Kim, Y. M.; Mendelsohn, J., Recombinant humanized anti-HER2 antibody (Herceptin (TM)) enhances the antitumor activity of paclitaxel and doxorubicin against HER2/neu overexpressing human breast cancer xenografts. *Cancer Research* **1998,** *58* (13), 2825-2831.

33. Lu, R. M.; Hwang, Y. C.; Liu, I. J.; Lee, C. C.; Tsai, H. Z.; Li, H. J.; Wu, H. C., Development of therapeutic antibodies for the treatment of diseases. *J Biomed Sci* **2020,** *27* (1), 1.

34. Wang, C.; Li, W.; Drabek, D.; Okba, N. M. A.; van Haperen, R.; Osterhaus, A. D. M. E.; van Kuppeveld, F. J. M.; Haagmans, B. L.; Grosveld, F.; Bosch, B. J., A human monoclonal antibody blocking SARS-CoV-2 infection. *Nat Commun* **2020,** *11* (1), 2251.

35. Singh, K.; Ejaz, W.; Dutta, K.; Thayumanavan, S., Antibody Delivery for Intracellular Targets: Emergent Therapeutic Potential. *Bioconjug Chem* **2019,** *30* (4), 1028-1041.

36. Hernandez, I.; Bott, S. W.; Patel, A. S.; Wolf, C. G.; Hospodar, A. R.; Sampathkumar, S.; Shrank, W. H., Pricing of monoclonal antibody therapies: higher if used for cancer? *Am J Manag Care* **2018,** *24* (2), 109-112.

37. Andrei, S. A.; Sijbesma, E.; Hann, M.; Davis, J.; O'Mahony, G.; Perry, M. W. D.; Karawajczyk, A.; Eickhoff, J.; Brunsveld, L.; Doveston, R. G.; Milroy, L. G.; Ottmann, C., Stabilization of protein-protein interactions in drug discovery. *Expert Opin Drug Discov* **2017,** *12* (9), 925-940.

38. Labrijn, A. F.; Janmaat, M. L.; Reichert, J. M.; Parren, P., Bispecific antibodies: a mechanistic review of the pipeline. *Nat Rev Drug Discov* **2019,** *18* (8), 585-608.

39. Suurs, F. V.; Lub-de Hooge, M. N.; de Vries, E. G. E.; de Groot, D. J. A., A review of bispecific antibodies and antibody constructs in oncology and clinical challenges. *Pharmacol Ther* **2019,** *201*, 103-119.

40. Topp, M. S.; Gökbuget, N.; Zugmaier, G.; Klappers, P.; Stelljes, M.; Neumann, S.; Viardot, A.; Marks, R.; Diedrich, H.; Faul, C.; Reichle, A.; Horst, H. A.; Brüggemann, M.; Wessiepe, D.; Holland, C.; Alekar, S.; Mergen, N.; Einsele, H.; Hoelzer, D.; Bargou, R. C., Phase II trial of the anti-CD19 bispecific T cell-engager blinatumomab shows hematologic and molecular remissions in patients with relapsed or refractory B-precursor acute lymphoblastic leukemia. *J Clin Oncol* **2014,** *32* (36), 4134-40.

41. Rual, J. F.; Venkatesan, K.; Hao, T.; Hirozane-Kishikawa, T.; Dricot, A.; Li, N.; Berriz, G. F.; Gibbons, F. D.; Dreze, M.; Ayivi-Guedehoussou, N.; Klitgord, N.; Simon, C.; Boxem, M.; Milstein, S.; Rosenberg, J.; Goldberg, D. S.; Zhang, L. V.; Wong, S. L.; Franklin, G.; Li, S.; Albala, J. S.; Lim, J.; Fraughton, C.; Llamosas, E.; Cevik, S.; Bex, C.; Lamesch, P.; Sikorski, R. S.; Vandenhaute, J.; Zoghbi, H. Y.; Smolyar, A.; Bosak, S.; Sequerra, R.; Doucette-Stamm, L.; Cusick, M. E.; Hill, D. E.; Roth, F. P.; Vidal, M., Towards a proteome-scale map of the human protein-protein interaction network. *Nature* **2005,** *437* (7062), 1173-8.

42. Chatr-aryamontri, A.; Breitkreutz, B. J.; Oughtred, R.; Boucher, L.; Heinicke, S.; Chen, D. C.; Stark, C.; Breitkreutz, A.; Kolas, N.; O'Donnell, L.; Reguly, T.;

Nixon, J.; Ramage, L.; Winter, A.; Sellam, A.; Chang, C.; Hirschman, J.; Theesfeld, C.; Rust, J.; Livstone, M. S.; Dolinski, K.; Tyers, M., The BioGRID interaction database: 2015 update. *Nucleic Acids Research* **2015,** *43* (D1), D470-D478.

43. Szklarczyk, D.; Franceschini, A.; Wyder, S.; Forslund, K.; Heller, D.; Huerta-Cepas, J.; Simonovic, M.; Roth, A.; Santos, A.; Tsafou, K. P.; Kuhn, M.; Bork, P.; Jensen, L. J.; von Mering, C., STRING v10: protein-protein interaction networks, integrated over the tree of life. *Nucleic Acids Research* **2015,** *43* (D1), D447-D452.

44. Makley, L. N.; Gestwicki, J. E., Expanding the number of 'druggable' targets: non-enzymes and protein-protein interactions. *Chem Biol Drug Des* **2013,** *81* (1), 22-32.

45. Modell, A. E.; Blosser, S. L.; Arora, P. S., Systematic Targeting of Protein-Protein Interactions. *Trends Pharmacol Sci* **2016,** *37* (8), 702-13.

46. Raj, M.; Bullock, B. N.; Arora, P. S., Plucking the high hanging fruit: a systematic approach for targeting protein-protein interactions. *Bioorg Med Chem* **2013,** *21* (14), 4051-7.

47. Tavassoli, A., SICLOPPS cyclic peptide libraries in drug discovery. *Curr Opin Chem Biol* **2017,** *38*, 30-35.

48. Delbridge, A. R.; Strasser, A., The BCL-2 protein family, BH3-mimetics and cancer therapy. *Cell Death Differ* **2015,** *22* (7), 1071-80.

49. Chipuk, J. E.; Moldoveanu, T.; Llambi, F.; Parsons, M. J.; Green, D. R., The BCL-2 family reunion. *Mol Cell* **2010,** *37* (3), 299-310.

50. Czabotar, P. E.; Lessene, G.; Strasser, A.; Adams, J. M., Control of apoptosis by the BCL-2 protein family: implications for physiology and therapy. *Nat Rev Mol Cell Biol* **2014,** *15* (1), 49-63.

51. Roberts, A. W.; Davids, M. S.; Pagel, J. M.; Kahl, B. S.; Puvvada, S. D.; Gerecitano, J. F.; Kipps, T. J.; Anderson, M. A.; Brown, J. R.; Gressick, L.; Wong, S.; Dunbar, M.; Zhu, M.; Desai, M. B.; Cerri, E.; Enschede, S. H.; Humerickhouse, R. A.; Wierda, W. G.; Seymour, J. F., Targeting BCL2 with Venetoclax in Relapsed Chronic Lymphocytic Leukemia. *New England Journal of Medicine* **2016,** *374* (4), 311-322.

52. Perciavalle, R. M.; Opferman, J. T., Delving deeper: MCL-1's contributions to normal and cancer biology. *Trends in Cell Biology* **2013,** *23* (1), 22-29.

53. Shamas-Din, A.; Brahmbhatt, H.; Leber, B.; Andrews, D. W., BH3-only proteins: Orchestrators of apoptosis. *Biochim Biophys Acta* **2011,** *1813* (4), 508-20.

54. Ivanov, A. A.; Khuri, F. R.; Fu, H., Targeting protein-protein interactions as an anticancer strategy. *Trends Pharmacol Sci* **2013,** *34* (7), 393-400.

55. Besbes, S.; Billard, C., First MCL-1-selective BH3 mimetics as potential therapeutics for targeted treatment of cancer. *Cell Death Dis* **2015,** *6*, e1810.

56. Ashkenazi, A.; Fairbrother, W. J.; Leverson, J. D.; Souers, A. J., From basic apoptosis discoveries to advanced selective BCL-2 family inhibitors. *Nature Reviews Drug Discovery* **2017,** *16* (4), 273-284.

57. Newman, R. H.; Fosbrink, M. D.; Zhang, J., Genetically Encodable Fluorescent Biosensors for Tracking Signaling Dynamics in Living Cells. *Chemical Reviews* **2011,** *111* (5), 3614-3666.

58. Welch, C. M.; Elliott, H.; Danuser, G.; Hahn, K. M., Imaging the coordination of multiple signalling activities in living cells. *Nature Reviews Molecular Cell Biology* **2011,** *12* (11), 749-756.

59. Wehr, M. C.; Rossner, M. J., Split protein biosensor assays in molecular pharmacological studies. *Drug Discovery Today* **2016,** *21* (3), 415-429.

60. Miller, K. E.; Kim, Y.; Huh, W. K.; Park, H. O., Bimolecular Fluorescence Complementation (BiFC) Analysis: Advances and Recent Applications for Genome-Wide Interaction Studies. *Journal of Molecular Biology* **2015,** *427* (11), 2039-2055.

61. Kerppola, T. K., Visualization of molecular interactions using bimolecular fluorescence complementation analysis: Characteristics of protein fragment complementation. *Chemical Society Reviews* **2009,** *38* (10), 2876-2886.

62. Wang, F.; Banerjee, D.; Liu, Y. S.; Chen, X. Y.; Liu, X. G., Upconversion nanoparticles in biological labeling, imaging, and therapy. *Analyst* **2010,** *135* (8), 1839-1854.

63. Handly, L. N.; Yao, J.; Wollman, R., Signal Transduction at the Single-Cell Level: Approaches to Study the Dynamic Nature of Signaling Networks. *Journal of Molecular Biology* **2016,** *428* (19), 3669-3682.

64. Yao, Z.; Petschnigg, J.; Ketteler, R.; Stagljar, I., Application guide for omics approaches to cell signaling. *Nature Chemical Biology* **2015,** *11* (6), 387-397.

65. Slavoff, S. A.; Liu, D. S.; Cohen, J. D.; Ting, A. Y., Imaging protein-protein interactions inside living cells via interaction-dependent fluorophore ligation. *J Am Chem Soc* **2011,** *133* (49), 19769-76.

66. Huttlin, E. L.; Bruckner, R. J.; Paulo, J. A.; Cannon, J. R.; Ting, L.; Baltier, K.; Colby, G.; Gebreab, F.; Gygi, M. P.; Parzen, H.; Szpyt, J.; Tam, S.; Zarraga, G.; Pontano-Vaites, L.; Swarup, S.; White, A. E.; Schweppe, D. K.; Rad, R.; Erickson, B. K.; Obar, R. A.; Guruharsha, K. G.; Li, K.; Artavanis-Tsakonas, S.; Gygi, S. P.; Harper, J. W., Architecture of the human interactome defines protein communities and disease networks. *Nature* **2017,** *545* (7655), 505-509.

67. Stelzl, U.; Worm, U.; Lalowski, M.; Haenig, C.; Brembeck, F. H.; Goehler, H.; Stroedicke, M.; Zenkner, M.; Schoenherr, A.; Koeppen, S.; Timm, J.; Mintzlaff, S.; Abraham, C.; Bock, N.; Kietzmann, S.; Goedde, A.; Toksoz, E.; Droege, A.; Krobitsch, S.; Korn, B.; Birchmeier, W.; Lehrach, H.; Wanker, E. E., A human protein-protein interaction network: a resource for annotating the proteome. *Cell* **2005,** *122* (6), 957-68.

68. Hoppe, A. D.; Scott, B. L.; Welliver, T. P.; Straight, S. W.; Swanson, J. A., N-way FRET microscopy of multiple protein-protein interactions in live cells. *PLoS One* **2013,** *8* (6), e64760.

69. Kuchenov, D.; Laketa, V.; Stein, F.; Salopiata, F.; Klingmuller, U.; Schultz, C., High-Content Imaging Platform for Profiling Intracellular Signaling Network Activity in Living Cells. *Cell Chem Biol* **2016,** *23* (12), 1550-1559.

70. Cabantous, S.; Nguyen, H. B.; Pedelacq, J. D.; Koraichi, F.; Chaudhary, A.; Ganguly, K.; Lockard, M. A.; Favre, G.; Terwilliger, T. C.; Waldo, G. S., A new protein-protein interaction sensor based on tripartite split-GFP association. *Sci Rep* **2013,** *3*, 2854.

71. Kamiyama, D.; Sekine, S.; Barsi-Rhyne, B.; Hu, J.; Chen, B.; Gilbert, L. A.; Ishikawa, H.; Leonetti, M. D.; Marshall, W. F.; Weissman, J. S.; Huang, B., Versatile protein tagging in cells with split fluorescent protein. *Nat Commun* **2016,** *7*, 11046.

72. Blakeley, B. D.; Chapman, A. M.; McNaughton, B. R., Split-superpositive GFP reassembly is a fast, efficient, and robust method for detecting protein-protein interactions in vivo. *Mol Biosyst* **2012,** *8* (8), 2036-40.

73. Luker, K. E.; Smith, M. C.; Luker, G. D.; Gammon, S. T.; Piwnica-Worms, H.; Piwnica-Worms, D., Kinetics of regulated protein-protein interactions revealed with firefly luciferase complementation imaging in cells and living animals. *Proc Natl Acad Sci U S A* **2004,** *101* (33), 12288-93.

74. Jester, B. W.; Cox, K. J.; Gaj, A.; Shomin, C. D.; Porter, J. R.; Ghosh, I., A Coiled-Coil Enabled Split-Luciferase Three-Hybrid System: Applied Toward Profiling Inhibitors of Protein Kinases. *Journal of the American Chemical Society* **2010,** *132* (33), 11727-11735.

75. Martell, J. D.; Yamagata, M.; Deerinck, T. J.; Phan, S.; Kwa, C. G.; Ellisman, M. H.; Sanes, J. R.; Ting, A. Y., A split horseradish peroxidase for the detection of intercellular protein-protein interactions and sensitive visualization of synapses. *Nat Biotechnol* **2016,** *34* (7), 774-80.

76. Wehr, M. C.; Laage, R.; Bolz, U.; Fischer, T. M.; Grunewald, S.; Scheek, S.; Bach, A.; Nave, K. A.; Rossner, M. J., Monitoring regulated protein-protein interactions using split TEV. *Nat Methods* **2006,** *3* (12), 985-93.

77. Gray, D. C.; Mahrus, S.; Wells, J. A., Activation of Specific Apoptotic Caspases with an Engineered Small-Molecule-Activated Protease. *Cell* **2010,** *142* (4), 637-646.

78. Thaminy, S.; Miller, J.; Stagljar, I., The split-ubiquitin membrane-based yeast two-hybrid system. *Methods Mol Biol* **2004,** *261*, 297-312.

79. Jones, K. A.; Kentala, K.; Beck, M. W.; An, W.; Lippert, A. R.; Lewis, J. C.; Dickinson, B. C., Development of a Split Esterase for Protein-Protein Interaction-Dependent Small-Molecule Activation. *ACS Cent Sci* **2019,** *5* (11), 1768-1776.

80. Hu, C. D.; Kerppola, T. K., Simultaneous visualization of multiple protein interactions in living cells using multicolor fluorescence complementation analysis. *Nat Biotechnol* **2003,** *21* (5), 539-45.

81. Galperin, E.; Verkhusha, V.; Sorkin, A., Three-chromophore FRET microscopy to analyze multiprotein interactions in living cells. *Nature Methods* **2004,** *1* (3), 209-217.

82. Shekhawat, S. S.; Ghosh, I., Split-protein systems: beyond binary protein-protein interactions. *Current Opinion in Chemical Biology* **2011,** *15* (6), 789-797.

83. Furman, J. L.; Badran, A. H.; Shen, S.; Stains, C. I.; Hannallah, J.; Segal, D. J.; Ghosh, I., Systematic evaluation of split-fluorescent proteins for the direct detection of native and methylated DNA. *Bioorg Med Chem Lett* **2009,** *19* (14), 3748-51.

84. Pu, J.; Zinkus-Boltz, J.; Dickinson, B. C., Evolution of a split RNA polymerase as a versatile biosensor platform. *Nat Chem Biol* **2017,** *13* (4), 432-438.

85. Filonov, G. S.; Moon, J. D.; Svensen, N.; Jaffrey, S. R., Broccoli: Rapid Selection of an RNA Mimic of Green Fluorescent Protein by Fluorescence-Based Selection and Directed Evolution. *Journal of the American Chemical Society* **2014,** *136* (46), 16299-16308.

86. Lee, J. H.; Daugharthy, E. R.; Scheiman, J.; Kalhor, R.; Yang, J. L.; Ferrante, T. C.; Terry, R.; Jeanty, S. S.; Li, C.; Amamoto, R.; Peters, D. T.; Turczyk, B. M.; Marblestone, A. H.; Inverso, S. A.; Bernard, A.; Mali, P.; Rios, X.; Aach, J.; Church, G. M., Highly multiplexed subcellular RNA sequencing in situ. *Science* **2014,** *343* (6177), 1360-3.

87. Satija, R.; Farrell, J. A.; Gennert, D.; Schier, A. F.; Regev, A., Spatial reconstruction of single-cell gene expression data. *Nature Biotechnology* **2015,** *33* (5), 495-U206.

88. Moffitt, J. R.; Hao, J. J.; Wang, G. P.; Chen, K. H.; Babcock, H. P.; Zhuang, X. W., High-throughput single-cell gene-expression profiling with multiplexed error-robust fluorescence in situ hybridization. *Proceedings of the National Academy of Sciences of the United States of America* **2016,** *113* (39), 11046-11051.

89. Li, S.; Xu, L. G.; Ma, W.; Wu, X. L.; Sun, M. Z.; Kuang, H.; Wang, L. B.; Kotov, N. A.; Xu, C. L., Dual-Mode Ultrasensitive Quantification of MicroRNA in Living Cells by Chiroplasmonic Nanopyramids Self-Assembled from Gold and Upconversion Nanoparticles. *Journal of the American Chemical Society* **2016,** *138* (1), 306-312.

90. Wabuyele, M. B.; Soper, S. A., PCR amplification and sequencing of single copy DNA molecules. *Single Mol* **2001,** *2* (1), 13-21.

91. Piepenburg, O.; Williams, C. H.; Stemple, D. L.; Armes, N. A., DNA detection using recombination proteins. *Plos Biology* **2006,** *4* (7), 1115-1121.

92. Zamft, B. M.; Marblestone, A. H.; Kording, K.; Schmidt, D.; Martin-Alarcon, D.; Tyo, K.; Boyden, E. S.; Church, G., Measuring cation dependent DNA polymerase fidelity landscapes by deep sequencing. *PLoS One* **2012,** *7* (8), e43876.

93. Pu, J.; Chronis, I.; Ahn, D.; Dickinson, B. C., A Panel of Protease-Responsive RNA Polymerases Respond to Biochemical Signals by Production of Defined RNA Outputs in Live Cells. *J Am Chem Soc* **2015,** *137* (51), 15996-9.

94. Church, G. M.; Elowitz, M. B.; Smolke, C. D.; Voigt, C. A.; Weiss, R., Realizing the potential of synthetic biology. *Nat Rev Mol Cell Biol* **2014,** *15* (4), 289-94.

95. Nunez, J. K.; Harrington, L. B.; Doudna, J. A., Chemical and Biophysical Modulation of Cas9 for Tunable Genome Engineering. *ACS Chem Biol* **2016,** *11* (3), 681-8.

96. Chappell, J.; Watters, K. E.; Takahashi, M. K.; Lucks, J. B., A renaissance in RNA synthetic biology: new mechanisms, applications and tools for the future. *Current Opinion in Chemical Biology* **2015,** *28*, 47-56.

97. Kalhor, R.; Mali, P.; Church, G. M., Rapidly evolving homing CRISPR barcodes. *Nature Methods* **2017,** *14* (2), 195-200.

98. Gilbert, L. A.; Horlbeck, M. A.; Adamson, B.; Villalta, J. E.; Chen, Y.; Whitehead, E. H.; Guimaraes, C.; Panning, B.; Ploegh, H. L.; Bassik, M. C.; Qi, L. S.; Kampmann, M.; Weissman, J. S., Genome-Scale CRISPR-Mediated Control of Gene Repression and Activation. *Cell* **2014,** *159* (3), 647-61.

99. Meighen, E. A., MOLECULAR-BIOLOGY OF BACTERIAL BIOLUMINESCENCE. *Microbiological Reviews* **1991,** *55* (1), 123-142.

100. Li, H. L.; Zhu, H.; Xu, C. J.; Yuan, J. Y., Cleavage of BID by caspase 8 mediates the mitochondrial damage in the Fas pathway of apoptosis. *Cell* **1998,** *94* (4), 491-501.

101. Lee, E. F.; Czabotar, P. E.; Van Delft, M. F.; Michalak, E. M.; Boyle, M. J.; Willis, S. N.; Puthalakath, H.; Bouillet, P.; Colman, P. M.; Huang, D. C. S.; Fairlie, W.

D., A novel BH3 ligand that selectively targets Mcl-1 reveals that apoptosis can proceed without Mcl-1 degradation. *Journal of Cell Biology* **2008,** *180* (2), 341-355.

102. Hemphill, J.; Chou, C.; Chin, J. W.; Deiters, A., Genetically encoded light-activated transcription for spatiotemporal control of gene expression and gene silencing in mammalian cells. *J Am Chem Soc* **2013,** *135* (36), 13433-9.

103. Soderquist, R. S.; Eastman, A., BCL2 Inhibitors as Anticancer Drugs: A Plethora of Misleading BH3 Mimetics. *Molecular Cancer Therapeutics* **2016,** *15* (9), 2011-2017.

104. Leverson, J. D.; Zhang, H.; Chen, J.; Tahir, S. K.; Phillips, D. C.; Xue, J.; Nimmer, P.; Jin, S.; Smith, M.; Xiao, Y.; Kovar, P.; Tanaka, A.; Bruncko, M.; Sheppard, G. S.; Wang, L.; Gierke, S.; Kategaya, L.; Anderson, D. J.; Wong, C.; Eastham-Anderson, J.; Ludlam, M. J.; Sampath, D.; Fairbrother, W. J.; Wertz, I.; Rosenberg, S. H.; Tse, C.; Elmore, S. W.; Souers, A. J., Potent and selective small-molecule MCL-1 inhibitors demonstrate on-target cancer cell killing activity as single agents and in combination with ABT-263 (navitoclax). *Cell Death Dis* **2015,** *6*, e1590.

105. Certo, M.; Del Gaizo Moore, V.; Nishino, M.; Wei, G.; Korsmeyer, S.; Armstrong, S. A.; Letai, A., Mitochondria primed by death signals determine cellular addiction to antiapoptotic BCL-2 family members. *Cancer Cell* **2006,** *9* (5), 351-65.

106. Meyer, A. J.; Ellefson, J. W.; Ellington, A. D., Directed Evolution of a Panel of Orthogonal T7 RNA Polymerase Variants for in Vivo or in Vitro Synthetic Circuitry. *ACS Synth Biol* **2015,** *4* (10), 1070-6.

107. Segall-Shapiro, T. H.; Meyer, A. J.; Ellington, A. D.; Sontag, E. D.; Voigt, C. A., A 'resource allocator' for transcription based on a highly fragmented T7 RNA polymerase. *Mol Syst Biol* **2014,** *10*, 742.

108. Magliery, T. J.; Wilson, C. G.; Pan, W.; Mishler, D.; Ghosh, I.; Hamilton, A. D.; Regan, L., Detecting protein-protein interactions with a green fluorescent protein fragment reassembly trap: scope and mechanism. *J Am Chem Soc* **2005,** *127* (1), 146-57.

109. Ran, T.; Douek, Y.; Milo, L.; Shapiro, E., A programmable NOR-based device for transcription profile analysis. *Sci Rep* **2012,** *2*, 641.

110. Farzadfard, F.; Lu, T. K., Synthetic biology. Genomically encoded analog memory with precise in vivo DNA writing in living cell populations. *Science* **2014,** *346* (6211), 1256272.

111. Xie, Z.; Wroblewska, L.; Prochazka, L.; Weiss, R.; Benenson, Y., Multi-input RNAi-based logic circuit for identification of specific cancer cells. *Science* **2011,** *333* (6047), 1307-11.

112. Gibson, D. G.; Young, L.; Chuang, R. Y.; Venter, J. C.; Hutchison, C. A., 3rd; Smith, H. O., Enzymatic assembly of DNA molecules up to several hundred kilobases. *Nat Methods* **2009,** *6* (5), 343-5.

113. Carlson, J. C.; Badran, A. H.; Guggiana-Nilo, D. A.; Liu, D. R., Negative selection and stringency modulation in phage-assisted continuous evolution. *Nat Chem Biol* **2014,** *10* (3), 216-22.

114. Eliseev, B.; Yeramala, L.; Leitner, A.; Karuppasamy, M.; Raimondeau, E.; Huard, K.; Alkalaeva, E.; Aebersold, R.; Schaffitzel, C., Structure of a human cap-dependent 48S translation pre-initiation complex. *Nucleic Acids Res* **2018,** *46* (5), 2678-2689.

115. Kim, S. J.; Fernandez-Martinez, J.; Nudelman, I.; Shi, Y.; Zhang, W.; Raveh, B.; Herricks, T.; Slaughter, B. D.; Hogan, J. A.; Upla, P.; Chemmama, I. E.; Pellarin, R.; Echeverria, I.; Shivaraju, M.; Chaudhury, A. S.; Wang, J.; Williams, R.; Unruh, J. R.; Greenberg, C. H.; Jacobs, E. Y.; Yu, Z.; de la Cruz, M. J.; Mironska, R.; Stokes, D. L.; Aitchison, J. D.; Jarrold, M. F.; Gerton, J. L.; Ludtke, S. J.; Akey, C. W.; Chait, B. T.; Sali, A.; Rout, M. P., Integrative structure and functional anatomy of a nuclear pore complex. *Nature* **2018,** *555* (7697), 475-482.

116. Plaschka, C.; Hantsche, M.; Dienemann, C.; Burzinski, C.; Plitzko, J.; Cramer, P., Transcription initiation complex structures elucidate DNA opening. *Nature* **2016,** *533* (7603), 353-8.

117. Soucek, L.; Whitfield, J. R.; Sodir, N. M.; Masso-Valles, D.; Serrano, E.; Karnezis, A. N.; Swigart, L. B.; Evan, G. I., Inhibition of Myc family proteins eradicates KRas-driven lung cancer in mice. *Genes Dev* **2013,** *27* (5), 504-13.

118. Souers, A. J.; Leverson, J. D.; Boghaert, E. R.; Ackler, S. L.; Catron, N. D.; Chen, J.; Dayton, B. D.; Ding, H.; Enschede, S. H.; Fairbrother, W. J.; Huang, D. C.; Hymowitz, S. G.; Jin, S.; Khaw, S. L.; Kovar, P. J.; Lam, L. T.; Lee, J.; Maecker, H. L.; Marsh, K. C.; Mason, K. D.; Mitten, M. J.; Nimmer, P. M.; Oleksijew, A.; Park, C. H.; Park, C. M.; Phillips, D. C.; Roberts, A. W.; Sampath, D.; Seymour, J. F.; Smith, M. L.; Sullivan, G. M.; Tahir, S. K.; Tse, C.; Wendt, M. D.; Xiao, Y.; Xue, J. C.; Zhang, H.; Humerickhouse, R. A.; Rosenberg, S. H.; Elmore, S. W., ABT-199, a potent and selective BCL-2 inhibitor, achieves antitumor activity while sparing platelets. *Nat Med* **2013,** *19* (2), 202-8.

119. Langan, R. A.; Boyken, S. E.; Ng, A. H.; Samson, J. A.; Dods, G.; Westbrook, A. M.; Nguyen, T. H.; Lajoie, M. J.; Chen, Z.; Berger, S.; Mulligan, V. K.; Dueber, J. E.; Novak, W. R. P.; El-Samad, H.; Baker, D., De novo design of bioactive protein switches. *Nature* **2019,** *572* (7768), 205-210.

120. van der Geer, P., Analysis of protein-protein interactions by coimmunoprecipitation. *Methods Enzymol* **2014,** *541*, 35-47.

121. Sun, Y.; Hays, N. M.; Periasamy, A.; Davidson, M. W.; Day, R. N., Monitoring protein interactions in living cells with fluorescence lifetime imaging microscopy. *Methods Enzymol* **2012,** *504*, 371-91.

122. Jones, K. A.; Zinkus-Boltz, J.; Dickinson, B. C., Recent advances in developing and applying biosensors forsynthetic biology. *Nano Futures* **2019,** *3* (042002).

123. Ozawa, T.; Kaihara, A.; Sato, M.; Tachihara, K.; Umezawa, Y., Split luciferase as an optical probe for detecting protein-protein interactions in mammalian cells based on protein splicing. *Anal Chem* **2001,** *73* (11), 2516-21.

124. Hall, M. P.; Unch, J.; Binkowski, B. F.; Valley, M. P.; Butler, B. L.; Wood, M. G.; Otto, P.; Zimmerman, K.; Vidugiris, G.; Machleidt, T.; Robers, M. B.; Benink, H. A.; Eggers, C. T.; Slater, M. R.; Meisenheimer, P. L.; Klaubert, D. H.; Fan, F.; Encell, L. P.; Wood, K. V., Engineered luciferase reporter from a deep sea shrimp utilizing a novel imidazopyrazinone substrate. *ACS Chem Biol* **2012,** *7* (11), 1848-57.

125. Wehr, M. C.; Rossner, M. J., Split protein biosensor assays in molecular pharmacological studies. *Drug Discov Today* **2016,** *21* (3), 415-29.

126. Tabor, S.; Richardson, C. C., A bacteriophage T7 RNA polymerase/promoter system for controlled exclusive expression of specific genes. *Proc Natl Acad Sci U S A* **1985,** *82* (4), 1074-8.

127. Shis, D. L.; Bennett, M. R., Library of synthetic transcriptional AND gates built with split T7 RNA polymerase mutants. *Proc Natl Acad Sci U S A* **2013,** *110* (13), 5028-33.

128. Pu, J.; Kentala, K.; Dickinson, B. C., Multidimensional Control of Cas9 by Evolved RNA Polymerase-Based Biosensors. *ACS Chem Biol* **2018,** *13* (2), 431-437.

129. Pu, J.; Disare, M.; Dickinson, B. C., Evolution of C-Terminal Modification Tolerance in Full-Length and Split T7 RNA Polymerase Biosensors. *Chembiochem* **2019,** *20* (12), 1547-1553.

130. Zinkus-Boltz, J.; DeValk, C.; Dickinson, B. C., A Phage-Assisted Continuous Selection Approach for Deep Mutational Scanning of Protein-Protein Interactions. *ACS Chem Biol* **2019**.

131. Xie, V. C.; Pu, J.; Metzger, B. P.; Thornton, J. W.; Dickinson, B. C., Contingency and chance erase necessity in the experimental evolution of ancestral proteins. *Elife* **2021,** *10*.

132. Pu, J.; Dewey, J. A.; Hadji, A.; LaBelle, J. L.; Dickinson, B. C., RNA Polymerase Tags To Monitor Multidimensional Protein-Protein Interactions Reveal Pharmacological Engagement of Bcl-2 Proteins. *J Am Chem Soc* **2017,** *139* (34), 11964-11972.

133. Agteresch, H. J.; Dagnelie, P. C.; van den Berg, J. W.; Wilson, J. H., Adenosine triphosphate: established and potential clinical applications. *Drugs* **1999,** *58* (2), 211-32.

134. Chakraborty, K.; Veetil, A. T.; Jaffrey, S. R.; Krishnan, Y., Nucleic Acid-Based Nanodevices in Biological Imaging. *Annu Rev Biochem* **2016,** *85*, 349-73.

135. Sambrook, J.; Russell, D. W.; Sambrook, J., *The condensed protocols from Molecular cloning : a laboratory manual*. Cold Spring Harbor Laboratory Press: Cold Spring Harbor, N.Y., 2006; p v, 800 p.

136. Kim, T. K.; Eberwine, J. H., Mammalian cell transfection: the present and the future. *Anal Bioanal Chem* **2010,** *397* (8), 3173-8.

137. Longo, P. A.; Kavran, J. M.; Kim, M. S.; Leahy, D. J., Transient mammalian cell transfection with polyethylenimine (PEI). *Methods Enzymol* **2013,** *529*, 227-40.

138. Jaremko, M. J.; Davis, T. D.; Corpuz, J. C.; Burkart, M. D., Type II non-ribosomal peptide synthetase proteins: structure, mechanism, and protein-protein interactions. *Nat Prod Rep* **2020,** *37* (3), 355-379.

139. Pawson, T.; Scott, J. D., Signaling through scaffold, anchoring, and adaptor proteins. *Science* **1997,** *278* (5346), 2075-80.

140. Li, J.; Mahajan, A.; Tsai, M. D., Ankyrin repeat: a unique motif mediating protein-protein interactions. *Biochemistry* **2006,** *45* (51), 15168-78.

141. Zeytuni, N.; Zarivach, R., Structural and functional discussion of the tetra-trico-peptide repeat, a protein interaction module. *Structure* **2012,** *20* (3), 397-405.

142. Cheng, F.; Zhao, J.; Wang, Y.; Lu, W.; Liu, Z.; Zhou, Y.; Martin, W. R.; Wang, R.; Huang, J.; Hao, T.; Yue, H.; Ma, J.; Hou, Y.; Castrillon, J. A.; Fang, J.; Lathia, J. D.; Keri, R. A.; Lightstone, F. C.; Antman, E. M.; Rabadan, R.; Hill, D. E.; Eng, C.; Vidal, M.; Loscalzo, J., Comprehensive characterization of protein-protein interactions perturbed by disease mutations. *Nat Genet* **2021,** *53* (3), 342-353.

143. Pardoll, D. M., The blockade of immune checkpoints in cancer immunotherapy. *Nat Rev Cancer* **2012,** *12* (4), 252-64.

144. Dang, C. V., MYC on the path to cancer. *Cell* **2012,** *149* (1), 22-35.

145. McCubrey, J. A.; Steelman, L. S.; Chappell, W. H.; Abrams, S. L.; Wong, E. W.; Chang, F.; Lehmann, B.; Terrian, D. M.; Milella, M.; Tafuri, A.; Stivala, F.; Libra, M.; Basecke, J.; Evangelisti, C.; Martelli, A. M.; Franklin, R. A., Roles of the Raf/MEK/ERK pathway in cell growth, malignant transformation and drug resistance. *Biochim Biophys Acta* **2007,** *1773* (8), 1263-84.

146. Caughey, B.; Lansbury, P. T., Protofibrils, pores, fibrils, and neurodegeneration: separating the responsible protein aggregates from the innocent bystanders. *Annu Rev Neurosci* **2003,** *26*, 267-98.

147. Chen, Y.; Dorn, G. W., 2nd, PINK1-phosphorylated mitofusin 2 is a Parkin receptor for culling damaged mitochondria. *Science* **2013,** *340* (6131), 471-5.

148. Cuadrado, A.; Rojo, A. I.; Wells, G.; Hayes, J. D.; Cousin, S. P.; Rumsey, W. L.; Attucks, O. C.; Franklin, S.; Levonen, A. L.; Kensler, T. W.; Dinkova-Kostova, A. T., Therapeutic targeting of the NRF2 and KEAP1 partnership in chronic diseases. *Nat Rev Drug Discov* **2019,** *18* (4), 295-317.

149. Kaminska, B., MAPK signalling pathways as molecular targets for anti-inflammatory therapy--from molecular mechanisms to therapeutic benefits. *Biochim Biophys Acta* **2005,** *1754* (1-2), 253-62.

150. Wynn, T. A., Cellular and molecular mechanisms of fibrosis. *J Pathol* **2008,** *214* (2), 199-210.

151. Bonacci, W.; Teng, P. K.; Afonso, B.; Niederholtmeyer, H.; Grob, P.; Silver, P. A.; Savage, D. F., Modularity of a carbon-fixing protein organelle. *Proc Natl Acad Sci U S A* **2012,** *109* (2), 478-83.

152. Divine, R.; Dang, H. V.; Ueda, G.; Fallas, J. A.; Vulovic, I.; Sheffler, W.; Saini, S.; Zhao, Y. T.; Raj, I. X.; Morawski, P. A.; Jennewein, M. F.; Homad, L. J.; Wan, Y. H.; Tooley, M. R.; Seeger, F.; Etemadi, A.; Fahning, M. L.; Lazarovits, J.; Roederer, A.; Walls, A. C.; Stewart, L.; Mazloomi, M.; King, N. P.; Campbell, D. J.; McGuire, A. T.; Stamatatos, L.; Ruohola-Baker, H.; Mathieu, J.; Veesler, D.; Baker, D., Designed proteins assemble antibodies into modular nanocages. *bioRxiv* **2020**.

153. Lajoie, M. J.; Boyken, S. E.; Salter, A. I.; Bruffey, J.; Rajan, A.; Langan, R. A.; Olshefsky, A.; Muhunthan, V.; Bick, M. J.; Gewe, M.; Quijano-Rubio, A.; Johnson, J.; Lenz, G.; Nguyen, A.; Pun, S.; Correnti, C. E.; Riddell, S. R.; Baker, D., Designed protein logic to target cells with precise combinations of surface antigens. *Science* **2020,** *369* (6511), 1637-1643.

154. Chen, Z.; Kibler, R. D.; Hunt, A.; Busch, F.; Pearl, J.; Jia, M.; VanAernum, Z. L.; Wicky, B. I. M.; Dods, G.; Liao, H.; Wilken, M. S.; Ciarlo, C.; Green, S.; El-Samad, H.; Stamatoyannopoulos, J.; Wysocki, V. H.; Jewett, M. C.; Boyken, S. E.; Baker, D., De novo design of protein logic gates. *Science* **2020,** *368* (6486), 78-84.

155. Nitta, T.; Wang, Y.; Du, Z.; Morishima, K.; Hiratsuka, Y., A printable active network actuator built from an engineered biomolecular motor. *Nat Mater* **2021**.

156. Choe, J. H.; Watchmaker, P. B.; Simic, M. S.; Gilbert, R. D.; Li, A. W.; Krasnow, N. A.; Downey, K. M.; Yu, W.; Carrera, D. A.; Celli, A.; Cho, J.; Briones, J. D.; Duecker, J. M.; Goretsky, Y. E.; Dannenfelser, R.; Cardarelli, L.; Troyanskaya, O.; Sidhu, S. S.; Roybal, K. T.; Okada, H.; Lim, W. A., SynNotch-CAR T cells

overcome challenges of specificity, heterogeneity, and persistence in treating glioblastoma. *Sci Transl Med* **2021,** *13* (591).

157. Yoshikawa, M.; Yoshii, T.; Ikuta, M.; Tsukiji, S., Synthetic Protein Condensates That Inducibly Recruit and Release Protein Activity in Living Cells. *J Am Chem Soc* **2021,** *143* (17), 6434-6446.

158. Scott, D. E.; Bayly, A. R.; Abell, C.; Skidmore, J., Small molecules, big targets: drug discovery faces the protein-protein interaction challenge. *Nat Rev Drug Discov* **2016,** *15* (8), 533-50.

159. Arkin, M. R.; Wells, J. A., Small-molecule inhibitors of protein-protein interactions: progressing towards the dream. *Nat Rev Drug Discov* **2004,** *3* (4), 301-17.

160. Arkin, M. R.; Tang, Y.; Wells, J. A., Small-molecule inhibitors of protein-protein interactions: progressing toward the reality. *Chem Biol* **2014,** *21* (9), 1102-14.

161. Lu, H.; Zhou, Q.; He, J.; Jiang, Z.; Peng, C.; Tong, R.; Shi, J., Recent advances in the development of protein-protein interactions modulators: mechanisms and clinical trials. *Signal Transduct Target Ther* **2020,** *5* (1), 213.

162. Gerry, C. J.; Schreiber, S. L., Unifying principles of bifunctional, proximity-inducing small molecules. *Nat Chem Biol* **2020,** *16* (4), 369-378.

163. Maniaci, C.; Ciulli, A., Bifunctional chemical probes inducing protein-protein interactions. *Curr Opin Chem Biol* **2019,** *52*, 145-156.

164. Zarzycka, B.; Kuenemann, M. A.; Miteva, M. A.; Nicolaes, G. A. F.; Vriend, G.; Sperandio, O., Stabilization of protein-protein interaction complexes through small molecules. *Drug Discov Today* **2016,** *21* (1), 48-57.

165. Schneekloth, A. R.; Pucheault, M.; Tae, H. S.; Crews, C. M., Targeted intracellular protein degradation induced by a small molecule: En route to chemical proteomics. *Bioorg Med Chem Lett* **2008,** *18* (22), 5904-8.

166. Lu, J.; Qian, Y.; Altieri, M.; Dong, H.; Wang, J.; Raina, K.; Hines, J.; Winkler, J. D.; Crew, A. P.; Coleman, K.; Crews, C. M., Hijacking the E3 Ubiquitin Ligase Cereblon to Efficiently Target BRD4. *Chem Biol* **2015,** *22* (6), 755-63.

167. Lai, A. C.; Toure, M.; Hellerschmied, D.; Salami, J.; Jaime-Figueroa, S.; Ko, E.; Hines, J.; Crews, C. M., Modular PROTAC Design for the Degradation of Oncogenic BCR-ABL. *Angew Chem Int Ed Engl* **2016,** *55* (2), 807-10.

168. Schapira, M.; Calabrese, M. F.; Bullock, A. N.; Crews, C. M., Targeted protein degradation: expanding the toolbox. *Nat Rev Drug Discov* **2019,** *18* (12), 949-963.

169. Paiva, S. L.; Crews, C. M., Targeted protein degradation: elements of PROTAC design. *Curr Opin Chem Biol* **2019,** *50*, 111-119.

170. Mayor-Ruiz, C.; Bauer, S.; Brand, M.; Kozicka, Z.; Siklos, M.; Imrichova, H.; Kaltheuner, I. H.; Hahn, E.; Seiler, K.; Koren, A.; Petzold, G.; Fellner, M.; Bock, C.; Muller, A. C.; Zuber, J.; Geyer, M.; Thoma, N. H.; Kubicek, S.; Winter, G. E., Rational discovery of molecular glue degraders via scalable chemical profiling. *Nat Chem Biol* **2020,** *16* (11), 1199-1207.

171. An, S.; Fu, L., Small-molecule PROTACs: An emerging and promising approach for the development of targeted therapy drugs. *EBioMedicine* **2018,** *36*, 553-562.

172. Gao, H.; Sun, X.; Rao, Y., PROTAC Technology: Opportunities and Challenges. *ACS Med Chem Lett* **2020,** *11* (3), 237-240.

173. Miles, L. E., Properties, variants, and applications of the immunoradiometric assay method. *Ric Clin Lab* **1975,** *5* (1), 59-72.

174. Ray, S. S.; Nowak, R. J.; Brown, R. H., Jr.; Lansbury, P. T., Jr., Small-molecule-mediated stabilization of familial amyotrophic lateral sclerosis-linked superoxide dismutase mutants against unfolding and aggregation. *Proc Natl Acad Sci U S A* **2005,** *102* (10), 3639-44.

175. Tan, Z.; Wortman, M.; Dillehay, K. L.; Seibel, W. L.; Evelyn, C. R.; Smith, S. J.; Malkas, L. H.; Zheng, Y.; Lu, S.; Dong, Z., Small-molecule targeting of proliferating cell nuclear antigen chromatin association inhibits tumor cell growth. *Mol Pharmacol* **2012,** *81* (6), 811-9.

176. Nemetski, S. M.; Cardozo, T. J.; Bosch, G.; Weltzer, R.; O'Malley, K.; Ejigiri, I.; Kumar, K. A.; Buscaglia, C. A.; Nussenzweig, V.; Sinnis, P.; Levitskaya, J.; Bosch, J., Inhibition by stabilization: targeting the Plasmodium falciparum aldolase-TRAP complex. *Malar J* **2015,** *14*, 324.

177. Sijbesma, E.; Visser, E.; Plitzko, K.; Thiel, P.; Milroy, L. G.; Kaiser, M.; Brunsveld, L.; Ottmann, C., Structure-based evolution of a promiscuous inhibitor to a selective stabilizer of protein-protein interactions. *Nat Commun* **2020,** *11* (1), 3954.

178. Ferrara, M.; Sessa, G.; Fiore, M.; Bernard, F.; Asteriti, I. A.; Cundari, E.; Colotti, G.; Ferla, S.; Desideri, M.; Buglioni, S.; Trisciuoglio, D.; Del Bufalo, D.; Brancale, A.; Degrassi, F., Small molecules targeted to the microtubule-Hec1 interaction inhibit cancer cell growth through microtubule stabilization. *Oncogene* **2018,** *37* (2), 231-240.

179. Li, Z.; Wang, C.; Wang, Z.; Zhu, C.; Li, J.; Sha, T.; Ma, L.; Gao, C.; Yang, Y.; Sun, Y.; Wang, J.; Sun, X.; Lu, C.; Difiglia, M.; Mei, Y.; Ding, C.; Luo, S.; Dang, Y.; Ding, Y.; Fei, Y.; Lu, B., Allele-selective lowering of mutant HTT protein by HTT-LC3 linker compounds. *Nature* **2019,** *575* (7781), 203-209.

180. Tang, C.; Mo, X.; Niu, Q.; Wahafu, A.; Yang, X.; Qui, M.; Ivanov, A. A.; Du, Y.; Fu, H., Hypomorph mutation-directed small-molecule protein-protein interaction

inducers to restore mutant SMAD4-suppressed TGF-beta signaling. *Cell Chem Biol* **2021,** *28* (5), 636-647 e5.

181. Hartman, A. M.; Elgaher, W. A. M.; Hertrich, N.; Andrei, S. A.; Ottmann, C.; Hirsch, A. K. H., Discovery of Small-Molecule Stabilizers of 14-3-3 Protein-Protein Interactions via Dynamic Combinatorial Chemistry. *ACS Med Chem Lett* **2020,** *11* (5), 1041-1046.

182. Sijbesma, E.; Somsen, B. A.; Miley, G. P.; Leijten-van de Gevel, I. A.; Brunsveld, L.; Arkin, M. R.; Ottmann, C., Fluorescence Anisotropy-Based Tethering for Discovery of Protein-Protein Interaction Stabilizers. *ACS Chem Biol* **2020,** *15* (12), 3143-3148.

183. Guillory, X.; Wolter, M.; Leysen, S.; Neves, J. F.; Kuusk, A.; Genet, S.; Somsen, B.; Morrow, J. K.; Rivers, E.; van Beek, L.; Patel, J.; Goodnow, R.; Schoenherr, H.; Fuller, N.; Cao, Q.; Doveston, R. G.; Brunsveld, L.; Arkin, M. R.; Castaldi, P.; Boyd, H.; Landrieu, I.; Chen, H.; Ottmann, C., Fragment-based Differential Targeting of PPI Stabilizer Interfaces. *J Med Chem* **2020,** *63* (13), 6694-6707.

184. Wolter, M.; Valenti, D.; Cossar, P. J.; Levy, L. M.; Hristeva, S.; Genski, T.; Hoffmann, T.; Brunsveld, L.; Tzalis, D.; Ottmann, C., Fragment-Based Stabilizers of Protein-Protein Interactions through Imine-Based Tethering. *Angew Chem Int Ed Engl* **2020,** *59* (48), 21520-21524.

185. Newman, M. J.; Benani, D. J., A review of blinatumomab, a novel immunotherapy. *J Oncol Pharm Pract* **2016,** *22* (4), 639-45.

186. Linke, R.; Klein, A.; Seimetz, D., Catumaxomab: clinical development and future directions. *MAbs* **2010,** *2* (2), 129-36.

187. Sedykh, S. E.; Prinz, V. V.; Buneva, V. N.; Nevinsky, G. A., Bispecific antibodies: design, therapy, perspectives. *Drug Des Devel Ther* **2018,** *12*, 195-208.

188. Arnold, F. H., Directed Evolution: Bringing New Chemistry to Life. *Angew Chem Int Ed Engl* **2018,** *57* (16), 4143-4148.

189. Bornscheuer, U. T.; Hauer, B.; Jaeger, K. E.; Schwaneberg, U., Directed Evolution Empowered Redesign of Natural Proteins for the Sustainable Production of Chemicals and Pharmaceuticals. *Angew Chem Int Ed Engl* **2019,** *58* (1), 36-40.

190. Liang, A. D.; Serrano-Plana, J.; Peterson, R. L.; Ward, T. R., Artificial Metalloenzymes Based on the Biotin-Streptavidin Technology: Enzymatic Cascades and Directed Evolution. *Acc Chem Res* **2019,** *52* (3), 585-595.

191. Davis, A. M.; Plowright, A. T.; Valeur, E., Directing evolution: the next revolution in drug discovery? *Nat Rev Drug Discov* **2017,** *16* (10), 681-698.

192. Kuchner, O.; Arnold, F. H., Directed evolution of enzyme catalysts. *Trends Biotechnol* **1997,** *15* (12), 523-30.

193. Brandenberg, O. F.; Chen, K.; Arnold, F. H., Directed Evolution of a Cytochrome P450 Carbene Transferase for Selective Functionalization of Cyclic Compounds. *J Am Chem Soc* **2019,** *141* (22), 8989-8995.

194. Waldo, G. S., Genetic screens and directed evolution for protein solubility. *Curr Opin Chem Biol* **2003,** *7* (1), 33-8.

195. Roodveldt, C.; Aharoni, A.; Tawfik, D. S., Directed evolution of proteins for heterologous expression and stability. *Curr Opin Struct Biol* **2005,** *15* (1), 50-6.

196. Clackson, T.; Hoogenboom, H. R.; Griffiths, A. D.; Winter, G., Making antibody fragments using phage display libraries. *Nature* **1991,** *352* (6336), 624-8.

197. Roberts, R. W.; Szostak, J. W., RNA-peptide fusions for the in vitro selection of peptides and proteins. *Proc Natl Acad Sci U S A* **1997,** *94* (23), 12297-302.

198. Hanes, J.; Pluckthun, A., In vitro selection and evolution of functional proteins by using ribosome display. *Proc Natl Acad Sci U S A* **1997,** *94* (10), 4937-42.

199. Esvelt, K. M.; Carlson, J. C.; Liu, D. R., A system for the continuous directed evolution of biomolecules. *Nature* **2011,** *472* (7344), 499-503.

200. Miller, S. M.; Wang, T.; Liu, D. R., Phage-assisted continuous and non-continuous evolution. *Nat Protoc* **2020,** *15* (12), 4101-4127.

201. Rix, G.; Watkins-Dulaney, E. J.; Almhjell, P. J.; Boville, C. E.; Arnold, F. H.; Liu, C. C., Scalable continuous evolution for the generation of diverse enzyme variants encompassing promiscuous activities. *Nat Commun* **2020,** *11* (1), 5644.

202. Berman, C. M.; Papa, L. J., 3rd; Hendel, S. J.; Moore, C. L.; Suen, P. H.; Weickhardt, A. F.; Doan, N. D.; Kumar, C. M.; Uil, T. G.; Butty, V. L.; Hoeben, R. C.; Shoulders, M. D., An Adaptable Platform for Directed Evolution in Human Cells. *J Am Chem Soc* **2018,** *140* (51), 18093-18103.

203. Hendel, S. J.; Shoulders, M. D., Directed evolution in mammalian cells. *Nat Methods* **2021,** *18* (4), 346-357.

204. English, J. G.; Olsen, R. H. J.; Lansu, K.; Patel, M.; White, K.; Cockrell, A. S.; Singh, D.; Strachan, R. T.; Wacker, D.; Roth, B. L., VEGAS as a Platform for Facile Directed Evolution in Mammalian Cells. *Cell* **2019,** *178* (3), 748-761 e17.

205. Choi, J.; Chen, J.; Schreiber, S. L.; Clardy, J., Structure of the FKBP12-rapamycin complex interacting with the binding domain of human FRAP. *Science* **1996,** *273* (5272), 239-42.

206. Yin, P.; Fan, H.; Hao, Q.; Yuan, X.; Wu, D.; Pang, Y.; Yan, C.; Li, W.; Wang, J.; Yan, N., Structural insights into the mechanism of abscisic acid signaling by PYL proteins. *Nat Struct Mol Biol* **2009,** *16* (12), 1230-6.

207. Zinkus-Boltz, J.; DeValk, C.; Dickinson, B. C., A Phage-Assisted Continuous Selection Approach for Deep Mutational Scanning of Protein-Protein Interactions. *ACS Chem Biol* **2019,** *14* (12), 2757-2767.

208. Tran, T. H.; Chan, A. H.; Young, L. C.; Bindu, L.; Neale, C.; Messing, S.; Dharmaiah, S.; Taylor, T.; Denson, J. P.; Esposito, D.; Nissley, D. V.; Stephen, A. G.; McCormick, F.; Simanshu, D. K., KRAS interaction with RAF1 RAS-binding domain and cysteine-rich domain provides insights into RAS-mediated RAF activation. *Nat Commun* **2021,** *12* (1), 1176.

209. Chen, L.; Willis, S. N.; Wei, A.; Smith, B. J.; Fletcher, J. I.; Hinds, M. G.; Colman, P. M.; Day, C. L.; Adams, J. M.; Huang, D. C., Differential targeting of prosurvival Bcl-2 proteins by their BH3-only ligands allows complementary apoptotic function. *Mol Cell* **2005,** *17* (3), 393-403.

210. Ghosh, I.; Hamilton, A. D.; Regan, L., Antiparallel Leucine Zipper-Directed Protein Reassembly: Application to the Green Fluorescent Protein. *Journal of the American Chemical Society* **2000,** *122* (23), 5658-5659.

211. Dewey, J. A.; Dickinson, B. C., Split T7 RNA polymerase biosensors to study multiprotein interaction dynamics. *Methods Enzymol* **2020,** *641*, 413-432.

212. Rogers, J. K.; Guzman, C. D.; Taylor, N. D.; Raman, S.; Anderson, K.; Church, G. M., Synthetic biosensors for precise gene control and real-time monitoring of metabolites. *Nucleic Acids Res* **2015,** *43* (15), 7648-60.

213. Dickinson, B. C.; Packer, M. S.; Badran, A. H.; Liu, D. R., A system for the continuous directed evolution of proteases rapidly reveals drug-resistance mutations. *Nat Commun* **2014,** *5*, 5352.

214. Wang, T.; Badran, A. H.; Huang, T. P.; Liu, D. R., Continuous directed evolution of proteins with improved soluble expression. *Nat Chem Biol* **2018,** *14* (10), 972-980.

215. Wirth, M.; Zhang, W.; Razi, M.; Nyoni, L.; Joshi, D.; O'Reilly, N.; Johansen, T.; Tooze, S. A.; Mouilleron, S., Molecular determinants regulating selective binding of autophagy adapters and receptors to ATG8 proteins. *Nat Commun* **2019,** *10* (1), 2055.

216. Roth, T. B.; Woolston, B. M.; Stephanopoulos, G.; Liu, D. R., Phage-Assisted Evolution of Bacillus methanolicus Methanol Dehydrogenase 2. *ACS Synth Biol* **2019,** *8* (4), 796-806.

217. Blum, T. R.; Liu, H.; Packer, M. S.; Xiong, X.; Lee, P. G.; Zhang, S.; Richter, M.; Minasov, G.; Satchell, K. J. F.; Dong, M.; Liu, D. R., Phage-assisted evolution of

botulinum neurotoxin proteases with reprogrammed specificity. *Science* **2021,** *371* (6531), 803-810.

218. Richter, M. F.; Zhao, K. T.; Eton, E.; Lapinaite, A.; Newby, G. A.; Thuronyi, B. W.; Wilson, C.; Koblan, L. W.; Zeng, J.; Bauer, D. E.; Doudna, J. A.; Liu, D. R., Phage-assisted evolution of an adenine base editor with improved Cas domain compatibility and activity. *Nat Biotechnol* **2020,** *38* (7), 883-891.

219. Daitoku, H.; Sakamaki, J.; Fukamizu, A., Regulation of FoxO transcription factors by acetylation and protein-protein interactions. *Biochim Biophys Acta* **2011,** *1813* (11), 1954-60.

220. Fontaine, F.; Overman, J.; François, M., Pharmacological manipulation of transcription factor protein-protein interactions: opportunities and obstacles. *Cell Regen* **2015,** *4* (1), 2.

221. Sun, C., The SF3b complex: splicing and beyond. *Cell Mol Life Sci* **2020,** *77* (18), 3583-3595.

222. Arís, A.; Villaverde, A., Engineering nuclear localization signals in modular protein vehicles for gene therapy. *Biochem Biophys Res Commun* **2003,** *304* (4), 625-31.

223. Xia, W.; Bringmann, P.; McClary, J.; Jones, P. P.; Manzana, W.; Zhu, Y.; Wang, S.; Liu, Y.; Harvey, S.; Madlansacay, M. R.; McLean, K.; Rosser, M. P.; MacRobbie, J.; Olsen, C. L.; Cobb, R. R., High levels of protein expression using different mammalian CMV promoters in several cell lines. *Protein Expr Purif* **2006,** *45* (1), 115-24.

224. Zengerle, M.; Chan, K. H.; Ciulli, A., Selective Small Molecule Induced Degradation of the BET Bromodomain Protein BRD4. *ACS Chem Biol* **2015,** *10* (8), 1770-7.

225. Zou, Y.; Ma, D.; Wang, Y., The PROTAC technology in drug development. *Cell Biochem Funct* **2019,** *37* (1), 21-30.